

Université de Montréal

**Bioresorbable coronary stents: Non-invasive quantitative assessment
of edge and intrastent plaque – a 256-slice computed tomography
longitudinal study**

Par

Evguenia Zdanovich

Programme de Sciences Biomédicales

Faculté de Médecine

Mémoire présenté en vue de l'obtention du grade de maîtrise

en Sciences Biomédicales, option Générale

Juillet 2019

© Evguenia Zdanovich, 2019

Université de Montréal

Programme de Sciences Biomédicales

Faculté de Médecine

Ce mémoire intitulé

**Bioresorbable coronary stents: Non-invasive quantitative assessment
of edge and intrastent plaque – a 256-slice computed tomography
longitudinal study**

Présenté par

Evguenia Zdanovich

A été évalué par un jury composé des personnes suivantes

Daniel Juneau

Président-rapporteur

Carl Chartrand-Lefebvre

Directeur de recherche

Samer Mansour

Codirecteur

Karl Sayegh

Membre du jury

Résumé

Les *bioresorbable stents* (BRS), en français intitulés tuteurs coronariens biorésorbables, sont constitués d'un polymère biorésorbable, plutôt que de métal, et ne créent pas d'artéfacts métalliques significatifs en tomодensitométrie (TDM). Cela permet une meilleure évaluation de la plaque coronarienne sous ces tuteurs en TDM qu'avec les anciens tuteurs qui sont en métal.

OBJECTIF: Évaluer l'évolution de la composition de la plaque, sa fraction lipidique (FL)— marqueur de vulnérabilité de la plaque, dans les 3 zones pré-tuteur (bord proximal), intra-tuteur et post-tuteur (bord distal), et le volume de la plaque entre 1 et 12 mois post-implantation de BRS.

MÉTHODOLOGIE: Il s'agit d'une étude observationnelle longitudinale réalisée chez 27 patients consécutifs (âge moyen 59,7 +/- 8,6 ans) et recrutés prospectivement pour une imagerie par TDM 256-coupes à 1 et 12 mois post-implantation de BRS (35 tuteurs total). Les objectifs primaires sont: volume de plaque totale et de FL (mm³) comparés entre 1 et 12 mois. Afin de tenir compte de la corrélation intra-patient, des analyses de variance des modèles linéaires mixtes avec ou sans *spline* sont utilisés avec deux facteurs répétés temps et zone/bloc (1 bloc= 5 mm en axe longitudinal). La valeur % FL= volume absolu du FL/ volume total de la plaque.

RÉSULTATS: Notre analyse par bloc ou par *spline* n'a pas démontré une différence significative dans les volumes de plaque ou des FL dans les zones pre- intra- and post-tuteur entre 1 et 12 mois.

CONCLUSION: Notre étude a réussi à démontrer la faisabilité d'une analyse non-invasive quantitative répétée de la plaque coronarienne et de la lumière intra-tuteur avec l'utilisation de TDM 256 coupes. Cette étude pilote n'a pas démontré de différence significative dans les volumes des plaques et atténuation entre 1- et 12- mois de follow-up post-implantation de BRS. Notre méthode pourrait être appliquée à l'évaluation des différents structures ou profils pharmacologiques de ces tuteurs.

Mots-clés : Tuteur biorésorbable, athérosclérose coronarienne, angiographie par tomographie par densité, plaque coronarienne, fraction lipidique, volume, analyse de variance, modèle linéaire mixte, humains

Abstract

Coronary bioresorbable stents (BRS) are made of a bioresorbable polymer rather than metal. Unlike metallic stents, BRS do not produce significant artifacts in computed tomography (CT) and are radiolucent in CT, making it possible to evaluate coronary plaque beneath an implanted stent.

PURPOSE: The purpose of our study was to evaluate the volumes of plaque and low attenuation plaque components (LAP —a marker of plaque vulnerability) of pre-, intra- and post-stent plaque location between 1 and 12 months post-implantation.

METHODS: In our prospective longitudinal study, we recruited 27 consecutive patients (mean age 59.7 +/- 8.6 years) with bioresorbable stents (n=35) for a 256-slice ECG-synchronized CT evaluation at 1 month and at 12 months post stent implantation. Total plaque volume (mm³) as well as absolute and relative (%) LAP volume per block in the pre-, intra- and post-stent zones were analyzed; comparison of 1 and 12 months post BRS implantation. Changes in these variables were assessed using mixed effects models with and without spline, which also accounted for correlation between repeated measurements with factors such as time and zone/block (1 block = 5 mm in longitudinal axis). The value % LAP= LAP absolute volume/ total plaque volume.

RESULTS: Our block or spline model analysis showed no significant difference in plaque or LAP volumes in pre-, intra- and post-stent zones measured at 1 month and at 12 months.

CONCLUSION: Our study demonstrates the feasibility of repeated non-invasive quantitative analysis of intrastent coronary plaque and in-stent lumen using a 256-channel CT scan. This pilot study did not show significant differences in plaque volume and attenuation between 1- and 12-month follow-up from stent implantation. The method we used could be applied to the evaluation of different stent structures or different pharmacological profiles of bioresorbable stents.

Keywords : Bioresorbable stent, coronary atherosclerosis, computed tomography angiography, coronary plaque, low-attenuation plaque, volume, analysis of variance, mixed effects model, humans

Table of contents

Résumé	5
Abstract	7
Table of contents	9
Tables list	15
Figures list	17
Boxes list	20
Abbreviations list	21
Symbols list	27
Remerciements	31
Introduction <i>avant-propos</i>	33
Chapter 1 – Coronary atherosclerosis	35
1.1. The epidemiology of coronary disease	36
1.2. Coronary anatomy	36
1.3. Arterial coronary micro-anatomy	38
1.4. Pathology of coronary artery disease	40
Chapter 2 – Coronary stents	47
2.1. Brief history of coronary artery obstructive disease treatment	48
2.2. Percutaneous coronary intervention era	48

2.3.	History and hemodynamics of stenting	51
2.4.	Stent types	52
2.4.1.	Bare-metal stents	52
2.4.2.	Drug-eluting stents	54
2.4.3.	Bioresorbable stents—an <i>avant-propos</i>	55
2.5.	A primer on bioresorbable stents	58
2.5.1.	Bioresorbable stent composition	58
2.5.2.	Bioresorbable stent lifespan and other related timelines.....	59
2.5.3.	Clinical outcomes of bioresorbable stents.....	65
2.5.4.	Bioresorbable stent complications	78
2.5.4.1.	Side branch complications in bioresorbable stents.....	78
2.6.	Imaging bioresorbable stents.....	82
2.6.1.	Bioresorbable stent imaging with conventional coronary angiography.....	83
2.6.2.	Bioresorbable stent imaging with intravascular ultrasound	84
2.6.3.	Bioresorbable stent imaging with optical coherence tomography	86
2.6.4.	Bioresorbable stent imaging with CT scan versus metallic stents	87
Chapter 3 –	Cardiac computed tomography.....	91
3.1.	Introduction to CT scan.....	92
3.1.1.	The technical aspects of CT	92
3.1.2.	Brief history of CT	93

3.2.	Physical and technical principles of coronary CT scan.....	95
3.2.1.	Temporal resolution in coronary CT scan.....	95
3.2.1.1.	Retrospectively ECG-gated helical acquisition.....	96
3.2.1.2.	Prospectively ECG-gated axial acquisition.....	97
3.2.2.	Spatial resolution in coronary CT scan	98
3.2.3.	Artifacts in coronary MDCT: detection and solutions	99
3.2.3.1.	Motion artifacts	99
3.2.3.1.1.	<i>Cardiac motion</i>	100
3.2.3.1.2.	<i>Respiratory motion</i>	107
3.2.3.2.	Metal or streak artifacts.....	108
3.2.4.	Cardiac CT radiation	109
3.3.	CT imaging of coronaries.....	109
3.3.1.	CT imaging of native coronary arteries.....	110
3.3.2.	CT imaging of coronary stents at present.....	111
Chapter 4 – Imaging coronary plaque		113
4.1.	Imaging coronary lumen and plaque.....	114
4.1.1.	Coronary CT imaging in action.....	114
4.1.2.	CT-based plaque composition and morphology imaging	115
4.1.3.	CT-based intrastent plaque imaging.....	118
4.1.4.	Clinical studies of BRS involving CT imaging.....	120

4.1.5.	CT-prediction of intrastent stenosis with plaque markers.....	124
4.1.6.	IVUS and CT studies of intra- and juxta-BRS plaque	129
4.1.6.1.	IVUS studies of intra- and juxta-BRS plaque imaging	129
4.1.6.2.	CT studies of intra- and juxta-BRS plaque imaging	131
Chapter 5 – The essence of my work		135
5.1.	Introduction and hypothesis	136
5.2.	Methods.....	137
5.2.1.	Study design	137
5.2.2.	Ethical considerations	137
5.2.3.	Study patients	137
5.2.3.1.	Novel implantation protocol.....	138
5.2.3.2.	CT study patients.....	138
5.2.4.	CT imaging.....	139
5.2.4.1.	Patient preparation.....	139
5.2.4.2.	CT acquisition protocol.....	139
5.2.4.3.	Contrast administration protocol.....	139
5.2.4.4.	CT image reconstruction and post-processing	139
5.2.4.5.	Radiation dose	140
5.2.5.	CT imaging analysis.....	140
5.2.6.	Statistical analysis	143

5.3.	Results	143
5.3.1.	Study patients	143
5.3.2.	CT plaque analysis	150
5.3.2.1.	Plaque volume analyses	150
5.3.2.2.	LAP volume analysis	152
5.3.2.3.	Relative LAP (%) analysis	154
5.4.	Discussion	156
	Conclusion and Perspectives	161
	Bibliography	163
	Appendices	195

Tables list

- Table 1. Bioresorbable stent clinical outcomes: comparison with drug-eluting metallic stents
- Table 2. BRS CCTA imaging: assessment parameters of the intrastent lumen and arterial walls
- Table 3. CT-based parameters measured in BRS-stented coronary arteries in recent studies
- Table 4. CT-based vulnerability markers of in-stent restenosis
- Table 5. Plaque area change assessments under bioresorbable stents by IVUS
- Table 6. Stent distribution parameters
- Table 7. Patient demographics
- Table 8. Scan parameters
- Table 9. Pre-implantation lesion characteristics as assessed with conventional angiography
- Table 10. Description of the different sizes of BRS in our study
- Table 11. Plaque volume at 1- and 12-month follow-up by block location (pre-, intra 1-, 2-, 3-, 4-, 5-, and post-stent blocks)
- Table 12. Plaque volume at 1- and 12-month follow-up by plaque location (pre-, 1st, 2nd, 3rd intrastent tertiles, and post-stent plaque)

- Table 13. Absolute LAP volume at 1- and 12-month follow-up by block location (pre-, intra 1-, 2-, 3-, 4-, 5-, and post-stent blocks)
- Table 14. Absolute LAP volume at 1- and 12-month follow-up by plaque location (pre-, 1st, 2nd, 3rd intrastent tertiles, and post-stent blocks)
- Table 15. Relative LAP volume at 1- and 12-month follow-up by block location (pre-, intra 1-, 2-, 3-, 4-, 5-, and post-stent blocks)
- Table 16. Relative LAP volume at 1- and 12-month follow-up by plaque location (pre-, 1st, 2nd, 3rd intrastent tertiles, and post-stent blocks)

Figures list

- Figure 1. Coronary anatomy with 256-slice ECG-gated coronary CT scan angiography
- Figure 2. A cross-sectional view of coronary vessel composition
- Figure 3. Current understanding of coronary lesion players in atherosclerosis development leading to vulnerable plaque
- Figure 4. Depiction of progressive changes in the atherosclerotic artery leading to lumen narrowing and positive remodeling
- Figure 5. Plain old balloon angioplasty
- Figure 6. Percutaneous coronary intervention
- Figure 7. Plasticised bare-metal cobalt-chromium stent
- Figure 8. CT imaging of bare-metal cobalt-chromium stent
- Figure 9. Drug-eluting in-stent restenosis
- Figure 10. ABSORB bioresorbable stent
- Figure 11. Composition and structure of ABSORB BRS and XIENCE V
- Figure 12. Histological and optical coherence tomography evolution in resorption of ABSORB BRS in a porcine coronary arteries model
- Figure 13. Longitudinal coronary healing process beneath bioresorbable scaffold captured in 5-year long imaging of the stented stenotic area
- Figure 14. Plaque and vessel progression over time after implantation of metallic or bioresorbable stents

- Figure 15. Outcomes from the three potential non-inferiority clinical trials
- Figure 16. Neointimal bridge formation after bioresorbable stent implantation
- Figure 17. Coronary catheterization room in Hôtel-Dieu Hospital in 2016
- Figure 18. Conventional coronary angiography
- Figure 19. Intravascular ultrasound post-implantation of a BRS in a patient with severe stenosis of mid left anterior descending artery
- Figure 20. Bioresorbable scaffold struts visualization with OCT, after BRS implantation in a patient with severe stenosis of mid left anterior descending artery
- Figure 21. Reduced stent blooming artifacts and improved strut definition with sharp (XCD) in comparison to smooth (XCB) kernel
- Figure 22. Bioresorbable stent visualized in mid-circumflex artery
- Figure 23. CT angiography correlation with conventional angiography
- Figure 24. Spiral or helical CT scanner
- Figure 25. Prospectively and conventionally retrospectively ECG-gated dual source CT
- Figure 26. Cardiac motion artifact
- Figure 27. Illustration of the image acquisition of dual-source computed tomography with two x-ray tubes and corresponding detectors positioned at 90° angles
- Figure 28. ECG editing performed in two patients

- Figure 29. Radiation-induced DNA damage can lead to either damage tolerance or DNA repair and regulatory responses mechanisms activation
- Figure 30. Non-invasive atherosclerotic plaque imaging
- Figure 31. Computational simulation of FFR volume rendering of left coronary artery tree
- Figure 32. Calculating remodeling index of BRS-scaffolded coronary artery based on CCTA imaging
- Figure 33. CCTA BRS imaging: plaque volume assessment with TeraRecon software
- Figure 34. Pre-, intra- and post-stent zones composition with 5-mm blocks
- Figure 35. Volumetric plaque analysis
- Figure 36. Intrastent stenosis

Boxes list

Box # 1	A reminder on the anatomy of the coronary arteries
Box # 2	Thin-cap fibroatheroma
Box # 3	Arterial remodeling
Box # 4	Spotty calcifications
Box # 5	Stent
Box # 6	Neointimal hyperplasia
Box # 7	Drug-eluting balloons (DEBs)
Box # 8	Arterial vasomotion
Box # 9	Dual anti-platelet therapy
Box # 10	Non-inferiority trials
Box # 11	Temporal resolution
Box # 12	Pitch
Box # 13	Spatial resolution
Box # 14	Voxel
Box # 15	Dual-source CT scanner
Box # 16	Attenuation
Box # 17	Radiation recommendations
Box # 18	FFR and FFR _{CT}
Box # 19	Kilovolt peak

Abbreviations list

A

ACC	—	American College of Cardiology
Ach	—	acetylcholine
ACS	—	acute coronary syndrome
AHA	—	American Heart Association
ASA	—	acetylsalicylic
AUC	—	area under the curve

B

BMS	—	bare-metal stent
BMI	—	body mass index
BRS	—	bioresorbable stents (also known as BVS – bioresorbable vascular scaffolds)

C

<i>CABG</i>	—	coronary artery bypass graft
CAC	—	coronary artery calcification
CAD	—	coronary artery disease
CCA	—	conventional coronary angiography
CCTA	—	coronary CT angiography
CE mark	—	certification mark
CHUM	—	centre hospitalier de l'Université de Montréal
CMR	—	coronary (or cardiac) magnetic resonance imaging
CT	—	computed tomography
Cx or LCx	—	circumflex coronary artery or left circumflex coronary artery

D

DEBs	—	drug-eluting balloons
DES	—	drug-eluting stents
DNA	—	deoxyribonucleic acid
DPL	—	dose-length product

E

ECG	—	electrocardiogram
EES	—	everolimus-eluting stent
ESC	—	European Society of Cardiology

F

FDA	—	Food and Drug Administration
FFR	—	fractional flow reserve
FFR _{CT}	—	fractional flow reserve computed tomography
F/U	—	follow-up

H

HR	—	hazard ratio
----	---	--------------

I

ISR	—	in-stent restenosis
IR	—	iterative reconstruction
IVUS	—	intravascular ultrasound

L

LAD	—	left anterior descending coronary artery
LCX	—	left circumflex coronary artery
LDL	—	low-density lipoprotein
LM	—	left main coronary artery

M

MACE	—	major adverse cardiovascular events
MI	—	myocardial infarction
MLA	—	minimum lumen area
MLD	—	minimal lumen diameter
MPR	—	multiplanar review
MRA	—	magnetic resonance angiography
MRI	—	magnetic resonance imaging
MSCT	—	multi-slice computed tomography
mTOR	—	mammalian target of rapamycin

O

OCT	—	optical coherence tomography
-----	---	------------------------------

OR — odds ratio

P

PCI — percutaneous coronary intervention

PDA — posterior descending coronary artery

PDLLA — poly (DL)-lactide

PO — *per os*

POBA — plain old balloon angioplasty

Q

QCA — quantitative coronary angiography

R

RAMQ — Régie de l'assurance maladie du Québec

RCA — right coronary artery

ReABSORB — ABSORB registry

S

SD — standard deviation

T

TCFA — thin-cap fibroatheroma

TLF — target lesion failure

TVMI — target vessel myocardial infarction

U

USA — United States of America

V

VH-IVUS — virtual histology intravascular ultrasound

Symbols list

bmp — beats per minute

cm — centimeter

Dr — doctor

Gy — gray

HU — Hounsfield unit

Inc. — incorporated

kVp — kilovolt peak

mAs — milliamperes

mg — milligram

mGy — milligray

mL — milliliter

mm — millimeter

mo — month

ms — millisecond

mSv — millisieverts

p — page

s — second

Sv — sieverts

2-D — two-dimensional

3-D — three dimensional

μm — micrometer

© — copyright

To the one and only who gave me the reason for it all

Remerciements

Je remercie sincèrement mon directeur principal, Dr Carl Chartrand-Lefebvre, mon co-directeur, Dr Samer Mansour, et mon parrain de maîtrise, Dr An Tang, pour:

M'avoir aidé avec la recherche de bourse de maîtrise.

M'avoir initié aux congrès internationaux et

M'avoir appris comment les choisir pour le bien de mon intérêt.

Avoir amélioré mon raisonnement scientifique.

M'avoir donné un avant-goût de gestion de mon projet.

Avoir amélioré ma collaboration scientifique et mon autonomie.

M'avoir rendu plus déterminée à réussir mes projets.

Avoir validé de mes travaux.

Avoir amélioré mon sens de travail accompli.

M'avoir beaucoup appris sur la priorisation et valorisation de mon travail et mon temps.

Surtout un grand merci de m'avoir appris comment trouver mon style de composition scientifique. Au plaisir de travailler avec vous de nouveau.

Mes remerciements à Mme Sylvie Babin pour son aide administrative dans la gestion de mon dossier et son souci d'accompagner les étudiants du département de radiologie dans leurs diverses démarches.

Merci aussi à Irina Boldeanu de m'avoir appuyé lors de mon apprentissage du logiciel TeraRecon.

Je remercie Charbel Naim, le fellow en cardiologie de Dr Mansour, pour m'avoir fourni et assisté avec les informations nécessaires pour amorcer mon projet de recherche.

Merci également à M. Miguel Chagnon pour m'avoir appris à avoir un raisonnement statistique et être disponible pour le support logistique.

Mes remerciements à Mme Assia Belblidia pour son prompt aide et ses démarches devant le comité d'éthique.

Je remercie aussi notre biostatisticien, le chirurgien cardiaque et PhD en statistique, Dr Louis-Mathieu Stevens, de nous être venu à la rescousse vers la fin de mon projet de maîtrise pour nous aider avec nos démarches statistiques rendues complexes et pour améliorer mes connaissances en statistiques.

Mes remerciements à Dr Daniel Juneau et Dr Karl Sayegh qui j'ai eu le privilège d'avoir en tant que président et membre du jury de mon mémoire de maîtrise.

Finalement, un grand merci à mes parents, Ирина Глазкова и Виктор Зданович, et mes proches pour tous les sacrifices qu'ils ont fait pour m'aider à devenir qui je suis aujourd'hui. Vous êtes toujours avec moi, même à des kilomètres.

Ma reconnaissance infinie va à mon conjoint, **عمر عرفة**, pour m'avoir donné de l'assurance de persévérer et un exemple de l'estime de soi ainsi que le courage de s'aimer et pour simplement avoir été à mes côtés.

Introduction *avant-propos*

This master's thesis manuscript begins with four chapters introducing an amalgam of concepts from cardiology and radiology—two disciplines I enjoy—with a focus on coronary atherosclerosis, coronary stents, cardiac computed tomography, and coronary plaque imaging. These introductory chapters accompany the reader to the main master's project in chapter 5: a prospective longitudinal study performed on novel coronary bioresorbable stents and imaged by cardiac CT scan.

I hope you enjoy this composition.

Chapter 1 – Coronary atherosclerosis

Presentation and objectives:

This chapter will introduce basic concepts pertaining to coronary atherosclerosis. First, a brief review of coronary artery disease epidemiology will be presented. Second, coronary anatomy will be depicted using computed tomography. Third, the American Heart Association coronary artery plaque classification system will be discussed. Lastly, the notion of coronary plaque vulnerability will be addressed.

1.1. The epidemiology of coronary disease

Despite advances in the medical field, coronary artery disease (CAD) remains one of the most prevalent causes of morbidity and mortality throughout the world.¹ In 2012, cardiovascular diseases resulted in 17.3 million deaths throughout the world despite unceasing improvement in the CAD survival rate. By 2030, this mortality rate is expected to increase to more than 23.6 million.²

In the United States, 50% of middle-aged men and 30% of middle-aged women will develop CAD of some type.³ However, from 1980 to 2002, CAD death rates fell by 52% in men and by 49% in women over 35 years of age.⁴ When addressing CAD risk factors, such as unhealthy diet, smoking, hypertension, obesity, high fasting plasma glucose, and physical inactivity, coronary artery disease tends to be preventable.³

1.2. Coronary anatomy

Usually, the proximal aorta gives rise to the left coronary artery which originates from the left posterior aortic sinus, and the right coronary arteries, which originates from the anterior aortic sinus.⁵ The left and right coronary arteries give rise to vessels that run partially through the main epicardial grooves, namely the left and right atrioventricular grooves and the anterior or posterior interventricular grooves (see box #1, p.38). The caliber and length of the coronary vessels and their side branches vary considerably.⁶

The proximal portion of the left coronary artery is called the left main coronary artery (LM) and is 0-15 mm in length. In most cases, the LM bifurcates into the left anterior descending coronary artery (LAD) and the left circumflex coronary artery (LCX), however, in 30% of the population, the LM trifurcates into an intermediate branch (also known as the ramus medianus) originating between the LAD and the LCX.⁶

The LAD runs through the anterior interventricular groove with its septal branches,

and vascularize the lateral and posterior of the left ventricle (LV) and the left atrium. In case of left dominance, the LCX gives branches to vascularize the inferior portion of the LV. The anterior, anteroseptal and anterolateral left ventricular segments are nourished by the LAD and its branches.⁶ In case of left dominance, the LCX gives branches that vascularize the infero-posterior wall of the LV⁷.

The LCX runs through the left atrioventricular groove with its major side branches, which are obtuse marginal branches (generally one to three) that irrigate the lateral and posterior portions of the left atrium and left ventricle if there is left-side dominance.⁶

The right coronary artery (RCA) runs in the right atrioventricular groove. The RCA gives rise to the acute marginal artery and the right posterior descending artery (PDA). In case of right dominance, the RCA irrigates the inferior, posterior and interventricular septum.⁶ In 7% of the population prevails co-dominance⁸, which means that both LCX and RCA supply the inferior wall of the left ventricle⁹.

Box # 1

A reminder on the anatomy of the coronary arteries¹⁰

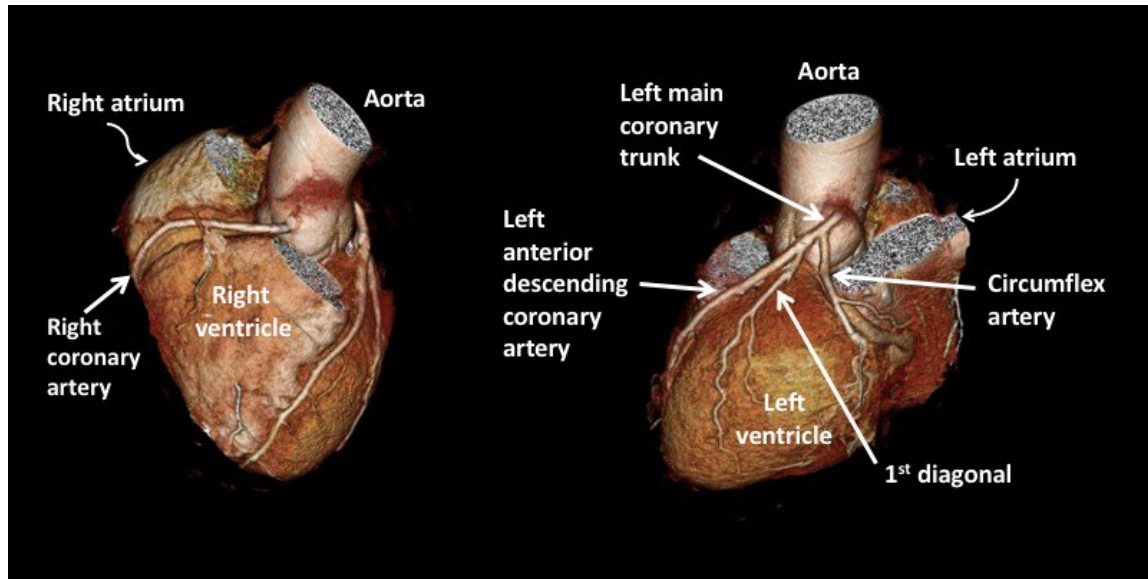


Figure 1. Coronary anatomy from 256-slice ECG-gated coronary CT scan angiography.

Copyright © 2018 [CHUM, E Zdanovich]

1.3. Arterial coronary micro-anatomy

Coronary arteries are composed of three layers: the tunica intima, tunica media, and tunica adventitia (see fig. 2, p.39). The most inner layer of the coronary vessel is the tunica intima, which is composed of an endothelial layer that offers a frictionless surface for blood movement.¹¹ The tunica media is the middle layer and consists of smooth muscle cells and elastin, which modulate the internal diameter of the coronary artery. The tunica adventitia (or tunica externa) is the most external layer that contributes to vessel shape and gives structural support.¹¹

The Structure of an Artery Wall

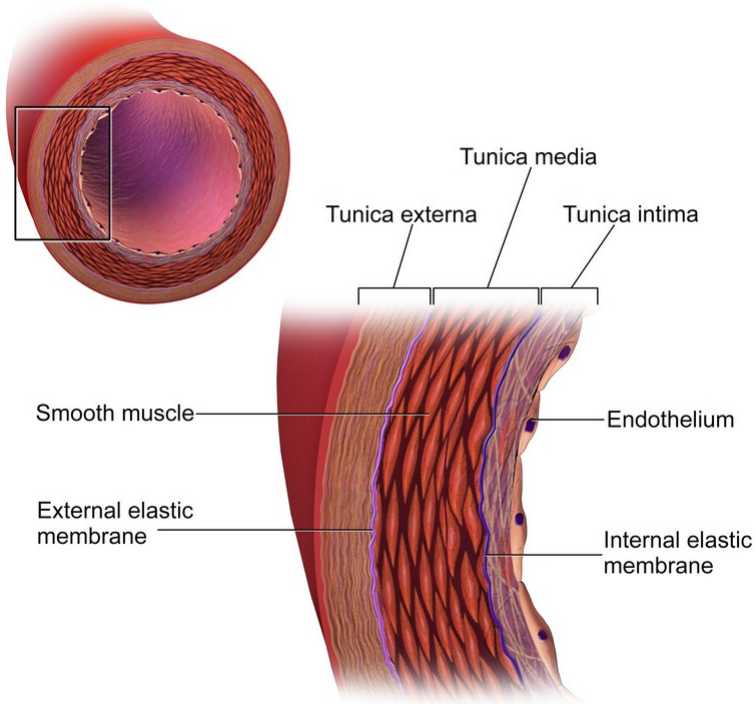


Figure 2. A cross-sectional view of the composition of a coronary vessel.

Reprinted with permission from Wikimedia Foundation, Inc; Blausen.com staff (2014) WikiJournal of Medicine [Creative Commons Attribution-ShareAlike] (2014), DOI:10.15347/wjm/2014.010 ISSN 2002-4436 ¹²License terms <https://creativecommons.org/licenses/by-sa/3.0/>

Coronary arteries supply organs with blood and nutrients and function under high pressure. This high pressure is accommodated by a greater ratio of elastic to muscle tissue. As previously described, the tunica media has elastic fibers. Likewise, the membrane between the tunica media and adventitia is also composed of an elastic connective tissue called the external elastic lamina or membrane. There is also an internal elastic membrane between the tunica intima and media (fig. 2, p.39). Elastin mediates variations in coronary artery size and diameter.¹¹

The size of a coronary vessel can be presented using a variety of parameters, such as minimal and maximal luminal diameters or cross-sectional area. The coronary vessel can be visualized and evaluated along its long or short axis. Coronary arteries are usually not perfectly round in their circumference; therefore, in a coronary cross-section (short-axis view), minimal and maximal diameters can be specified. When luminal diameter is measured, three diameters can be obtained: the minimal, mean and maximal luminal diameters. Cross-sectional area refers to the area of a given cross-section of the coronary vessel. The cross-sectional area of any components of the vessel, for example, a lumen or the external elastic membrane, can be measured.

1.4. Pathology of coronary artery disease

In 1856, Rudolph Virchow described how injury to an artery could lead to atherosclerosis of that vessel.¹³ Subsequently, in 1977, Russell Ross described a process of coronary atherosclerosis formation in which endothelial wall injury led to platelet adhesion to the wound, with activation of intimal smooth muscle cell proliferation resulting in plaque progression.^{13,14} Ross described atherosclerosis as an excessive inflammatory-proliferative process in the arterial wall, involving numbers of growth factors and vasoactive molecules.¹⁴

In the late 1990s, Libby and Hansson hypothesized on a complex interaction between clinical risk factors, such as hypercholesterolemia, innate and adaptive immunity status, and atherogenesis.¹⁵⁻¹⁷ In parallel, a complementary theory of plaque progression emerged due to the work of Fuster et al.¹⁸ The latter authors described atherogenesis as a series of events where endothelium is injured first, followed by denudation of the endothelial layer and damage to the intima, which then leads to further media damage in the advanced stages of the disease.¹⁸ In the same period of time, a new theory of atherogenesis emerged, which hypothesized that fissures in plaque led to coronary thrombosis and occurred mainly in soft, lipid-rich plaques covered with a thinning fibrous cap.¹⁹

In 1995, an expert committee from the American Heart Association (AHA) proposed a histological classification of coronary atherosclerotic lesions, from type I to type VI, from least to most clinically consequential.²⁰ Type I represents initial intimal thickening. In type II, there is formation of a fatty streak composed of macrophages and lipid-rich smooth muscle cells. Type III is an intermediate state of atheroma that may be associated with clinical symptoms. In type IV, the lipid-rich core of the atheroma becomes more confluent and vulnerable. Type V is called fibroatheroma and is characterized by the presence of fibrous connective tissue. Type VI lesions can be either calcified or fibrosed. Such lesions tend to fissure and lead to hematoma.²⁰

However, the concept of precursor lesions that would lead to clinical events was not addressed in the aforementioned classification of types of AHA lesion.^{1,21} Structural plaque characteristics and plaque vulnerability were subsequently studied and described with the following terms: adaptive intimal thickening, intimal xanthoma or fatty streak, pathological intimal thickening and fibroatheroma.^{1,20-22} It has also been revealed that the presence of a large necrotic core, an acellular lipid-rich milieu like that found in a vulnerable thin-cap fibroatheroma can convert a stable asymptomatic lesion into an unstable plaque with the potential to rupture.²³ Therefore, the notion of thin-cap fibroatheromas (TCFA) arose and was subsequently associated with plaque vulnerability (box # 2, p.44).^{1,24} It was found that as TCFA grows, vessel lumen does not always narrow, since a vessel can exhibit adaptive positive remodeling, which can, like TCFA, also be a plaque vulnerability marker (box # 3, p.45).²⁵ Finally, spotty calcification (defined as foci of calcifications measuring 3 mm or less) is another potential plaque component and marker that can be associated with plaque vulnerability (box # 4, p.46)²⁶.

Plaque healing was also not addressed in the AHA classification. Healing of the ruptured plaque can lead to sequelae such as a rise in plaque burden (where cross-sectional areas of plaque and media are divided by the vessel's external elastic membrane²⁷), negative remodeling (see box # 3, p.45) leading to luminal narrowing, or chronic total occlusion.^{1,22}

A new mechanism of unorganized atherogenesis as a precursor to plaque progression was investigated. In a recent review article by Wang et al.²⁸, a link was determined between vulnerable plaque, coronary wall shear stress (a force parallel to the vessel producing shear blood flow), and

atherogenesis (e.g., vasa vasorum proliferation).²⁸ These authors stated that shear stress at a given point in the coronary artery results in anarchic neovascularization of the vessel wall, leading to the formation of vulnerable plaque due to intraplaque hemorrhage and microvascular leakage of red blood cells, inflammatory cells, and lipid/lipoproteins. Figure 3 (p.43) illustrates some of the key components of the above-described generic vulnerable plaque.

Finally, it has been shown that inflammation prevails in the atherosclerotic region from early atherosclerotic lesions or “fatty streak” to acute plaque erosion and rupture.²⁹ An association between acute myocardial infarction and inflammatory factors has been described in the literature for over 50 years, which is partly due to the latter’s role in plaque progression and rupture.³⁰ Nonetheless, it is still unclear whether this correlation between atherogenesis and inflammation is of a causal nature or not, or if inflammation is merely the result of injured cardiac tissue.²⁹ Low-density-lipid (LDL) cholesterol-lowering drugs called statins may have a role in reducing inflammation. Indeed, they directly decrease activity of a nuclear factor, which regulates inflammatory genes, while indirectly lowering free cholesterol and oxidized-LDL levels, which act as proinflammatory mediators.²⁹

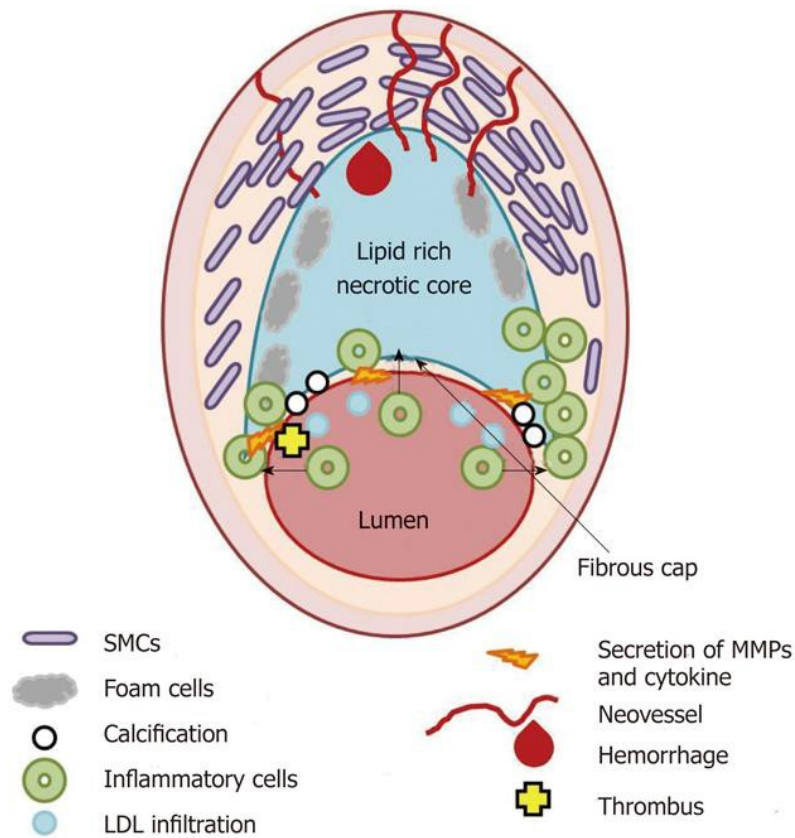


Figure 3. Current understanding of coronary lesion players in atherosclerosis development leading to vulnerable plaque. Vulnerability markers represented here include positive remodeling (oval shape of cross-section), necrotic core, and spotty calcifications, which can complicate via hemorrhage and/or thrombus.

SMCs = smooth muscle cells, which proliferate and maintain plaque formation and growth; LDL = low-density lipoprotein, which can migrate through intima and form lipid core with cholesterol crystals; MMPs = matrix metalloproteases, which upregulate matrix degradation and tend to switch from stable plaque to thin-cap fibroatheroma; macrophage = a kind of inflammatory cell; foam cells = macrophages that have engulfed lipid particles, which can accumulate and form a necrotic core.

Reprinted by permission from *World of J Radiol: Progress in atherosclerotic plaque imaging* by G. Soloperto and S. Casciaro © (2012 Baishideng Publishing Group Co.) Aug 28, 2012; 4(8): 353-371.

Doi : [10.4329/wjr.v4.i8.353](https://doi.org/10.4329/wjr.v4.i8.353)²⁵

Box # 2

Thin-cap fibroatheroma

As histological studies show, the most common type of vulnerable plaque is thin-cap fibroatheroma (TCFA). It consists of a lipid-rich necrotic core covered with a thin cap rich in macrophages, which are white blood cells that cleanse the body of foreign substances.³¹ TCFA is quantitatively characterized as an atheroma with a fibrous cap of <65 μm in thickness^{1,32} with a lipid-rich necrotic core representing about 35% of plaque volume, infiltrated with macrophages of >25 cells per 0.3 mm diameter field.³³ Major predictors of acute coronary syndrome are the thickness of TCFA and the dimensions of the lipid-rich necrotic core.³⁴

Box # 3

Arterial remodeling

Arterial remodeling occurs when atheromatous plaque in the coronary arteries expands. This remodeling can either expand the vessel outward, a process called positive remodeling, or shrink it inward, in negative remodeling.³⁵

Positive remodeling represents a compensatory mechanism that initially protects the vessel lumen from the expanding intimal plaque and is therefore called adaptive positive remodeling.^{36,37} Later on in the life of atherosclerotic plaque, extensive positive remodeling can be considered a marker of plaque vulnerability, along with a large lipid core and increased macrophage lesion influx (inflammation markers).^{38,39} Exaggerated positive remodeling tends to be associated with plaque rupture and unstable coronary syndromes.^{35,40} As the Glagov principle states, coronary arteries enlarge with the growing plaque area, which delays functionally important lumen stenosis provided that the plaque area remains less than 40% of the internal elastic lamina area (fig. 4, below)³⁷.

$$\text{Remodeling index}^{35} = \frac{\text{External elastic membrane area at the lesion site}}{\text{External elastic membrane of the reference}}$$

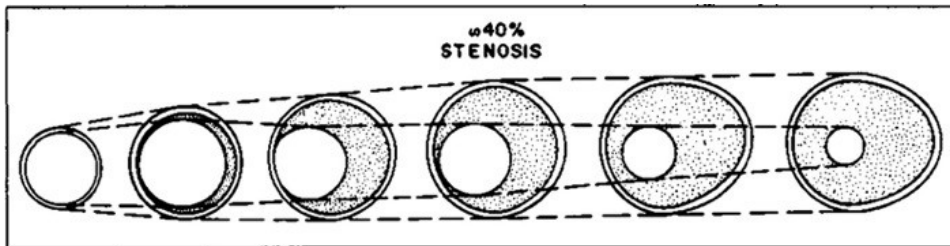


Figure 4. Depiction of progressive changes in the atherosclerotic artery leading to lumen narrowing and positive remodeling. With occurrence of positive remodeling, an almost normal lumen cross-sectional area is preserved with 40% stenosis. Reproduced with permission from the New England Journal of Medicine, Compensatory enlargement of

human atherosclerotic coronary arteries by Glagov S et al 1987; 316:1371-1375. Copyright Massachusetts Medical Society.³⁷

Box # 4

Spotty calcifications

Atheromatous plaques of patients with acute coronary syndromes were shown to include small calcifications in a spotty pattern.^{41,42} Some studies have demonstrated that spotty micro-calcifications can bring an increase in biomechanical plaque stress, thus becoming one of the possible pathways to plaque rupture.^{43,44} Spotty calcifications can possibly activate inflammatory cytokines and fragilize plaque morphology, which can lead to local inflammation and plaque instability.²⁶

Finally, under certain patient and plaque characteristics, coronary atherosclerosis can lead to plaque rupture, which in turn can result in luminal thrombosis. Addressing these characteristics that give rise to vulnerable plaque is currently an investigation target in the field of cardiovascular research.

Chapter 2 – Coronary stents

Presentation and objectives:

This chapter will introduce the reader to coronary angioplasty and will describe the main types of coronary stents that are implanted to treat coronary stenosis in all settings of acute coronary syndrome or stable angina. Most of the chapter will discuss the novel bioresorbable stents. The composition of bioresorbable stents, the associated clinical outcomes and the imaging of these stents using modalities such as conventional coronary angiography, intravascular ultrasound, optical coherence tomography and computed tomography will be covered.

2.1. Brief history of coronary artery obstructive disease treatment

At the turn of the twentieth century, acute coronary artery disease (CAD) (or acute coronary syndromes) was difficult to treat. Bed rest, oxygen and intravenous fluids were the main treatments.

With the 1980's came the thrombolytic era⁴⁵, during which thrombolytic agents such as streptokinase or tissue plasminogen activator were administered, dissolving coronary thrombus and restoring coronary blood flow.

Even when thrombolysis was successful, re-occlusions occurred.⁴⁶ Thus, despite improved clinical outcome with thrombolytic therapy, one third of patients did not gain adequate coronary reperfusion.^{47,48}

There were also some contraindications to the use of thrombolytics, such as presence of active bleeding, recent surgery, uncontrolled hypertension and history of stroke. It was observed that patients of 75 years and older had side effects such as major risk of haemorrhagic stroke.^{47,49}

By the end of the 1970's, besides medical treatment, two major options of CAD treatment had evolved: 1) surgical coronary revascularization with bypass grafting; and 2) plain old balloon (no stent) angioplasty (POBA). Despite bypass surgery being an appealing alternative, POBA was also promptly adopted as a treatment of CAD.^{46,50,51}

2.2. Percutaneous coronary intervention era

Cardiac catheterization is performed to diagnose and assess cardiac heart disease.⁵² Worldwide, this cardiac procedure is used widely. The term cardiac catheterization can be used for both right and left or either of the heart catheterizations. Interventional cardiologists perform this procedure either to diagnose or to treat the cardiac heart disease such as with POBA and PCI. The cardiac catheterization is conducted by inserting a catheter into the heart such as into a ventricle (ventriculography) or a coronary artery (coronarography). This procedure has no absolute

definitive contraindications except for the relative contraindications that depend on the patient's comorbidities.⁵³

POBA was performed first on an awake patient by Dr. Andreas Gruentzig in 1977 in Zurich, Switzerland. Dr. Gruentzig also developed the first balloon inflation device⁵¹ (fig. 5, below). POBA mechanism in the treatment of MI and/or myocardial ischemia involves the compression and redistribution of the culprit atherosclerotic plaque, then improving the coronary artery lumen patency.⁵⁴ However, work done on human cadavers and in vivo animal experiments have also suggested that during balloon deployment some changes were comprised of intima rupture and its separation from the media.⁵⁵ Moreover, the limits of POBA are also represented by its critical risk factor—small vessel size.⁵⁶

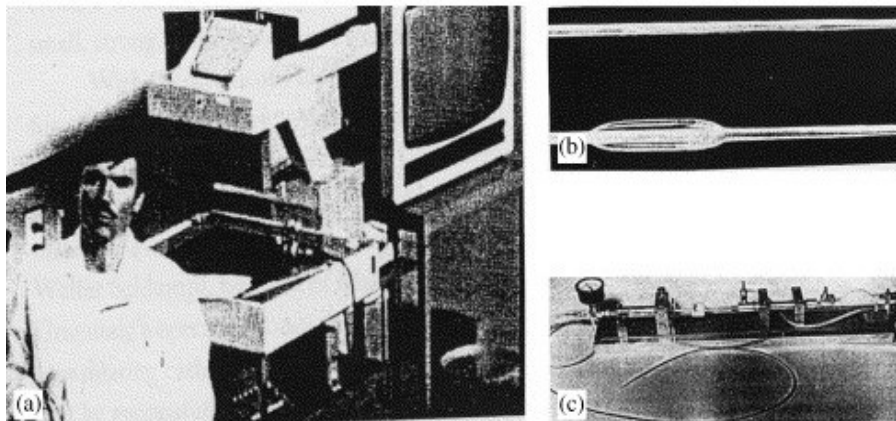


Figure 5. Plain old balloon angioplasty. A) Dr. Andreas Gruentzig and his lab; B) Gruentzig's balloon catheter uninflated and inflated; and C) Gruentzig's inflation device that was used to inflate the balloon catheter. Reprinted from "Tactile VR for hand-eye coordination in simulated PTCA"; YY Cai et al. Computers in Biology and Medicine 2006; 36: 167-180. Copyright (2018) with permission from Elsevier.⁵⁷

Restenosis can happen after an angioplasty, is defined as the decrease in the diameter of the vessel lumen and frequently leads to the target lesion failure.⁵⁸ Mechanisms of restenosis in POBA are comprised of vessel remodeling and elastic recoil.⁵⁹

Studies showed less residual stenosis following POBA and higher rates of patency in the weeks after reperfusion in comparison to thrombolysis.⁴⁶ POBA technique was nonetheless far from ideal. Up to 30-50% of patients, in the first year, had occurrences of restenosis, occlusions and early recoil.⁴⁶

Another non-surgical procedure followed POBA called percutaneous coronary intervention (PCI), or also known formerly as angioplasty with stent, that with help of a catheter introduces a stent into a blood vessel to treat stenosis.⁶⁰

Percutaneous coronary intervention can be performed through radial artery access with small-caliber catheters using the Seldinger technique (fig. 6, below) or through femoral artery access.

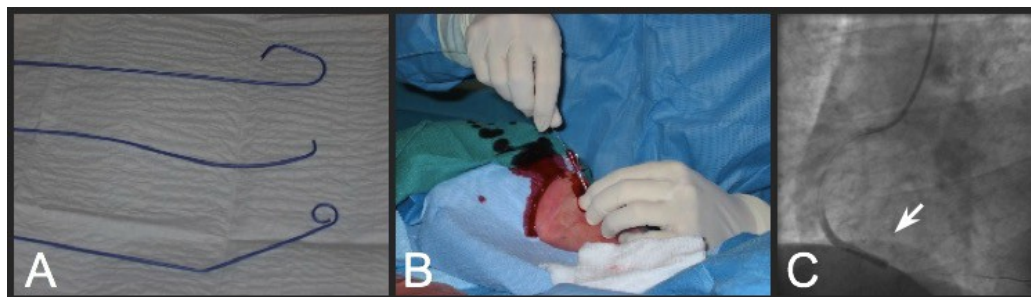


Figure 6. Percutaneous coronary intervention. A) Coronarography catheters. B) Radial artery intervention — Seldinger technique, radial artery. C) Inflated balloon catheter visualization during PCI. With permission from Dr. Carl Chartrand-Lefebvre 2017.

As opposed to POBA, in-stent PCI angioplasty restenosis is defined as excessive tissue proliferation also called neointimal proliferation. It is also defined by the atherosclerotic process of a novel occurrence named neoatherosclerosis.⁶¹ These notions were discussed in chapter 1 and will further be discussed in the current chapter.

2.3. History and hemodynamics of stenting

Box # 5

Stent

The term “stent” comes from the name of Charles Thomas Stent (1807-1885), an English dentist who invented Stent’s dental compound.⁶² This compound was used by plastic surgeons in 1917 during the First World War to attach facial skin grafts to war wounds.⁶³ In 1972, Goodwin et al. defined the term stent as “a compound (that holds) some form of graft in place”.⁶²

It was in March of 1986 that the first coronary stent was implanted by Jacques Puel and Ulrich Sigwart in Toulouse, France.^{62,64} In French, the “stent” became the “endo-prothèse coronarienne autoexpansive”. Nowadays, a vascular stent is also called, in French— a “tuteur”, a term used in botany for a stake that holds a plant straight.

The first coronary stents were invented by Julio Palmaz and Richard Schatz⁶⁵ to circumvent two significant limitations of balloon angioplasty: acute elastic recoil and restenosis. The stent’s mechanical scaffolding supports the vessel and prevents early recoil, allowing a laminar flow and decreasing the shear stress on the vessel, which reduces intimal thickening. The struts of the stent also cover open subintimal spaces, thus preventing contact of the thrombogenic substrate with platelets and aggregating factors. This reduces the possibility of local thrombi formation and their incorporation into a restenotic lesion.⁶⁶

Further developments happened in the mid- and late-1980’s.⁵¹ Early stents were far from ideal because of their thrombogenic potential.⁶⁶ The three main categories of stents used in recent years are bare-metal stents, drug-eluting stents and bioresorbable stents. In the province of Quebec, based on the RAMQ (Régie de l’assurance maladie du Québec) records of 2007-2008,

approximately 15,630 coronary angioplasties were performed in a total of 15 centers practicing angioplasty.⁶⁷

2.4. Stent types

A timeline of the different types of stents to be discussed in this chapter is presented as follows:

Timeline:

1986 – First implantation of bare-metal stent in a human coronary artery

1994 – FDA (Food and Drug Administration) approval of coronary stents for use in clinical settings

2002-2004 – Drug-eluting stent homologation by FDA⁵¹

2016 – FDA approval of the bioresorbable vascular scaffold⁶⁸

2.4.1. Bare-metal stents

As previously mentioned, the first intracoronary stent implantation was performed by Puel and Sigwart in 1986.^{62,64} A stainless-steel auto-expansive multifilament system without eluting medication was deployed. In the early 1980's, stent implantation was reserved for patients with the following indications: restenosis after a successful initial angioplasty, acute vessel occlusion after balloon angioplasty (bail-out stenting), and stenosis of aorto-coronary bypass. The U.S. Food and Drug Administration (FDA) approved the use of coronary stents in clinical settings in 1994.⁵¹ Figures 7 and 8 on the next pages show modern cobalt-chromium bare-metal stents (BMS).



Figure 7. Plasticised bare-metal cobalt-chromium stent. With permission from Hôtel-

Dieu (patient information stand), CHUM 2017.

A large randomized controlled trial named the CADILLAC trial (Controlled Abciximab and Device Investigation to Lower Late Angioplasty Complications), which enrolled 2082 patients with myocardial infarction (MI), demonstrated a lower death, revascularization, reinfarction, or stroke composite endpoint in patients who were implanted with a BMS in comparison to those treated solely with a POBA (11.5 vs. 20.0 %, $p < 0.001$).⁶⁹

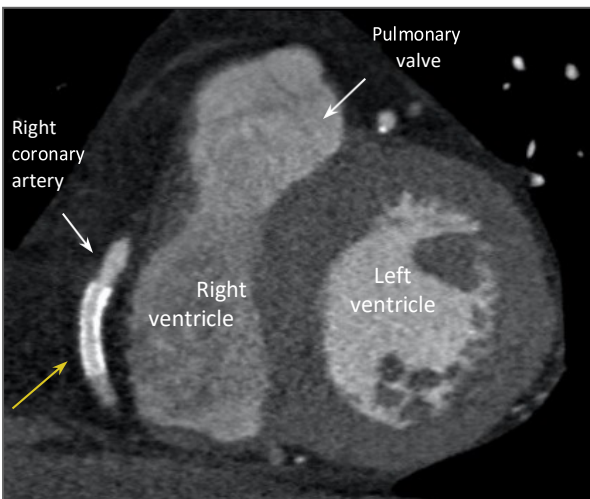


Figure 8. CT imaging of a bare-metal cobalt-chromium stent. A 54-year-old man with a permeable cobalt-chromium bare-metal stent (4.0x20 mm) implanted into his right coronary artery (yellow arrow). This coronary angiogram was performed using a 256-slice CT scanner with ECG-synchronized acquisition (Brilliance iCT, Philips Healthcare, Best, The Netherlands). Copyright © 2017 [E Zdanovich]

2.4.2. Drug-eluting stents

BMS implantation allowed a decreased number of urgent (recoil) and non-urgent revascularisation events in patients with PCI than in stand-alone POBA. However, in-stent restenosis was observed in 10-40% of patients by 6 months post-PCI due to neointimal hyperplasia (see box # 6, below).⁶⁹ With the goals of reducing neointimal hyperplasia and improving clinical outcomes, drug-eluting stents were created.

Box # 6

Neointimal hyperplasia

Neointimal hyperplasia is defined as an increase in thickness in the intimal layer of the coronary artery, called neointima due to proliferation and migration of smooth muscle cells.⁷⁰

Drug-eluting stents (DES) offer delayed release of an anti-proliferative drug such as sirolimus or paclitaxel from a strut coating that impedes proliferation of smooth muscle cells.⁷⁰ In comparison to BMS, DES have been associated with lower rates of death, stent thrombosis, binary stenosis, target-vessel and target-lesion revascularization.⁶⁹ However, a certain level of in-stent restenosis has been associated with DES (fig. 9, below).

There are two types of DES: first and second generation. The second generation is thinner, more deliverable, leads to less inflammation response and procures more rapid re-endothelialisation (vessel healing).⁷¹ Drug-eluting balloons (DEBs) will be discussed in box # 7, next page.



Figure 9. Drug-eluting in-stent restenosis. In-stent restenosis of about 50% (arrows) in a drug-eluting stent located in the right coronary artery of a 47-year-old woman. A) Curved multiplanar reconstruction; B) Orthogonal view of restenosis. Copyright © 2016 [C Chartrand-Lefebvre]

Box # 7

Drug-eluting balloons (DEBs):

DEBs recently emerged as yet another way of addressing restenosis. The balloons are usually coated with paclitaxel due to its rapid absorption and good retention.

2.4.3. Bioresorbable stents—an *avant-propos*

Bioresorbable stents (BRS) are also commonly referred to as bioresorbable vascular scaffolds.⁵¹ In July 2016, the FDA approved the first bioresorbable vascular scaffold stent in the U.S.⁶⁸ Recently, the European Society of Cardiology (ESC) / European Association of Percutaneous Coronary Interventions (EAPCI) stated that bioresorbable stent (BRS) is a more appropriate term than bioresorbable vascular scaffold (BVS), since a scaffold might suggest only a temporary need for coronary support.⁷²

BRS offer potential advantages over their predecessors. After PCI, once the vessel is healed, there is potentially no further necessity for permanent vessel scaffolding and drug delivery. Permanent metallic stent implantation interferes with surgical revascularization, produces artifacts in non-invasive imaging and precludes reactive vasomotion (definition in box # 8, below).⁷³

Box # 8

Arterial vasomotion:

What is it?

A cyclic variation of the vessel diameter moderated by medial smooth-muscle cells, which react to vasoactive molecules of the endothelium such as acetylcholine and nitroglycerine.^{74,75}

How is it measured?

A **vasomotion test** can be performed as follows:

Mean in-stent and distal lumen diameters are measured by quantitative coronary angiography (QCA, section 2.6.1) after sequential infusions of saline, 10^{-8} , 10^{-7} and 10^{-6} M Acetylcholine (Ach), and a vasoconstrictor, through a microcatheter.^{76,77} Nitrate (200 mg), a potent vasodilator, is administered at the very end of the process to help the artery return to its natural vasoactive tone.

Vasoconstriction to Ach is established when there is $\geq 3\%$ decrease in the lumen diameter from baseline (saline) after infusion of highest dose of Ach.^{76,78,79}

The BRS soft scaffold preserves better physiologic vasomotion of the stented segment with the native angulation of the arterial curvature and shear stress, which becomes even more

physiologic after BRS resorption, thus reducing the atherogenic potential. It also allows late luminal gain and late expansive arterial remodeling^{80,81} (see section 2.5.2 for more details).

Furthermore, once bioresorption is completed, lengthy dual anti-platelet therapy (see box # 9, below) can be discontinued, since the iatrogenic material is no longer present.⁸⁰ Moreover, hypothetically, this would allow bypass grafts on stented segments.

Box # 9

Dual anti-platelet therapy consists of two agents:

1) Aspirin, or acetylsalicylic acid (ASA), which prevents thromboxane production by platelets and their agglomeration into clots.⁸² It is prescribed for those who have had a myocardial infarction, stenting procedure, or coronary artery bypass graft (CABG) surgery. Aspirin therapy is continued for the rest of the patient's life.⁸³

2) P2Y12 inhibitor, which irreversibly blocks the adenosine diphosphate P2Y12 receptor, to prevent platelet agglomeration. The P2Y12 inhibitor prescribed can be either clopidogrel, prasugrel, or ticagrelor. It is usually taken for months or years, concurrently with aspirin therapy.⁸³

There are five bioresorbable stents that have received CE Mark approval in Europe. Among them are Absorb (Abbott Vascular), DESolve (Elixir Medical), ART Pure (ART) and Magmaris (Biotronik).^{84,85} Only Absorb has been approved in the U.S. and Canada.^{84,86} An Absorb bioresorbable stent in its deployed and non-deployed state is shown in figure 10 on next page.

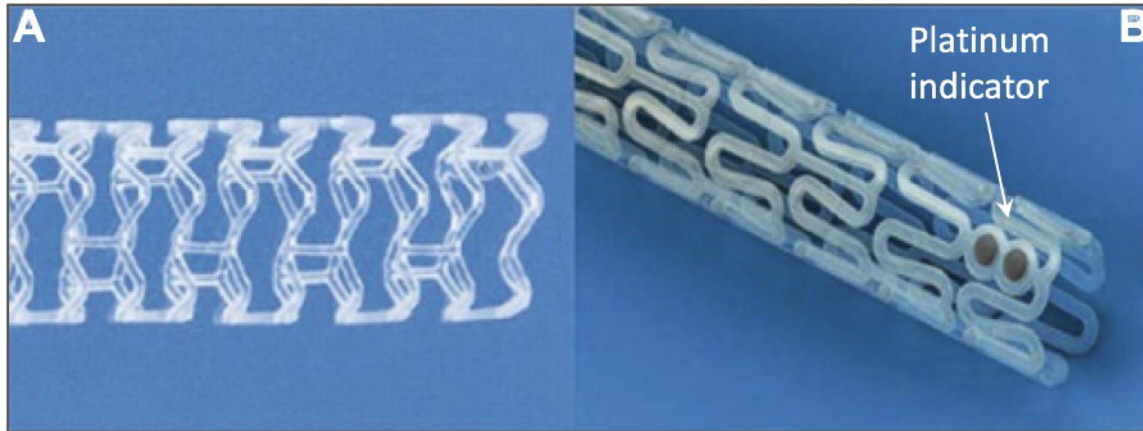


Figure 10. Absorb bioresorbable stent. A) Deployed B) Not deployed, with platinum indicator visible. (Image modified) Reprinted from “Biodegradable vascular scaffold Absorb BVS™ - scientific evidence and methods of implantation”; Rzeszutko L, Depukat R, Dudek D, *Postepy Kardiol Interwencyjnej* 2013; 9(1): 22–30; Copyright (2018) with permission from Open Access article from Creative Common Public Domain.⁸⁷

2.5. A primer on bioresorbable stents

2.5.1. Bioresorbable stent composition

The Absorb and DESolve BRS, the bioresorbable stents used most frequently, are composed of a poly-L-lactic acid (PLLA) scaffold with a poly-D,L-lactic acid (PDLLA) coating⁸⁸ (fig.11, below).

These are each associated with an antiproliferative agent – everolimus in the Absorb model and novolimus in the DESolve model,^{76,80} which reduces proliferation of smooth muscle cells in the stented segment. Even though the struts in the Absorb BRS are thicker (157 μm) than in the Xience DES (89 μm), the dose densities of everolimus that the Absorb releases are similar to the Xience model (fig. 11, below).⁸⁹

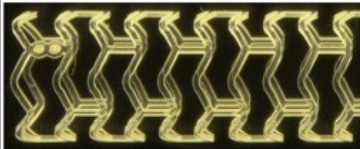
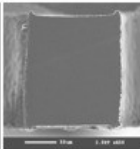
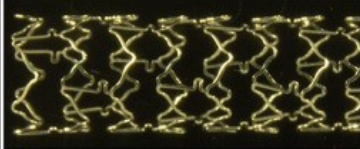
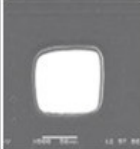
	Macroscopic appearance	Material	Cross-section	Strut thickness
Absorb BVS		PLLA + PDLLA		157 μm
Xience V		Co-Cr + durable fluoropolymer		89 μm

Figure 11. Composition and structure of the Absorb BRS and Xience V. Co-Cr = cobalt–chromium; PLLA = poly-L-lactide; PDLA = poly-D,L-lactide; BVS= bioresorbable vascular scaffold (synonym of BRS). Reprinted from “Clinical Outcomes of Small Side Branch Occlusion After Implantation of Bioresorbable Vascular Scaffold”; T. Muramatsu et al., *JACC Cardiovasc Int*, 2013 Mar;6(3):247-57, Copyright (2018) with permission from Elsevier.⁸⁸

2.5.2. Bioresorbable stent lifespan and other related timelines

A BRS resorbs into the bloodstream after 2 to 3 years on average, in contrast to bare-metal or drug-eluting stents which will remain in the body throughout the patient's life (fig. 12, below).^{81,90,91} Optical coherence tomography (OCT) (see section 2.6) and histologic evaluation have been performed on porcine coronary artery models. At 6, 12 and 24 months post-implantation of BRS, struts appeared as acellular regions with well-circumscribed borders (fig. 12, first three columns). At 30 and 36 months, there were minimal to no residual polymer struts remaining.^{80,81} Histology shows that the original struts were replaced by an acellular provisional matrix and stained both Movat's pentachrome and hematoxylin-eosin. At 48 months, struts were barely visible and had become part of the surrounding tissue.

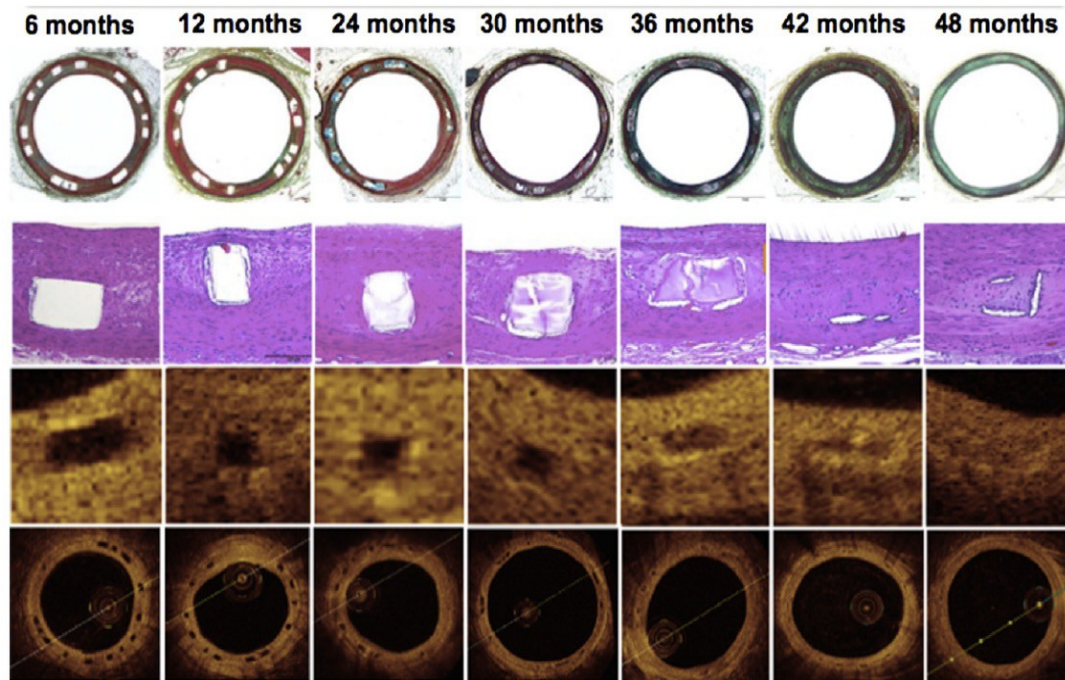


Figure 12. Histological and optical coherence tomography (OCT) evolution in resorption of ABSORB BRS in a porcine coronary arteries model. Movat's pentachrome (MP), 2X objective (top row) and hematoxylin and eosin (HE), 20X objective, top row center. Histological images show imperceptible to mild inflammation, no calcification of struts and no fibrin deposition. OCT images show struts as a preserved box at 6, 12, 24 and 30 months, then an open box at 36 months, a dissolved box at 42 months and an almost imperceptible box at 48 months. Reprinted from "Bioresorbable scaffold — A magic bullet for the treatment of coronary artery disease?" D. Brie et al. *Int J. Cardiol* 2016; 215: 47–59. Copyright (2018), with permission from Elsevier.⁸⁰

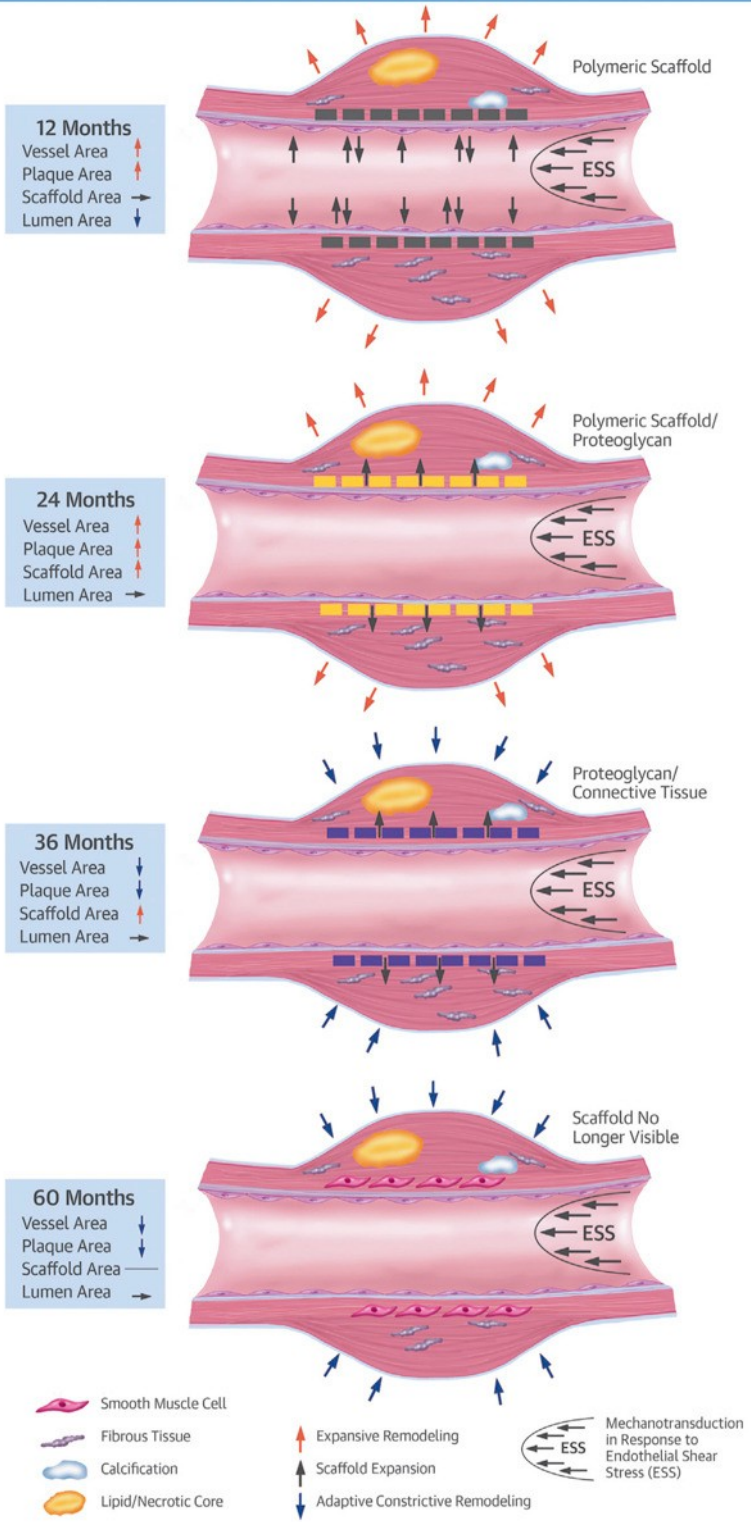
The ABSORB Cohort B trial enrolled a total of 101 patients. Of this group, 45 patients were assigned to the Cohort B1 study and given 6-month and 2-year angiographic follow-ups, while 56 patients were assigned to Cohort B2 and given a 1-year angiographic follow-up. The ABSORB Cohort B1 and B2 studies have both provided up to 5-year follow-up intravascular imaging post BRS implantation, which gives objective data on scaffold resorption and coronary healing in patients. This data showed that coronary vasomotion was observed within 6-12 months post-

deployment, and an increase in lumen area with adaptive vascular remodeling (see box # 3, p.45) was observed close to 1 year post-deployment.⁷⁵

It was also observed that after quantitative coronary angiography was performed at different points of time post-deployment of metallic stent, the coronary intra-stent minimal lumen diameter (MLD) progressively decreased.⁷⁵

However, QCA post-deployment of the Absorb BRS showed lumen preservation, and even expansion, over time. Likewise, serial intravascular ultrasounds (IVUS, section 2.6.2) performed over time, post-implantation of the Absorb BRS, revealed an increase in stent and vessel area from 6-24 months. Such adaptive remodeling accommodates the observed increase in plaque area that subsequently decreases from 2-5 years (see fig. 13, next page).^{75,92}

Restored Vasomotion ↑ / ↓ Cyclin Strain



Serruys, P.W. et al. J Am Coll Cardiol. 2016; 67(7):766-76.

Figure 13. Longitudinal coronary healing process beneath bioresorbable scaffold captured in 5-year-long imaging of stented stenotic area.

Scaffold polymer resorption takes nearly 36 months. Mechanical support provided by the scaffold remains unchanged for up to 6 months. A 3-month elution of everolimus (a cytostatic agent) from the struts prevents excessive neointimal hyperplasia.

At close to 12 months, the scaffold's mechanical support disappears and vasomotor tone begins to return. Such changes allow cyclical strain and physiological endothelial shear stress to again be transferred to the stented coronary wall (mechano-transduction), which becomes a possible mechanism for vessel remodeling.

At close to 24 months, scaffold expansion maintains lumen patency by compensating for neointimal growth. During this period, the vessel and plaque areas increase.

At close to 36 months, the lumen area remains unchanged, while the vessel and plaque area begin to decrease.

At close to 60 months, scaffold struts resorption and dissolution are complete and the void is filled with connective tissue. There is now a new layer of tissue between the lumen and the plaque, which is called the endoluminal tissue layer or neomedia.

Reprinted from "A Polylactide Bioresorbable Scaffold Eluting Everolimus for Treatment of Coronary Stenosis: 5-Year Follow-Up"; Serruys P.W. et al., J. Am Coll Cardiol., 2016 Feb 23;67(7):766-76. Copyright (2018), with permission from Elsevier.⁹²

Thus, it has been observed that changes in vessel and plaque area with BRS accompany a preservation of, or even an increase in, mean lumen area (late lumen gain). OCT performed post-implantation over several time points demonstrates an early increase in stent area (from 6-12 months), in parallel to an early growth in the neointimal area, which helps to preserve the mean lumen area. Such late luminal preservation or even luminal gain post BRS deployment has been related to the gradual dissolution of scaffold struts and their replacement with a fibroelastic matrix (neomedia), which retracts over time and gives space for lumen normalization. This neomedia tends to seal plaques with a necrotic core, which could impede future plaque rupture. The aforementioned concepts are presented in artistic rendering (see fig. 14.a, p.64) and with serial OCT at different time points (fig. 14.b, p.64).^{93,94}

Furthermore, the return of vessel vasomotor sensitivity to vasoactive stimuli (acetylcholine or nitroglycerine) is documented at 6-12 months after Absorb BRS implantation.⁷⁵ After 5 years, coronary vasodilation in response to administered nitroglycerine was observed by QCA in more than 80% of Absorb BRS-containing vessels.^{75,93} However, coronary vasomotor sensitivity does not return post-deployment of a metal stent.⁷⁵ The return to natural vasomotion of the vessels in the stented segment after implantation of bioresorbable stents allows for normalized arterial flow and shear stress.^{80,81}

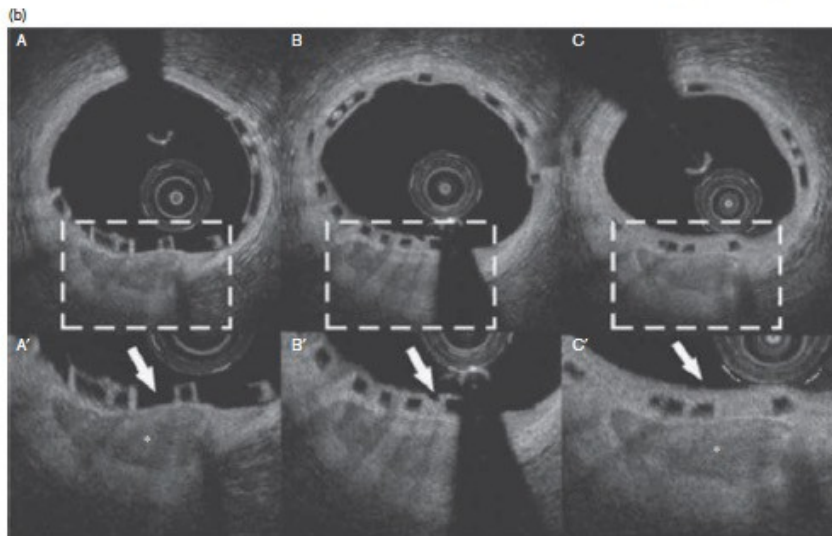
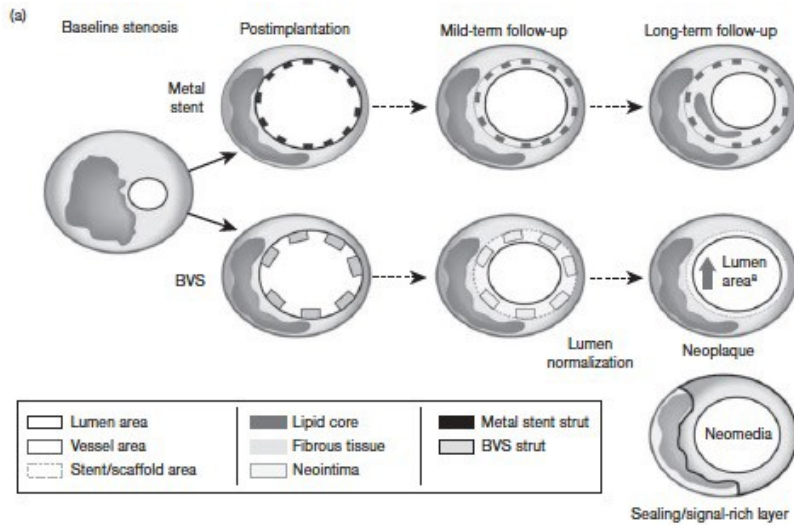


Figure 14. Plaque and vessel progression over time after implantation of metallic or bioresorbable stents.

(a) Longitudinal coronary healing response in metal versus bioresorbable stents.

(b) Neointimal appearance observation with optical coherence tomography following ABSORB BRS implantation.

A, B, C = healing process within 12 months following ABSORB BRS deployment.

A', B', C' = zoom view (arrows) of the re-epithelized healing regions.

* = Necrotic core plaque. BVS = bioresorbable vascular scaffold.

Reprinted from "Bioresorbable vascular scaffolds for the treatment of coronary artery disease: What have we learned from randomized-controlled clinical trials?", Rizik D. G. et al., *Coron Artery Dis.*, 2017 Jan;28(1):77-89. Copyright (2018), with permission from Wolters Kluwer Health, Inc.⁷⁵

2.5.3. Clinical outcomes of bioresorbable stents

In earlier studies of BRS, reported clinical outcomes of BRS were similar to those of DES, with similar composite outcomes of target lesion revascularization, target vessel myocardial infarction and cardiac death events (table 1, p.67). For example, the ABSORB II trial – a single-blind, multicenter, randomized control trial performed by Serruys P.W. et al., compared clinical events with the everolimus-eluting BRS versus the everolimus drug-eluting stent (DES) in 501 patients, guided by intravascular ultrasound (IVUS).⁹⁵ Between 2011 and 2013, the trial enrolled 335 patients with BRS (364 lesions) and 166 patients with metallic stents (182 lesions). Clinical outcomes with the BRS and DES were similar at the 1-year follow-up (respectively 5% vs. 3%, $p=0.35$). The thrombosis rate was also similar at 0.9% in the BRS and 0% in the DES ($p=0.55$) (see table 1, p.67). However, the authors of the ABSORB II study reported that generalizability of the study may be limited, since the lesions analyzed were simpler than in daily practice of cardiologists.

In the ABSORB II 3-year follow-up trial published by Serruys et al. in Lancet in 2016,⁹⁶ there were 23 (7% of 325 study patients – 6% with the BRS Absorb vs. 1% with the DES Xience, $p=0.0108$) documented target vessel myocardial infarctions, of which 13 (5% – 4% with Absorb vs. 1% with Xience, $p=0.16$) were peri-procedural. Within 1 to 3 years of follow-up in the population of 329 study patients, there were a total of 6 (2%) definite very late scaffold thromboses documented in the Absorb group and none in the Xience group. The percentage of thrombosis out of the total number of stents was not indicated.⁹⁶

In the ABSORB II 4-year follow-up study published by Chevalier et al. in EuroIntervention in 2018,⁹⁷ follow-up at 4 years was conducted with 86% (288/335) of the initial cohort patients in the Absorb group and with 84% (139/166) of the Xience group. The target vessel myocardial infarction rate was not documented in this study, as it was in the 3-year follow-up. However, target lesion failure rate was reported to have increased from 10.5% to 11.5% in the Absorb group and from 5.0% to 6.0% in the Xience group between the 3- and 4-year follow-up with no statistical significance at 4-year rates ($p=0.063$). Between the 3- and 4-year follow-up, no additional very late scaffold or stent thrombosis was documented in either group. Overall, the 4-year rate of very late scaffold or stent thrombosis was 3.0% in the Absorb group and 0.0% in the Xience group ($p=0.035$) (visit table 1, p.67).

There are some limitations to the two aforementioned studies. The PCI surgeons were not as experienced with the implantation of the BRS scaffold as with metallic stents, and the optimum implantation techniques that are currently recommended were not yet known,⁹⁸ which may have affected scaffold thrombosis rates. This study did not perform IVUS or OCT imaging analysis of very late scaffold thrombosis to understand its etiology. Further studies are needed to understand this mechanism.

Following the beginning of the ABSORB II trial, a large, multi-center, randomized control trial called ABSORB III enrolled 2008 patients with stable or unstable angina.⁹⁹ These patients were randomly assigned in a 2:1 ratio to receive either an Absorb BRS scaffold (1322 patients) or an everolimus-eluting cobalt-chromium (Xience) stent (686 patients). The trial's primary end point was target-lesion failure (a composite of cardiac death, ischemia-driven target-lesion

revascularization, or target-vessel myocardial infarction) at 1-year post stent implantation. Also, in-scaffold and in-segment measurements were performed by quantitative coronary angiography.

Study/ Author	Study start year	Stents implanted	No of patients	Follow-up	Clinical outcomes [†]		Stent/device thrombosis ^{‡§}
ABSORB cohort A	2006	Absorb BRS	30	5 years	ischemia-driven major adverse cardiac events	3.4% at 4 years	0%
ABSORB cohort B	2009	Absorb BRS	101	2 years		10.2%	0%
ABSORB EXTEND	2010	Absorb BRS	512	1 year	ischemia-driven target-lesion revascularization	4.3%	0.8%
ABSORB II	2011	Absorb BRS/ Xience EES	335 / 166	1 year	DOCE and MACE rates [†]	5% / 3% (p=0.35)	0.9% / 0% (p=0.55)
			288 / 139 remaining	4 year	Target lesion failure [‡]	11.5% / 6.0% (p=0.063)	3% / 0% (p=0.035)
ABSORB III	2012	Absorb BRS/ Xience EES	1322 / 686	1 year	ischemia-driven target-lesion revascularization	3% / 2.5% (p=0.5)	1.5% / 0.7% (p=0.13)
				3 years	Target lesion failure [‡]	13.4% / 10.4% (p=0.06)	2.3% / 0.7% (p=0.01)
Ali et al.	Meta-analysis	Absorb BRS/ EES	3261 / 2322	2 years	Target vessel-related myocardial infarction	5.8 % / 3.2 % (p=0.0003)	2.3 % / 0.7 % (p<0.0001)
		Absorb BRS/ CCEE	2164 / 1225	3 years	Target lesion failure [‡]	11.7% / 8.1% (p=0.006)	2.4% / 0.6% (p=0.001)
ABSORB IV	2014	Absorb BRS/ Xience EES	1296 / 1308	1 year	Target lesion failure [‡]	7.8% / 6.4% (p _{non-inferiority} = 0.0006)	0.7% / 0.3% (p=0.1586)

To be continued on the next page

Real-world BRS trial	Population	N	Intervention	Duration	MACE event-free survival rate with and without PSP	Stent thrombosis-free survival rate with and without PSP
ReABSORB registry published by Haddad et al.	Canadian consecutive dual-center all-comers with high prevalence ACS enrolled between 2012 and 2016	125 (97 PSP/ 28 non-PSP)	Predilation-sizing-postdilation BRS implantation technique	Clinical and angiographic follow-up of up to 4 years	95.8%/ 74.0% (p=0.001)	2.1%/ 7.1% (p=0.175)

Table 1. Bioresorbable stent clinical outcomes: comparison with drug-eluting metallic stents^{95-97,99-108}

EES = everolimus eluting-stents (e.g., Xience); [†]Clinical outcomes (or major adverse cardiovascular events also known as MACE) are reported as published, such as a composite of target lesion revascularization, target vessel myocardial infarction and cardiac death; DOCE = device-oriented composite endpoint [‡]Definite or probable thrombosis; mo = months; [∇] Target lesion failure (TLF) is measured and defined as a composite of cardiac death, myocardial infarction resulting from target vessel thrombosis, or ischemia-driven target lesion revascularization; CCEE- cobalt-chromium everolimus-eluting stent.

ACS = acute coronary syndrome. PSP = predilation-sizing-postdilation, a BRS implantation technique. Copyright © (2019) Evguenia Zdanovich.

The study showed non-inferiority of BRS for target lesion failure at 1-year follow-up (p = 0.007) with data collection still ongoing.⁹⁹ At 1-year post implantation of stents, the percent thrombosis of stented segments was slightly higher with BRS than with DES, although it did not reach statistical significance (i.e., 1.5% vs. 0.7%, p=0.13)⁹⁹ (see table 1, p.67).

Some limitations of the ABSORB III study were noted by the authors. For instance, the trial enrolled patients with relatively stable angina symptoms and simple coronary lesions. Thus, study findings may not be generalizable to patients with more complex coronary lesions. Finally, low-frequency events such as cardiac death or scaffold thrombosis were underpowered in this study. Therefore, interpretations of rates of such events should be carried out with caution, especially as pertaining to the non-significant difference between stents.⁹⁹

In 2017, Kereiakes et al.¹⁰² published ABSORB III study results from a 3-year follow-up post stent implantation. The number of patients in each group (Absorb vs. Xience) and the endpoints in the ABSORB III study at 3-year follow-up are specified in the text above. The main results showed that target lesion failure (TLF) at 3-year follow-up occurred more frequently with BRS than DES, although this did not reach statistical significance (13.4% vs. 10.4% of patients, $p=0.06$) (see table 1, p.67). In addition, target vessel myocardial infarction (TVMI) was more prevalent with BRS (8.6% vs. 5.9%, $p=0.03$). Likewise, there were more thrombotic events with BRS (2.3% vs. 0.7%, $p=0.01$). Thus, even though 1-year follow-up data showed non-inferiority of BRS in TLF, the results of a 3-year follow-up show higher adverse event rates in BRS, especially for TVMI and thrombosis.

A recent clinical meta-analysis of randomized trials on Absorb stents was performed by Ali et al.¹⁰¹ and published in Lancet in 2017. The authors analyzed seven randomized trials that randomly assigned patients (5583 in total) to either everolimus-eluting Absorb BRS or metallic everolimus-eluting stent DES (also called EES), which were subsequently clinically followed for at least 2 years. Device-oriented composite endpoint was the primary outcome measure. This composite endpoint included cardiac mortality, ischemia-driven target lesion revascularization, or target vessel myocardial infarction. Definite or probable device thrombosis was the primary safety outcome. The meta-analysis showed that as compared to EES, BRS had increased rates of composite device-oriented adverse events and in-stent thrombosis at 2 years and between 1 and 2 years post implantation. For instance, BRS had higher rates than EES of target vessel myocardial infarction (respectively 5.8% vs. 3.2%, $p=0.0003$). During the first two years post implantation, in-stent thrombosis was also higher with BRS than with EES (2.3% vs 0.7%, $p<0.0001$) (see table 1, p.67).¹⁰¹

There are several limitations to this meta-analysis. First, Ali et al. identified some subgroups that systematically had better or worse outcomes with BRS than with EES. For instance, patients with diabetes had better 2-year patient-oriented composite endpoint results when implanted with BRS than with EES. In contrast, patients with non-complex lesions were identified to have better 2-year stent-oriented composite endpoint outcomes when implanted with EES than with BRS. Therefore, as the authors mention, since statistical multiplicity, or multiple comparisons¹⁰⁹, was not accounted for in these additional analyses, these analyses should be considered hypothesis-generating.¹⁰¹

A second limitation of the Ali et al. meta-analysis was that a large number of high-risk patients and complex lesions were excluded from the analyzed ABSORB randomized control trials. Thus, it is necessary to design supplemental studies to observe BRS performance under the aforementioned conditions.

A third limitation mentioned by Ali et al. is that only a few patients in the early ABSORB studies were implanted using optimal BRS implantation technique. Further trials are necessary to determine whether this technique improves patient outcomes.

In his 2018 study, Ali et al.¹⁰⁸, safety and efficacy of BRS were also investigated but at 3-year outcome. Meta-analysis was comprised of 4 randomized ABSORB trials (total 3389 patients) with 2164 everolimus-eluting Absorb BRS and 1225 everolimus-eluting stents. Target lesion failure that consisted of cardiac mortality, target vessel myocardial infarction, or ischemia-driven target lesion revascularization was the primary efficacy outcome. Device thrombosis was the primary safety outcome. The results are shown in table 1 (p. 67) and parallel the 2-year follow-up with even higher MACE and similar thrombosis rates were observed in BRS stents.

The second Ali et al. study has some limitations. No high-risk patients and complex lesions were included in the 4 ABSORB trials. These aspects will be considered in the ongoing dedicated studies¹⁰⁸. Finally, conclusions from the results can only be analyzed with regards to the 1st generation of Absorb BRS, which is no longer manufactured.

Another recent meta-analysis performed by Kang et al.¹¹⁰ also analyzed the long-term efficacy and safety of BRS. The analysis was conducted in a total of 91 randomized controlled trials or 105842 patients with either BRS or one of the metallic stents with the mean follow-up time of 3.7 years. It has been demonstrated that target lesion failure and definite or probable stent thrombosis were higher in the BRS group than in any other DES groups.

A limitation of this study was in BRS sample size that was small in comparison to other device groups. Longer follow-up times and larger BRS sample sizes are currently being investigated in the ongoing studies that analyze the efficacy, safety and overall BRS performance.¹¹⁰

To address the adverse results in the latest BRS studies, a collaborative large-scale study was conducted by Stone et al.¹¹¹ with principal investigators of the 5 prospective studies including ABSORB II, ABSORB China, ABSORB Japan, the ABSORB III randomized trials, and the ABSORB EXTEND nonrandomized registry (see table 1, p.67). The objective of this study was to determine whether TLF and stent thrombosis at 3-year follow-up post BRS implantation was dependent on surgical techniques such as selection of vessel size and pre- and post-dilation variables. Thus, TLF and stent thrombosis were assessed in 2973 patients (with 3149 BRS-treated coronary lesions) and outcomes of 3-year follow-up were determined according to the investigators' pre-specified parameters of optimal technique (pre- and post-dilation and vessel sizing). Adjustment of differences in up to 18 patients and lesion parameters was performed by multivariable analysis.¹¹¹

Their results showed that in BRS-treated lesions, selection of vessel size based on reference diameters of between ≥ 2.25 mm and ≤ 3.75 mm was performed in 81.6% of patients. Also, optimal pre-dilation, defined as the reference vessel diameter ratio of ≥ 1.1 derived from balloon to core laboratory, was performed with 59.2% of patients. Lastly, optimal post-dilation, defined as a noncompliant balloon at ≥ 18 atm and larger than the nominal stent diameter, but not exceeding it by more than 0.5 mm, was observed in 12.4% of patients.¹¹¹

In addition, it was found that when the vessels were properly sized, BRS implantation was an independent predictor of freedom from TLF at 1-year follow-up (hazard ratio [HR]: 0.67; $p = 0.01$) and at 3-year follow-up (HR: 0.72; $p = 0.01$), and from stent thrombosis at 1-year follow-up (HR:

0.36; $p = 0.004$). Moreover, when the pre-dilation was performed aggressively (i.e. discordantly to the vessel size), it became an independent predictor of freedom from stent thrombosis between 1 and 3 years of follow-up (HR: 0.44; $p = 0.03$). Finally, when post-dilation was optimally performed, it became an independent predictor of freedom from TLF (HR: 0.55; $p = 0.05$) between 1 and 3 years of follow-up. Thus, after multivariable adjustments of lesion and baseline patient parameters, this large-scale analysis of the main ABSORB studies showed that surgical technique and vessel sizing had strong association with BRS-related outcomes through to 3-year follow-up.¹¹¹

Stone et al. mention a number of limitations of this large-scale collaborative study. First, the definitions of the pre-specified optimal techniques are somewhat arbitrary and relied on smaller prior cases and reports. Second, even though all studies were prospective, the analysis was *post hoc* since a number of variables were not collected for multiple comparisons. Third, systematic sequential intravascular imaging, missing from the studies, would be necessary to confirm and understand the beneficial effect that aggressive pre-dilation has on very late stent thrombosis. Fourth, the authors' analysis did not adjust for the effects of compliance with long-term dual antiplatelet therapy, a complicating factor that should be accounted for in analysis with varied durations of therapy.¹¹¹

Fifth, the above study determined the effects of pre- and post-dilation techniques at 3-year follow-up, when struts are usually completely resorbed.⁹¹ However, it is not yet known whether there is an association between an implantation technique and the outcome at 3-year follow-up. Lastly, only first-generation Absorb BRS were included in this study. It is likely that the discovered concepts overall are generalizable among scaffolds, but further studies are required to address the effects of vessel sizing and implantation techniques on the outcomes of next-generation BRS and other scaffolds.¹¹¹

In 2018 in the Lancet, Stone et al.¹⁰⁴ published the results of the largest trial to date, titled ABSORB IV (Trial identifier: NCT02173379)¹⁰¹, in which the Absorb BRS and Xience DES were compared. In this trial, 2604 patients with acute coronary syndromes or stable coronary artery disease were randomly assigned in a one-to-one ratio to the Absorb BRS or Xience DES group (1296 to 1308,

respectively) in five countries (147 sites). Optimized techniques were used for BRS implantation, such as predilation of the target lesion and dilation of the BRS post-implantation, the latter strongly recommended.^{104,112}

The results of the study showed that 30-day major adverse cardiovascular events (MACE) composed of cardiac death, target vessel myocardial infarction and target lesion failure were documented in 64 (5.0%) of the Absorb patients and 48 (3.7%) of the Xience patients (one-sided $p_{\text{non-inferiority}} = 0.0244$ (see box # 10, below)). The 1-year target lesion failure rate showed similar results with 98 (7.8%) of the Absorb patients and 84 (6.4%) of the Xience patients (one-sided $p_{\text{non-inferiority}} = 0.0006$.) As for scaffold/stent thrombosis at 1-year follow-up, there was no statistically significant difference between Absorb and Xience patients (0.7% vs. 0.3% respectively, $p = 0.1586$) (see table 1, p.67).^{104,112}

Box # 10

Non-inferiority trials

Non-inferiority trials (see fig. 15, below) are usually conducted to show that a new intervention or treatment is better than a placebo, and non-inferior to an existing intervention.¹¹³ A new intervention can be shown to offer more advantages than the established treatment in terms of cost, compliance, and safety, as is the case with the ABSORB IV trial.¹¹⁴ In ABSORB IV, the non-inferiority margin (or delta Δ) for 30-day risk difference between Absorb and Xience was 2.9%, and the 1-year non-inferiority margin for target lesion failure was 4.8%.¹⁰⁴

95% non-inferiority confidence intervals for three different intervention pairs represented by lines

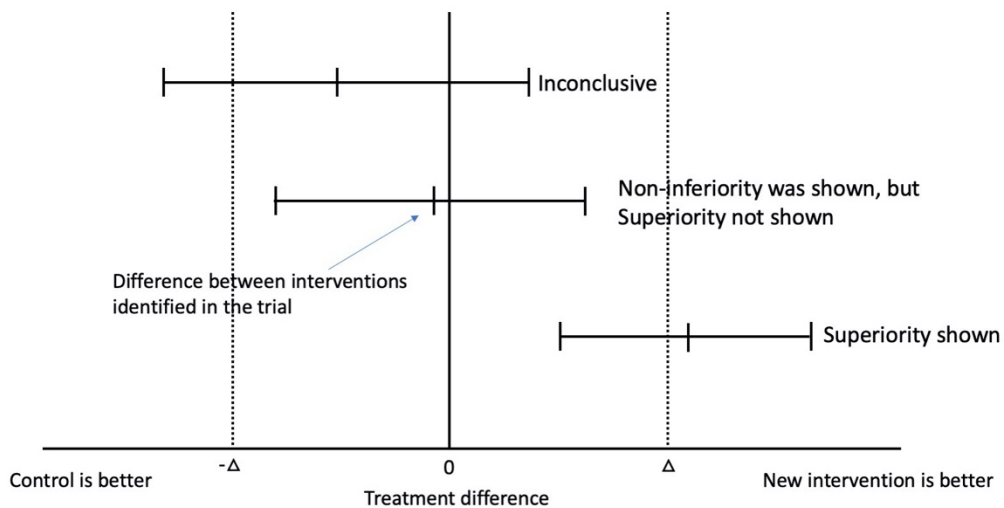


Figure 15. Outcomes from the three potential non-inferiority clinical trials.

D- non-inferiority margin.

Adapted from "Understanding the null hypothesis (H_0) in non-inferiority trials"; Jihad Mallat. *Crit Care*. 2017; 21: 101. Title was modified. Copyright © (2019) with permission from Open Access article from Creative Commons Public Domain 4.0¹¹³
<https://creativecommons.org/licenses/by/4.0/>

As compared to the previously-mentioned ABSORB II and III trials, more favorable outcomes were observed in the ABSORB IV trial. As reported by Stone et al.,¹⁰⁴ in a larger patient population with improved BRS implantation technique and enhanced lesion selection, the BRS performed at an improved non-inferiority level in 30-day and 1-year MACE rates as compared to the Xience stent. The MACE rates in the Absorb group are nevertheless higher than in the Xience group. The study did not reach statistical significance in differences of rates of thrombosis between the two groups, but there was a trend for a higher thrombosis rates in the Absorb group.¹⁰⁴

In 2018, a new Absorb study was published by Haddad et al.,¹⁰⁵ which examined real-world long-term (up to 4 years of follow-up) efficacy and safety of BRS in an all-comers cohort of 125 consecutively-enrolled patients diagnosed with high prevalence of acute coronary syndrome (ACS). The same BRS implantation guidelines were recommended to the cardiologists as had been advised in the ABSORB IV trial, including predilation-sizing-postdilation technique for appropriate vessel preparation through predilation, vessel and BRS sizing, and reducing BRS struts nonapposition through post-dilation.¹⁰⁵ Ninety-seven patients benefitted from the predilation-sizing-postdilation technique, while 28 patients had other implantation techniques than the aforementioned.¹⁰⁵

The Haddad et al. study encompassed a total of 163 treated lesions among which 23% were type A, 64% type B (1 or 2, visit table IX, p. 124, for explanation of subtypes) and 13% type C.¹⁰⁵ These lesion types were based on a system of classification of coronary lesions published by the ACC (American College of Cardiology) / AHA (American Heart Association).¹¹⁵ According to this classification, lesion type A is discrete, concentric with smooth contours and absence of thrombus. Lesion type B is tubular, eccentric with some thrombus potentially present. Lesion type C is diffuse and high risk, and is present in tortuous and extremely angulated coronary segments.¹¹⁵

The 4-year major cardiac event-free survival rate was 90.7% overall as demonstrated by Kaplan-Meier analysis.¹⁰⁵ Kaplan-Meier estimation is known as one of the best methods for projecting post-treatment survival of participants over a given amount of time.¹¹⁶ The predilation-sizing-postdilation technique resulted in a 95.8% rate of event-free survival compared to 74.0% without

this technique ($p=0.001$).¹⁰⁵ The 4-year thrombosis-free survival rate was 96.8% overall, as 4 stent thromboses were observed in 4 patients total: 2 (2.1%) patients with and 2 (7.1%) patients without the predilatation-sizing-postdilatation technique ($p=0.175$) (see table 1, p.67).¹⁰⁵

The Haddad et al. study is the first to have investigated the long-term (up to 4-years) efficacy and safety of BRS implantation in Canadian all-comers patients with a high prevalence of acute coronary syndrome (ACS). Furthermore, it is currently the best available study in the literature for comparison of the long-term results of implantation with predilatation-sizing-postdilatation technique versus implantation without this technique, making a potential follow-up randomized trial that includes the control technique unethical. However, there are some limitations to this study. The study is non-randomized and has no BRS comparator group, which limits generalizability of the results to a larger clinical cohort. In addition, at present, follow-up data for most patients in this study is not available beyond 3 years. Therefore, further studies are advised to monitor potential very late clinical events in a similar BRS cohort.¹⁰⁵

A recent study by Zhao et al.¹¹⁷ addressed high incidences of BRS in-stent thrombosis by performing *in vitro* cell proliferation assays on BRS coating seeded with nanoparticles, which are loaded with sirolimus (2000 cells per well, 96 wells). The authors hypothesized that a continuous sheath of the BRS non-proliferative drug coating could successfully prevent (undesirable) proliferation of coronary smooth muscle cells and endothelial cells. After stent implantation, the endothelium is fragile and needs to grow to protect the coronary media from exhibiting pro-thrombotic factors leading to thrombosis. Therefore, to address the issue with monolayered BRS coating, Zhao et al. developed a new coating made of biodegradable polymer poly-(DL)-lactide (PDLLA) nanoparticles with a mean size of 300 nm loaded with sirolimus. *In vitro* results demonstrated an adequate and continuous release of sirolimus from the BRS coating seeded with nanoparticles. Cell culture assays revealed that the sirolimus-loaded nanoparticles coating effectively inhibited smooth muscle cell proliferation while still allowing fast growth and multiplication of endothelial cells. Such a discovery could prevent in-stent restenosis and thrombotic events.¹¹⁷

To summarize, early BRS studies showed that BRS clinical outcomes and thrombotic events were similar or non-inferior to DES outcomes. At 3-year follow-up, the ABSORB III study determined that target vessel myocardial infarction and thrombotic events were significantly more prevalent in Absorb BRS than in Xience DES.¹⁰² Subsequently, a recent meta-analysis (5583 patients) by Ali et al.¹⁰¹ showed that, compared to DES, BRS had higher incidence of device-oriented adverse events and scaffold thrombosis at 2 years and between 1- and 2-year follow-ups. Another recent study by Stone et al.¹⁰⁴ (2973 patients) investigated whether target lesion failure and stent thrombosis at 3 years post BRS implantation was dependent on surgical technique. It was determined that with properly-sized vessels, BRS implantation becomes a significant independent predictor of freedom from TLF at 1- and 3-year post implantation follow-ups and also from scaffold thrombosis at 1-year follow-up. A real-world study published in 2018 by Haddad et al.¹⁰⁵ with a Canadian cohort of 125 patients with high prevalence of acute coronary syndrome (ACS), demonstrated that predilation-sizing-postdilation BRS implantation technique is significantly associated with higher MACE-event-free survival rate. In addition, the novel *in vitro* study by Zhao et al.¹¹⁷ demonstrated a potential solution to BRS in-stent thrombosis through BRS coating with nanoparticles loaded with a non-proliferative agent. As of September 14th, 2017, the Absorb-BRS-producing company Abbott Vascular reportedly stopped commercial sales of Absorb BRS in all countries because of low demand.¹¹⁸ Nevertheless, the company states that it will continue evaluation of long-term outcomes in ongoing clinical trials.¹¹⁸

Supplemental *in vivo* studies are crucial in order to address the adverse clinical events and relatively-high scaffold thrombosis rates that occur after bioresorbable stent implantation.

2.5.4. Bioresorbable stent complications

2.5.4.1. Side branch complications in bioresorbable stents

ABSORB BRS are proven to be effective in treating non-bifurcated coronary lesions.^{73,119,120} However, questions have been raised about the fate of side branch permeability when branches are covered by BRS. The current BRS strut thickness of 157 μm versus 89 μm in Xience DES (see section 2.5.1., fig. 11, p.59) may be associated with higher rates of side branch occlusions, which can lead to periprocedural myocardial infarction.¹²¹⁻¹²⁵ In a 2010 study, Okamura et al. proposed a mechanism of side branch occlusions. They coined the phrase “neointimal bridge” for a phenomenon where a neointimal layer starts to grow at the ostia covered by a BRS (see fig. 16 on the next page). The authors explained that the creation of such a bridge results from interaction of the bioresorbable struts, vessel wall and shear stress.¹²⁶

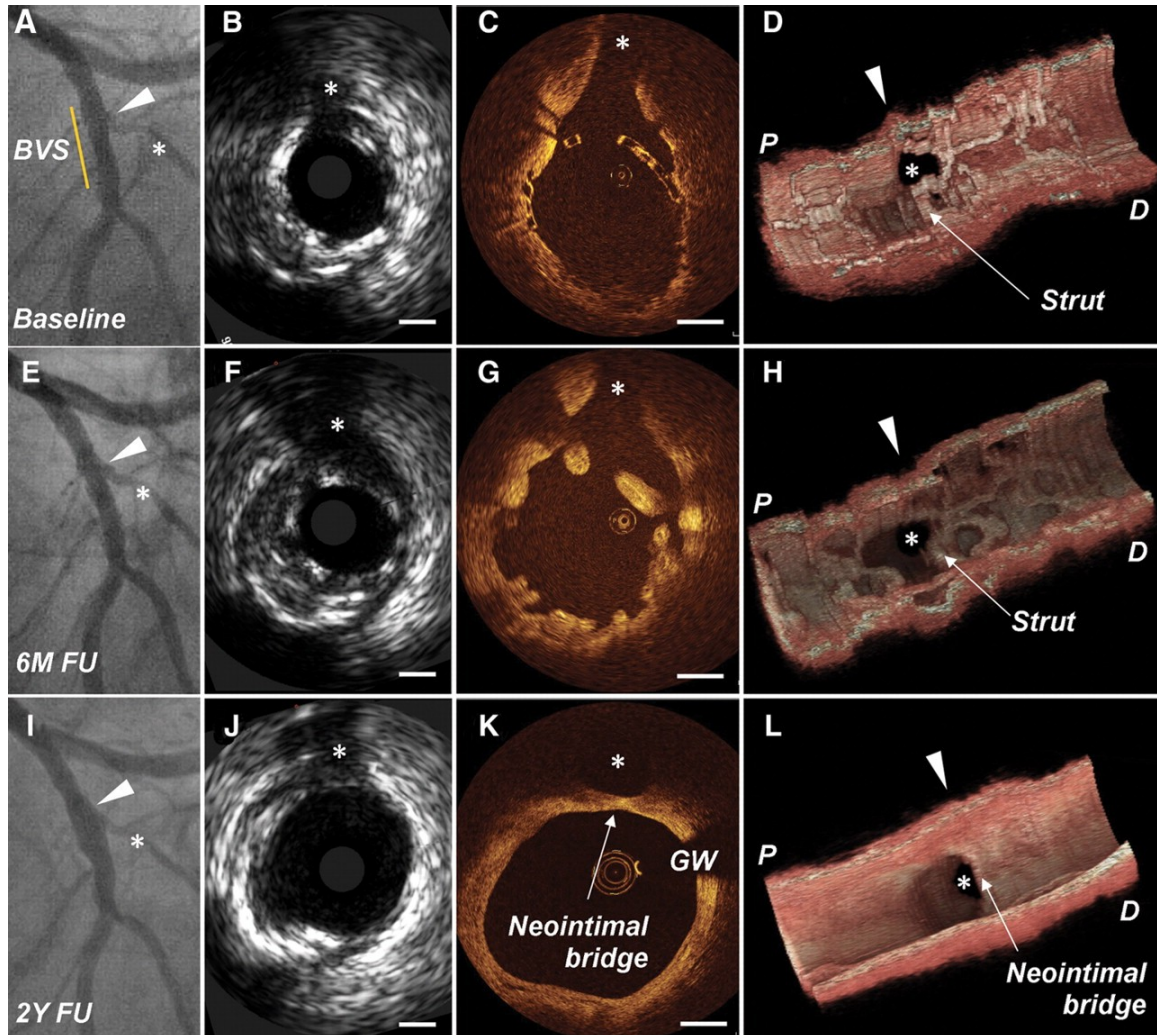


Figure 16. Neointimal bridge formation after bioresorbable stent implantation. Implantation of a 3.0/12 bioresorbable everolimus-eluting stent was performed in the left anterior descending coronary artery of a 64-year-old woman with stable anginal symptoms over the ostium of a diagonal branch. Conventional angiography demonstrated no residual stenosis post stent dilatation (panel A). The patient experienced no complications after intervention and was discharged with dual antiplatelet therapy within 24 h after procedure. Serial intravascular ultrasound and optical coherence tomography were performed at 6 months and 2 years after BRS implantation. At baseline, the BRS was well expanded with its struts jailing the diagonal branch (panels B and C). At 6 months, OCT showed a good lumen with creased appearance and stent struts with visible changes (panels E-G). At 2 years, the scaffold struts were no longer identifiable, and the lumen was extensively patent with smooth borders (panels I-K).

When BRS struts resorb, they are replaced by a neointimal neocarina, a proteoglycan bridge. Three-dimensional reconstructions of OCT can be visualized in panels D, H and L which demonstrate the intricate spatial relationship between the BRS and the side branch ostium in an easily comprehensible way.

Panels A–L. Asterisk identifies a BRS-jailed side branch. P = proximal; D = distal; GW = guide wire artefact; bar = 1 mm.

Reprinted from the European Heart Journal; Okamura T., Serruys P.W. and Regar E. “The fate of bioresorbable struts located at a side branch ostium: serial three-dimensional optical coherence tomography assessment”; 2010 Sep; 31(17):2179. Copyright (2018), with permission from Oxford Academic.¹²⁷

In a recent prospective study by Ojeda et al.¹²⁸, 140 patients were studied with a total of 346 side branches at risk of occlusion post BRS implantation: 181 small (<1 mm in diameter), 102 intermediate (1-2 mm in diameter) and 63 large (>2 mm in diameter). Quantitative coronary angiography was performed pre and post percutaneous intervention to collect the following data at the stented vessels: luminal diameters, lesion lengths and stenosis percentage. Angiographic analysis included all visible bifurcating branches from the scaffolded segments or their nearby five proximal or distal margins. Starting from six months post implantation of BRS, patency of covered intermediate or large branches was studied by coronary computed tomography (CT).

Rapid occlusions immediately post BRS implantation occurred in 31 (9%) branches: 22 (12%) small, 8 (8%) intermediate and 1 (1.6%) large side branches. There were no late side branch occlusions detected at 7 ± 3 months.¹²⁸

This study showed that two main predictors of side branch occlusions are small side branches ($p < 0.05$) and post-implantation stenosis of > 50% at side branch origin ($p < 0.01$). Occurrences and adverse clinical outcomes of side branch occlusions were rare when side branches of >1 mm in diameter were covered.¹²⁸

The authors mention a limitation to this study, which is that in order to prevent interpretation mistakes of the sizes and events of ostia stenosis, two expert cardiologists agreed on the classification criteria. To prevent such limitation, authors suggest that the services of an independent core laboratory could have been used.¹²⁸

In the most recent study published by Onuma et al in 2017,¹²⁹ a retrospective 5-year 3-dimensional OCT analysis of the ABSORB Cohort B trial was performed with data collected from 29 patients (with a total of 85 side branch ostia). In a repeated-measures mixed model analysis with time as a fixed variable and a dependent variable of an ostial area free from stent struts, a decrease in estimated ostial area free from struts was shown (0.75 mm² to 0.68 mm² to 0.63 mm², baseline versus first follow-up visit at 6 or 12 months versus second visit at 2 or 3 years). In the pairwise comparison, the ostial area was not statistically different between the baseline and the first visit ($p = 0.621$) or between the first and second follow-up visit ($p = 0.999$). However, there was a statistically significant increase in ostial area from the second visit to the 5-year follow-up, from 0.63 to 0.89 mm² ($p < 0.001$; p values adjusted with Bonferroni).

It was also shown that struts that covered side branches divided their ostium into compartments and that the number of these compartments decreased with time. Onuma et al. observed that large compartments potentially become larger over time after struts resorption and integration of neighbouring smaller compartments. Moreover, it was determined that there was a higher flow through large compartments giving higher shear stresses, which impedes neointimal formation in such ostial compartments and thus, its occlusion.¹²⁹

To prevent side branch occlusion, performance of side branch balloon dilatation post implantation at safe pressures has been suggested. Different safe dilatation pressure thresholds exist for each type of stent to prevent strut fractures. For instance, metallic stents have thinner struts and greater radial strength than bioresorbable scaffolds.¹³⁰ Thus, safely dilating side branches post implantation creates one large compartment, which may be more likely to remain patent with time.

There were some limitations to the study by Onuma et al. First, most of the side branches were <2.0 mm, thus study results could not be generalized for side branches >2.0 mm. Second, it was a single-arm study with no comparison to metallic drug-eluting stents. Third, only 29 patients were enrolled in the study, generating a small number of side branch ostia. Fourth, some patients did not undergo a 5-year follow-up invasive angiography. Thus, some data was missing in the longitudinal assessment of ostia. A simple comparative analysis between 2 longitudinal follow-up points would therefore have led to bias. Consequently, a repeated-measures mixed model analysis was performed in order to include all the collected data points and to account for the interdependent data, such as multiple measurements done at a specific time point at the same ostium. Finally, guidewire shadows at times partly or completely masked side branches and thereby impeded ostial side branch analysis. Such a problem is, however, a common limitation of any OCT study.¹²⁹

2.6. Imaging bioresorbable stents

Most clinical trials with BRS were performed using invasive techniques such as quantitative or conventional coronary angiography (CCA) (figs. 17-18, pp 83-84), intravascular ultrasound (IVUS) (fig. 19, p.86) or optical coherence tomography (OCT) (fig. 20, p.87). These invasive imaging techniques and their measurement modalities will be addressed in the following subsections. Imaging of BRS with computed tomography will be briefly discussed. However, most information on computed tomography imaging of BRS will be presented in chapter 3.

2.6.1. Bioresorbable stent imaging with conventional coronary angiography



Figure 17. Coronary catheterization room in Hôtel-Dieu Hospital in 2016 (Centre Hospitalier de l'Université de Montréal).

CCA or QCA is the standard reference test for radiological imaging of lumen of the coronary arteries, hence for diagnosis of coronary stenosis. During CCA and prior to PCI, parameters such as coronary luminal diameter and degree of stenosis are measured.⁵⁵

First, as previously described, a balloon angioplasty is performed in which the artery is cannulated with a catheter that effectively treats coronary stenosis by crushing atheromatous plaque in the unhealthy coronary wall.^{84,131} After the plaque is displaced, a stent is deployed at the affected site to prevent restenosis.¹³¹ CCA is not only performed prior to PCI but is also useful per-PCI since it can guide the cardiologists to perform efficient coronary intervention.

During CCA stent implantation, it is important to adjust final stent dimensions to the lumen diameter, as stent under-expansion was found to play a role in early stent thrombosis and in-stent restenosis in BMS, DES and BRS stents in the mid- and long-term.^{132,133} CCA allows measurement of estimated lumen diameter for stent implantation by interpolating proximal and distal reference segments to stenosis.¹³⁴

Figure 18 below shows CCA images from before and after BRS implantation. The platinum indicators at stent extremities, while not visible here, are sometimes faintly visible on CCA images. The rest of the BRS structure is not visible.

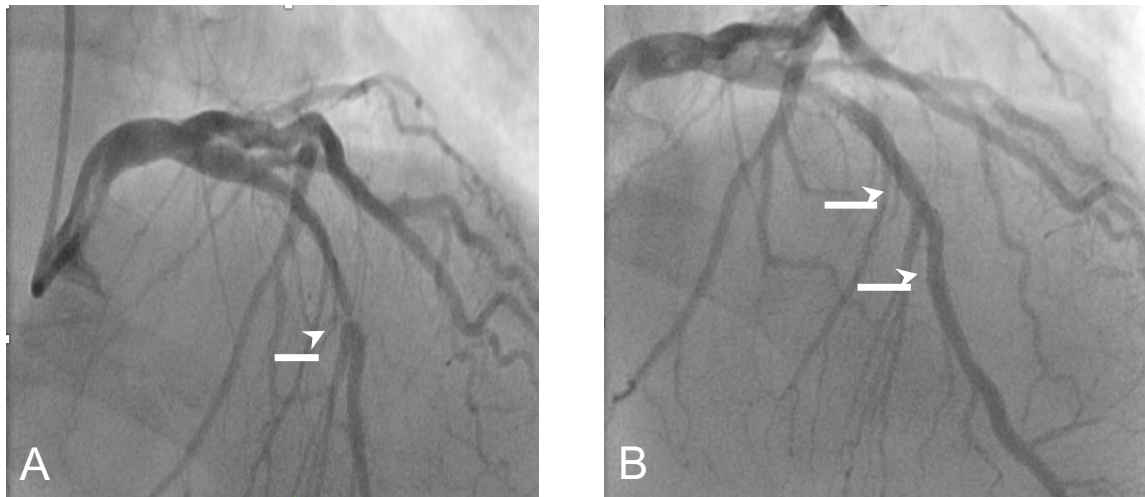


Figure 18. Conventional Coronary Angiography (CCA). A) Severe stenosis of mid left anterior descending artery (arrow), prior to stenting. B) Angiography after bioresorbable stent (3.0 mm x 18 mm) implantation, with an excellent angiographic result (arrows). The small platinum indicators at stent extremities are not visible, nor is the bioresorbable scaffold itself. Copyright © 2016 Samer Mansour.

2.6.2. Bioresorbable stent imaging with intravascular ultrasound

Another invasive coronary imaging technique, used in many stent studies, is intravascular ultrasound (IVUS). IVUS is the second-most-used intracoronary imaging technique after conventional coronary angiography. It can be performed prior, during and after PCI. At present, in the coronary catheterization room, IVUS plays a major role in diagnosis and follow-up of CAD.⁵⁵

IVUS technology is based on detection and conversion of sound waves into a medical image. The sound waves are emitted by piezoelectric crystals. When these crystals are stimulated electrically, they vibrate, becoming transducers of electric impulses that generate sound waves of the needed frequency, an ultrasound frequency. After being emitted by the crystals, if these ultrasound waves meet an obstacle such as an organ, they are reflected (echoed) back to the crystals and transformed again into electric impulses by the piezoelectric transducer. IVUS creates an image from the transformed echoed impulses.^{55,135}

The penetration of IVUS waves into tissue is > 5 mm,¹³⁵ and IVUS images can be collected through blood flow. Grey-scaled IVUS with its axial resolution of 100-200 μm allows slight differentiation of plaque components, while virtual histology (VH)-IVUS can detect necrotic core, fibrous or fibrofatty plaque and dense calcium, with the exception of the thin fibrous cap.¹³⁶

BRS struts are only moderately visible with IVUS (fig. 19, p.86). Post-implantation follow-up analysis with IVUS generally allows the measurement of vessel, scaffold and plaque areas, mean lumen, plaque and calcification volumes and remodeling index.^{137,138} One of the advantages of IVUS is that it allows measurement of the cross-sectional area, which is not possible with conventional angiography. For instance, the minimum lumen area (MLA), frequently measured by IVUS, has a strong correlation with the physiological repercussions of lumen stenosis. The reported MLA thresholds of stenoses in arteries other than the left main coronary artery are about 3.0 mm^2 or 4 mm^2 .^{139,135} A smaller minimum lumen area indicates significant stenosis.

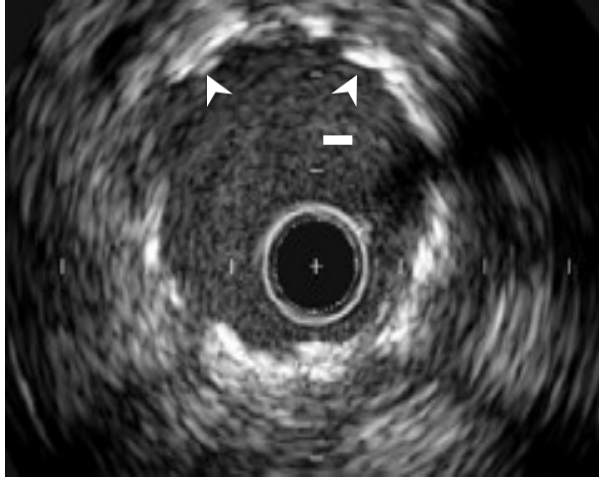


Figure 19. Intravascular ultrasound (IVUS) post-implantation of a BRS in a patient with severe stenosis of mid left anterior descending artery (same patient shown in Figure 18, p. 84) Adequate strut apposition is shown (arrows). Stent struts are usually moderately visible in IVUS, as seen here. Copyright © 2016 Samer Mansour.

2.6.3. Bioresorbable stent imaging with optical coherence tomography

Optical coherence tomography (OCT) is another invasive coronary imaging technique used in BRS stent studies. In contrast to IVUS, which builds images from sound waves, OCT images are obtained from light waves.¹³⁵ The emitted 1300 nm infrared light is reflected by the tissue and is then converted into an image.⁵⁵

OCT axial spatial resolution, which at 10-15 μm is superior to IVUS resolution of 100-200 μm ,³² provides good specificity and sensitivity in determination of plaque type and allows measurement of the thickness of a fibrous cap. For instance, it can detect thin-cap fibroatheroma (TCFA, chapter 1, box # 2, p.44), a predictor of plaque rupture.³³ However, OCT's higher resolution makes image acquisition in the artery segment filled with blood difficult since erythrocytes disperse infrared light and attenuate the image.³² Thus, to clear the artery of blood, OCT acquisitions require intracoronary rinse with either a saline or contrast agent.

The fibrous cap is well visualized by OCT, but differentiation of the lipid pool from calcium is limited. Moreover, OCT's shallow penetration of 1 to 3 mm makes assessment of the entire plaque volume challenging.¹³⁶ However, in comparison with IVUS, OCT's good spatial resolution

allows better characterization of the scaffold architecture of stents (see fig. 20 below). OCT allows visualization of stent edge dissections, incomplete stent appositions and tissue protrusions that cannot be seen by conventional angiography or IVUS.¹³⁵

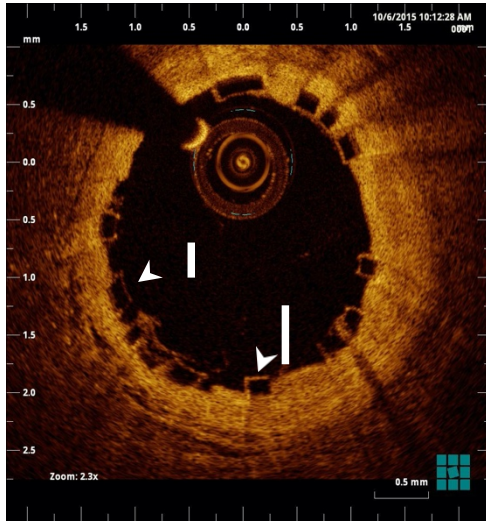


Figure 20. Bioresorbable scaffold struts visualization with OCT, after BRS implantation in a patient with severe stenosis of mid left anterior descending artery (same patient shown in Figures 18 and 19, pp. 84 and 86). Struts typically appear as black boxes with OCT (arrows). Copyright © 2016 Samer Mansour.

2.6.4. Bioresorbable stent imaging with CT scan versus metallic stents

This is an introductory section that discusses BRS imaging by CT scan. Further information about the cardiac CT scan and coronary lumen and plaque CT imaging under BRS will be described in chapters 3 and 4.

Most stents have a metallic scaffold which causes CT blooming artifacts (see fig. 21 on next page), potentially leading to severe impairment of diagnosis of intrastent restenosis, especially in stents measuring less than 3 mm in diameter.¹⁴⁰

There are many aspects of the imaging techniques and stent structure itself that can reduce blooming. For example, bare metallic stents' struts are now thinner than they used to be therefore allowing better visualisation of stented segments. Also, in the early 2000's, high definition CT (vs standard definition) was introduced with higher spatial resolution allowing also better evaluation of stented segments. Edge-enhancing kernels¹⁴¹ are another blooming

reduction strategy (see fig. 21, below); despite improved stent strut definition with these dedicated reconstruction algorithms, significant artificial thickening of the old metallic stents' walls persists.

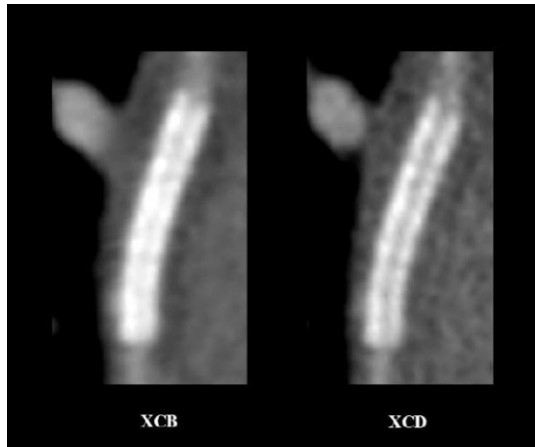


Figure 21. Reduced stent blooming artifacts and improved strut definition with sharp (XCD) versus smooth (XCB) kernel (filter), in first obtuse marginal artery stent implanted in

69-year-old woman, 256-slice CT acquisition with prospective ECG-gating, and image reconstruction with medium-soft (XCB, left) and edge-enhancing

(XCD, right) reconstruction kernels, multiplanar reformat. Copyright © 2015 Carl Chartrand-Lefebvre.

The BRS platform, on the other hand, is made of degradable polymers, with metal-free struts that do not cause blooming artifacts.⁸⁰ BRS struts are totally invisible in coronary CT angiography, even after immediate implantation. BRS can however be identified in CT by the small platinum indicators at their extremities⁸⁰ (figs. 22-23, pp.89-90). More about bioresorbable stents and CT imaging in chapter 3.

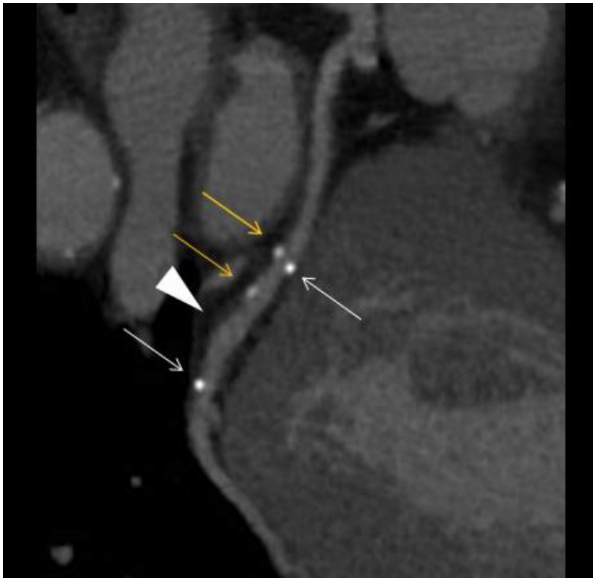


Figure 22. Bioresorbable stent visualized in mid-circumflex artery of a 58-year-old man. Conventional angiography showed 80% mid-circumflex stenosis and followed with implementation of a bioresorbable stent (BRS, Abbott Absorb 3.5 x 28 mm).

Under the CHUM BRS clinical register (Dr. Samer Mansour et al.), a 256-slice CT scan with prospective ECG-synchronization was performed one month following angioplasty. Only two proximal and distal metallic markers are visible on scan (white arrows). Positive remodelling can also be seen (arrowhead) and two calcification loci (orange arrows) proximal to positive remodeling site. Good permeability of stent is observed. No significant artifacts are visualized. Copyright © 2015 [C. Chartrand-Lefebvre]

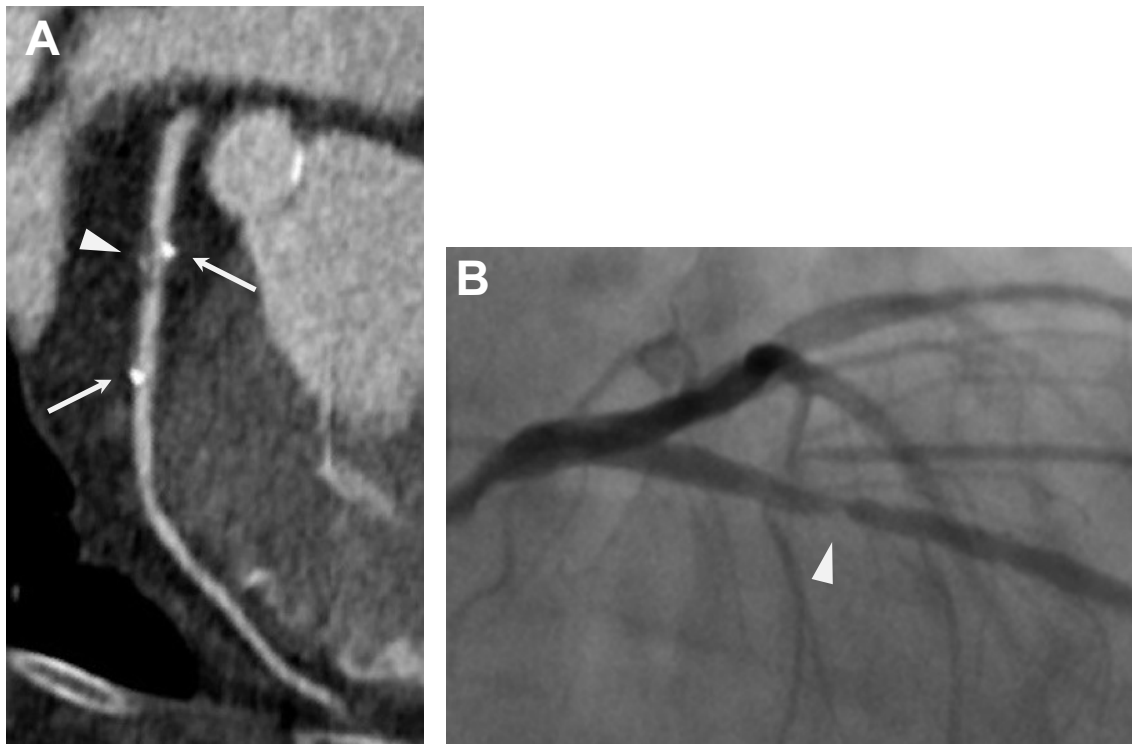


Figure 23. CT angiography correlation with conventional angiography.

A) 256-slice ECG-gated CT angiography. Bioresorbable stent (2.5 x 18 mm) in left anterior descending artery, 14 months after implantation. Mixed intrastent plaque with severe lumen stenosis (arrowhead). Platinum markers (arrows). B) Conventional coronary angiography. Severe intra-stent stenosis was confirmed (arrowhead). Platinum markers are not visible. Copyright © 2015 [C. Chartrand-Lefebvre]

To summarize, this chapter addresses coronary stents with an emphasis on bioresorbable stents, their clinical studies and imaging by different modalities. The following chapter will discuss cardiac computed tomography with its physical and technical principles, its artifacts, and native and stented coronary imaging.

Chapter 3 – Cardiac computed tomography

Presentation and objectives:

This chapter will discuss coronary computed tomography angiography (CCTA) beginning with its physical principles, its evolution and its different types. It will also review improvements in the spatial and temporal resolution of CCTA modalities and the artifacts that can make coronary image interpretation challenging. Radioprotection will be discussed briefly as well. Finally, a review of literature will be conducted on CCTA imaging of the native coronaries and metallic and bioresorbable stents through time.

3.1. Introduction to CT scan

Computed tomography (CT) was invented in 1972 by Godfrey Newbold Hounsfield and Allan Cormack, for which they shared a Nobel Prize in Physiology or Medicine in 1979.¹⁴² Hounsfield was an electrical engineer working at the Central Research Laboratory of Electric and Musical Industries, better known as EMI Records.¹⁴² One rumour states that the success of the Beatles' record sales at EMI helped to fund CT research and, to some extent, the invention of the first CT unit, which later led to evolved CT systems as we know them today.^{143,144}

CT is a relatively rapid and non-invasive imaging technique for stenosis detection in the coronaries. Together with a specialized software, CT takes a snapshot of a rapidly-moving heart, unfortunately sometimes with artifacts, and transforms it into series of sliced static images. This three-dimensional technique is achieved through high temporal and spatial resolution.¹⁴⁵ This section will discuss the technical aspects of CT and a brief history of CT.

3.1.1. The technical aspects of CT

During CT scanning, the patient lies on a table in the center of the gantry, the latter supporting the rotating x-ray tube as well as the sensor matrix. A collimated x-ray beam is sent from the tube through the patient's body and is detected by sensors (detectors) at the opposite end of the CT gantry, which rotate synchronously with the x-ray tube (fig. 24, below). The sensors transform the received x-ray beam into an electrical signal of proportional intensity.¹⁴⁴ The degree to which the patient's body absorbs the x-ray beam affects the strength of electrical signal generated by the sensors. For instance, as the x-ray beam passes through dense bone structures, some of the beam is absorbed, resulting in a weaker beam reaching the sensors, and proportionally less transmission of electrical signal. By contrast, when the x-ray beam passes through less dense tissue, such as the lungs and the air they contain, less radiation is absorbed, leaving more to be transmitted to the sensors, which in turn give a stronger electrical signal. The electrical signals are rapidly transformed into digital data that are processed by various reconstruction algorithms

(filter or kernel), which are designed with a small mathematical matrix that performs image modification.^{55,145,146}

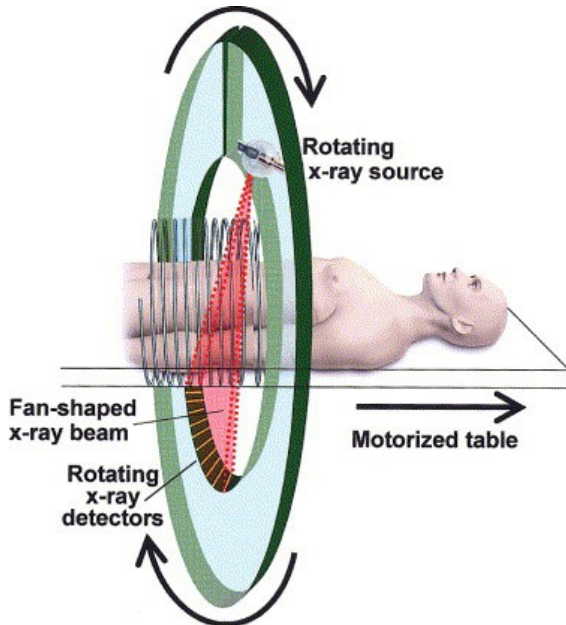


Figure 24. Spiral or helical CT scanner. The x-ray source, and on the opposite side, x-ray sensors that rotate around the patient. In earlier CT scanners that used only the axial mode (see Section 3.1.2.), the table did not move, and a single image slice of the patient was created for each gantry rotation. With more modern scanners such as helical scanners, simultaneous and continuous movement of the table and patient in one direction during gantry rotation

allows volumetric (spiral or helical) CT acquisition, as illustrated here. This image shows a single row of sensors, however, in modern scanners multiple sensors are aligned alongside each other, which gives thinner slice widths and allows shorter scan times. Reprinted from *Gastroenterology*, David J. Brenner and Maria A. Georgsson, "Mass Screening with CT Colonography: Should the Radiation Exposure Be of Concern?", 2005 Jul;129(1):328-37. Copyright (2017), with permission from Elsevier.¹⁴⁷

3.1.2. Brief history of CT

Since the invention of the CT scan by the previously-mentioned doctors Hounsfield and Cormack, axial (or conventional) tomography has become useful to diagnostic radiology. Early CT systems involved conventional axial (transverse) acquisitions of the body. The spatial resolution achieved in early CT machines was from 1 to 2 mm.¹⁴⁸ Subsequent CT machines had helical (spiral) systems with a tube that rotated around the moving patient on the CT table instead of the conventional

axial CT system where the table was still (fig. 24, p.93). Data acquisition speed with these newer helical CT systems depends on the speed of tube rotation around the patient and on the speed of information capture. Shortly after spiral CT invention, the tube required 18-20 s for a single rotation and 1 min to return to its initial position for the new cycle, thus creating motion artifacts.¹⁴⁴

Helical CT systems offered a considerable improvement of image quality through faster data acquisition and more reproducible diagnostic information. In fact, images were now captured not only in one axial plane, but could be reconstructed in axial, coronal, sagittal and curved planes providing a three-dimensional representation of the target organ and allowing more diagnostic possibilities.¹⁴⁵ However, even with the more advanced helical CT machines, acquisition time was still longer than what would be required to capture the heart in diastole in its stillest state.¹⁴⁵

The next generation of CT scans, called multi-slice CT (MSCT), appeared at the beginning of the 21st century. In MSCT the higher acquisition speed is due to a more performant data-acquisition system with multiple rows of detectors. There is also a larger collimation of the x-ray beam, which allows all detectors to receive the beam at the same time and a larger anatomical area to be evaluated in one gantry rotation (larger z-coverage or longitudinal coverage).¹⁴⁵

Four-row detectors were among the first MSCT systems to be used in cardiac imaging, but greater advancement came with 16-row detectors that could image coronary arteries with fewer artifacts and better resolution.¹⁴⁴ Subsequently CT scans were developed with more detectors, able to acquire 64 slices during one rotation, then 128 slices, 256 slices and presently, 320 slices.¹⁴⁹ With wide detectors CTs (256- and 320-row), the entire human heart can be imaged in a single heartbeat.¹⁴⁴

Coronary CT angiography (CCTA) was developed to allow visualization of coronary artery lumen and walls. CCTA involves high rate intravenous administration of iodinated contrast agent¹⁵⁰ and ECG-gating. Physical and technical aspects of CCTA are discussed below.

3.2. Physical and technical principles of coronary CT scan

Beginning with the 64-slice MDCT and the more advanced scanners that followed, CCTA gained enough temporal and spatial resolution to be able to offer visualization of the lumen and the coronary segments that lie distally.¹⁵⁰

3.2.1. Temporal resolution in coronary CT scan

Box # 11

Temporal resolution

Temporal resolution is the ability to accurately image a non-static object over time.¹⁵¹

In a CT scan, good temporal resolution is important when organs that move, such as the heart, are imaged¹⁵² (see box # 13, p.98, for a definition of spatial resolution).

Given the small size of the coronary arteries, CCTA image quality can be undermined by cardiac movement.⁵⁵ One held breath during thoracic image acquisition can usually eliminate respiratory movement, but during standard CT coronary imaging, cardiac movement usually leads to artifacts (see section 3.2.3.1.1). To acquire good coronary images without motion artifacts at cardiac frequency <70 bpm, a temporal resolution in diastole should be at least 250 ms, and in systole, at least 50 ms.¹⁵³ For instance, Leschka et al. demonstrated that image quality was improved when patient heart rate was low,¹⁵⁴ or when beta-blockers were administered.¹⁵⁵ With increasing cardiac frequency, better temporal resolution is required. To improve temporal resolution, systems have been created that enable ECG-coupling to MDCT acquisition or reconstruction. Various ECG-synchronization modules exist, such as retrospectively ECG-gated helical acquisition or prospectively ECG-gated axial acquisition.⁵⁵

3.2.1.1. Retrospectively ECG-gated helical acquisition

Retrospectively ECG-gated helical acquisition was a very popular technique in the first years of CCTA, especially with 4- and 16-slice MDCT. Retrospective ECG-coupled CCTA made it possible, after initial acquisition of imaging data, to retrospectively reconstruct the images of a given cardiac cycle phase. A phase is expressed as a percentage of an RR interval.⁵⁵ The choice of cardiac phase, the purpose of which is to allow better visualization of the coronary arteries free of artifacts, relies on patient heart rate during acquisition.^{156,157} In patients with a heart rate of ≤ 70 bpm, the temporal reconstruction window associated with the fewest movement artifacts should be in the middle or at the end of diastole.^{156,157,158} In patients with a heart rate of >70 bpm, the best reconstruction window is located in late systole and early diastole.¹⁵⁷

Retrospective ECG-gating requires continuous helical acquisition with a low pitch (box # 12, below). Thus, during the whole heart cycle, the x-ray beam from consecutive gantry rotations penetrates the same anatomical region of the heart, leading to acquisition overlap and exposing patients to relatively high doses of radiation.⁵⁵ Retrospective ECG-gated MDCT acquisitions require a mean effective radiation dose of 15 to 18 mSv with 16- or 64-slice CT scanners, while conventional angiography requires 6 mSv.^{159,160} When patient heart rate is relatively low during retrospective 64-slice ECG-gated MDCT acquisition, an optional modulation of the tube current permits decreased tube output during systole. This can reduce emitted radiation by 30 to 50%.¹⁶¹

Box # 12

Pitch

Pitch is defined as the table displacement distance during 360° rotation of the tube divided by the width of the collimated x-ray beam.⁵⁵

3.2.1.2. Prospectively ECG-gated axial acquisition

An alternative to retrospective ECG-gated MDCT helical acquisition is prospective ECG-gated axial acquisition (fig. 25, p.98). This acquisition technique, also called step-and-shoot, is triggered by prospective ECG-gating. This mode of ECG-synchronization is available on more recent MDCT machines.⁵⁵

With prospective technique, the ECG signal determines when MDCT acquisition will take place. This acquisition is called axial, as opposed to helical, because the scanning table does not move during acquisition. It is called step-and-shoot because only one cardiac cycle out of two is used for image acquisition.⁵⁵

Unlike retrospective helical ECG-gating technique, prospective axial ECG-gating technique doesn't overlap during acquisitions and thus allows a reduction in radiation exposure for the patient. Indeed, as initial studies from the literature have shown, the latter technique offers more than 80% radiation reduction with effective doses of 1.5 to 3.0 mSv.^{55,162} Locally, at the Centre Hospitalier de l'Université de Montréal (CHUM), the introduction of prospective ECG-gated axial technique on a 256-slice scanner has allowed reduction of the mean effective dose from 15.3 to 4.2 mSv (70% reduction) as compared to retrospective helical ECG-gated technique.⁵⁵

Usually, at low heart rates (<65 bpm), better image quality with less cardiac movement artifacts will be obtained in mid-diastole at 75% of the RR cardiac cycle. The operator can choose to increase the width of the acquisition window by manually adding data at the beginning or the end of a scanned segment. This optimization tool of the reconstruction image phases is called "padding".⁵⁵ However, padding increases the patient's radiation exposure. Indeed, a 100 ms increase in padding corresponds with a 45% increase in radiation exposure. Thus, the slightest reduction of padding offers a substantial reduction in radiation exposure.¹⁶³ Prospective ECG-synchronization technique is more effective when patient heart rate is stable and low.^{55,162}

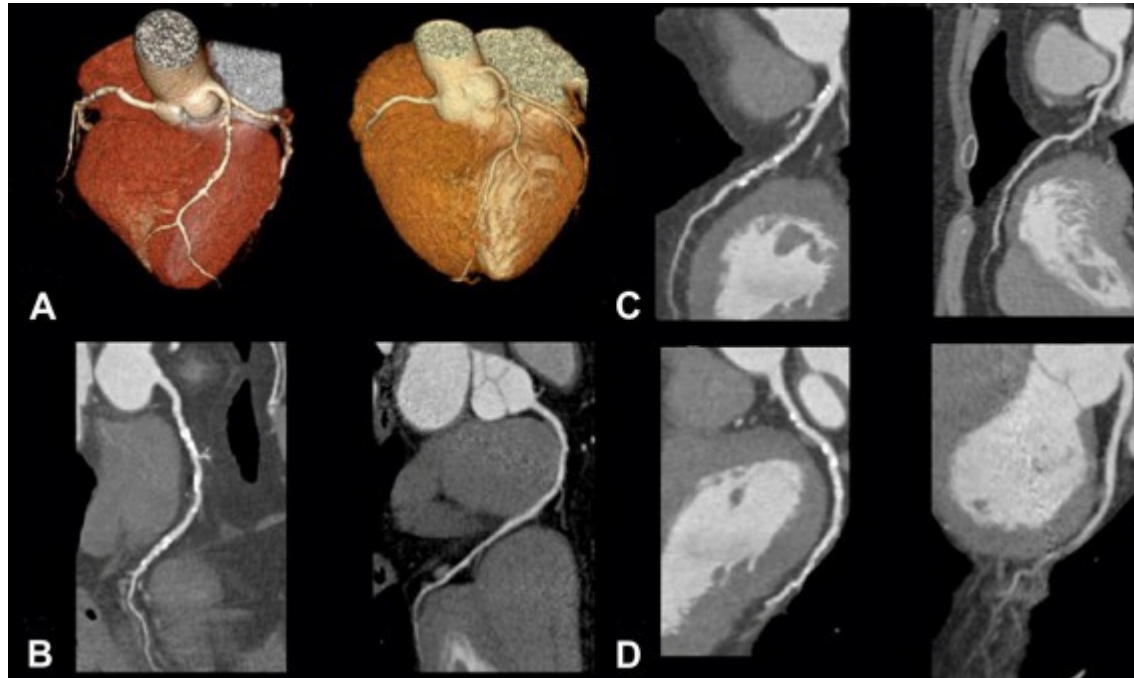


Figure 25. Prospectively and conventional retrospectively ECG-gated dual source CT. Prospectively ECG-gated dual source CT with advanced arrhythmia annulment algorithm (**left**) and conventional retrospectively ECG-triggered dual source CT (box # 15, p.103) (**right**). 3D volume-rendered reconstruction illustrating 3 proximal coronary arteries free of motion artifacts (**A**) Curved multiplanar images of right coronary artery (**B**) left anterior descending artery (**C**) left circumflex artery (**D**) depicting excellent image quality free of motion artifacts. Reprinted from Lee A.M. et al. "Coronary computed tomography angiography during arrhythmia: Radiation dose reduction with prospectively ECG-triggered axial and retrospectively ECG-gated helical 128-slice dual-source CT"; 2012 May-Jun;6(3):172-183.e2. Copyright (2018), with permission from Elsevier.¹⁶⁴

3.2.2. Spatial resolution in coronary CT scan

Box # 13

Spatial resolution (also known as image sharpness) is defined as the minimal distance between two imaged adjacent entities of high contrast at which these given entities can be discerned from each other.⁵⁵

A decade ago, standard definition MDCT scanners had 0.5-0.625 mm spatial resolution in the longitudinal or z-axis and about 0.5 mm in the x- and y-axes. To obtain good multiplanar reconstruction, one of the basic requirements is for resolution to be isotropic, i.e. equal in all directions. The aforementioned MDCT resolution is not adequate for optimal coronary stenosis grading. Indeed, proximal coronaries measure about 5 mm and distal coronaries about ≤ 2 mm in diameter. Therefore, a distal coronary artery of 2 mm diameter can be represented in CT acquisition by no more than 4 voxels (see box #14 below), which is insufficient for accurate stenosis grading.¹⁶⁵ By contrast, with 64-slice single- and double-source CT, isotropic resolution is about 0.4 mm.¹⁶⁶ Novel high-definition CT have a z-spatial resolution of 0.23 mm, allowing better non-invasive assessment of coronary stents and smaller caliber vessels.¹⁶⁷

Box # 14

A **voxel** is “a volume element, which is the basic unit of CT or MRI reconstruction, represented as a pixel in the display of the CT or MRI image.”¹⁶⁸ To put it simply, a pixel is a 2-D square and a voxel is a 3-D cube. Each 2-D pixel can be represented by a 3-D brain cube, or voxel.¹⁶⁹

3.2.3. Artifacts in coronary MDCT: detection and solutions

Computed tomography is subject to a variety of artifacts. This includes artifacts specific to patients or to an imaging modality, some of which are unique to cardiac imaging.¹⁷⁰ In this subsection, we will discuss motion artifacts and blooming.

3.2.3.1. Motion artifacts

The most common cause of an artifact is motion that either originates from the patient’s body, heart or respiration.¹⁷⁰

3.2.3.1.1.

Cardiac motion

As discussed in Section 3.2.1, obtaining high-resolution images of the beating heart is one of the main challenges of cardiac CT. A slow and regular heartbeat is better for cardiac CT acquisitions and data reconstructions since it allows for better image quality. The most common cause of the cardiac motion artifact is a high heart rate, which can be further exacerbated by premature beats or irregular rhythms.¹⁷¹

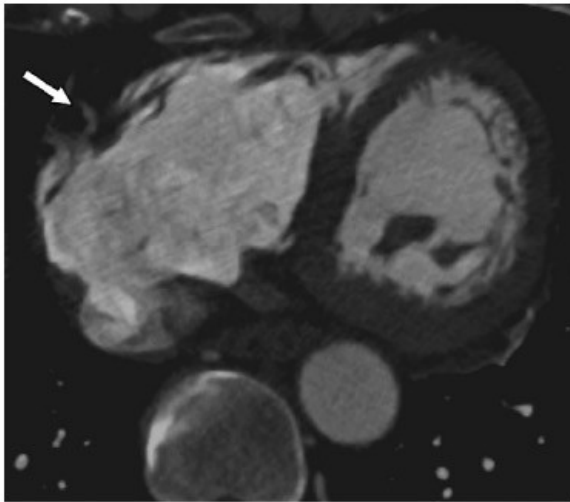
In an xy-plane, motion artifacts that happen within a single heartbeat usually appear as blurs (see fig. 26a, p.101), areas of ghosting (see fig. 26b, p.101) or winging (see fig. 26c, p.101). Moreover, some regions of the heart change their position more than others. For instance, the right coronary artery has the greatest positional shift in the xy-axis and the highest velocity movement across the cardiac cycle,¹⁷² followed by the left circumflex, left main and anterior descending arteries.^{173,174}

Stepladder artifacts, or stair-stepping, can occur along the z-axis when premature beats or irregular rhythms cause motion between sequential heartbeat reconstructions. This kind of artifact can manifest as a discontinuity region of anatomic structures and can thus interfere with finding stenosis by mimicking it (see fig. 26d, p.101).^{170,171,175} When the heart changes position during consecutive beats due to arrhythmias, linear bands can appear on coronal, sagittal, or three-dimensional reconstructions (see fig. 26e, p.102).^{170,171}

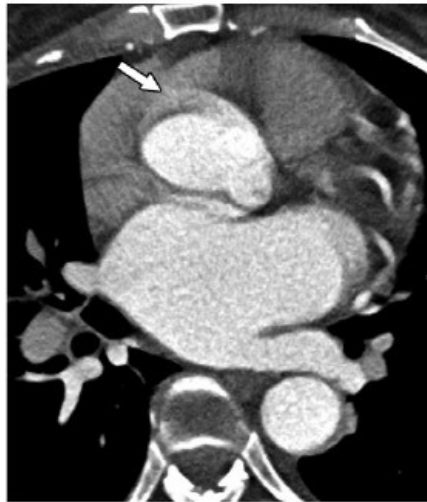
To reduce cardiac motion artifacts, several methods exist that can be implemented before, during or after scanning. One option is to reduce heart motion, for instance through administration of β -blockers. Another option is to modify scanning parameters so that images are acquired in shorter periods of time.¹⁷⁰

It should be noted that the heart rate varies during breath holding at the scanning session, initially increasing and subsequently decreasing.¹⁷⁶ This variation can result in stepladder motion artifacts in distal coronary arteries when the scanning direction is craniocaudal. This kind of artifact can also be exacerbated by an inappropriate selection of pitch (see box # 12, p.96), which can result in variation of the heart rate. Some modern scanners automatically select an appropriate pitch

based on the patient's heart rate. Other solutions to minimize stepladder artifacts include teaching patients effective breath-holding techniques and decreasing the duration of breath holding.^{170,171}



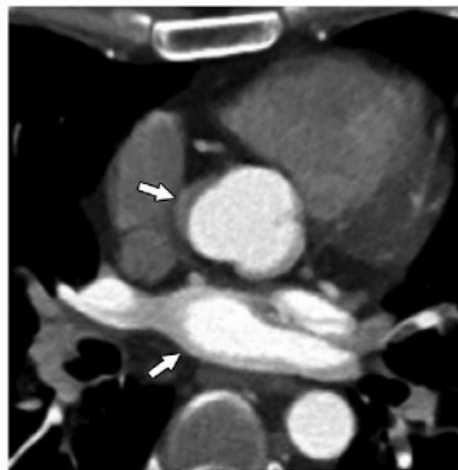
a.



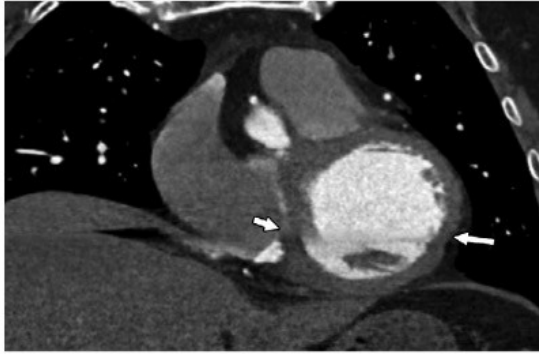
b.



c.



d.



e.

Figure 26. Cardiac motion artifact. (a) Blurring of the right coronary artery (arrow) shown on axial CT image. (b) Ghosting of the right coronary artery and the ascending aorta (arrow) visualized on axial CT image. (c) Winging manifestation of the right coronary artery (arrow) on the axial CT image. (d,e) Misregistration or stepladder artifacts¹⁷⁵ visible on axial CT image as motion of the aortic root¹⁷⁷ (see arrows in d) and on coronal reconstruction as a linear band of misregistration (see arrows in e). Reprinted from *RadioGraphics*, Kalisz K. et al. *Artifacts at Cardiac CT: Physics and Solutions*, 2016 Nov-Dec;36(7):2064-2083. Copyright (2018), with permission from the Radiological Society of North America (RSNA®).¹⁷⁰

Stepladder artifacts can be reduced by increasing the z-axis coverage per rotation.¹⁷⁸ Scanning more cardiac anatomy per rotation decreases opportunities for misregistrations after data combination.¹⁷⁹ Wide-area detectors, of for example 16 cm, can eliminate stepladder artifacts by imaging the entire heart in one heartbeat within a single gantry rotation.¹⁸⁰ Another way to reduce artifacts is with dual-source scanners (see box # 15, below), since data from the second tube completes data gaps, which helps avoid artifacts.¹⁷⁰

Box # 15

Dual-source CT scanner

Dual-source CT comprises two x-ray tubes paired to two corresponding detectors. The detectors are engineered at an angular offset of 90° in the gantry (see fig. 27 below). By contrast, there is only one x-ray tube in a conventional multislice CT. In a dual source CT, it takes half the time to capture image data as compared to conventional CT,¹⁸¹ which improves temporal resolution.

Dual-source CT is mainly used in cardiac units, emergency, acute care and dual-energy imaging. Dual-energy imaging implies that the scan sends two different energy magnitudes simultaneously from two corresponding x-ray sources. By relying on the unique energy-dependent attenuations (see box #16, p.104) of different scanned entities, it is possible to differentiate fat from soft tissue and bone, and even identify calcifications in an iodinated contrast media.¹⁸¹

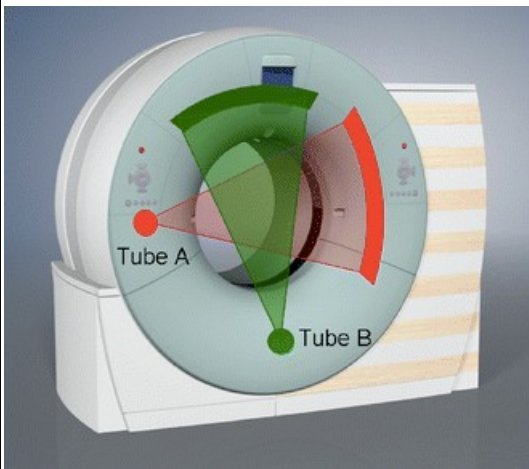


Figure 27. Illustration of image acquisition with dual-source computed tomography using two x-ray tubes and corresponding detectors positioned at 90° angles. Temporal resolution of this type of scanner represents a quarter of the gantry rotation time, no matter what the patient's heart rate is. Adapted with permission from Springer Nature (licensor): on behalf of Cancer Research UK: Springer Nature; European Radiology; (First performance evaluation of a dual-source CT (DSCT) system, Flohr TG et al.), © (2018).¹⁸²

Box # 16

Attenuation is defined as “the change in a beam of radiation as it passes through the matter”.¹⁸³

Increased attenuation implies that more x-ray beams are being attenuated, or stopped, by matter, which is thus an area displayed more brightly in the image.¹⁸⁴ In other words, when an x-ray beam is said to be “attenuated” by passing through matter it means that the beam’s intensity has been decreased. This decrease could be due to scatter of beam photons or to the absorption of the beam by the matter. Beam intensity that passes through matter varies with beam energy and matter atomic number.¹⁸⁵ For instance, when an x-ray beam passes easily through matter, such as air in lungs, these areas are displayed as dark images. When an x-ray beam passes through dense matter like bones, more of the beam is blocked, resulting in the bones being displayed as white.

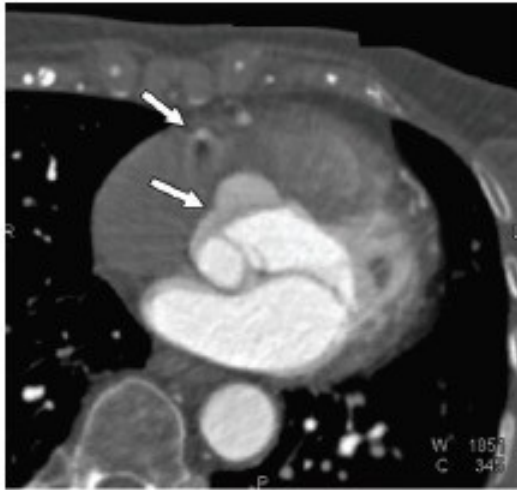
Correction algorithms exist that correct coronary motion by using data from adjacent cardiac phases to determine vessel movement (path and velocity) within a given cardiac cycle. These algorithms localize the position of the vessel of interest at the target phase and compensate for motion in that given phase.¹⁷⁰ Thanks to motion-correction algorithms, there have been improvements in image quality, diagnostic accuracy and interpretability, even in patients with high and irregular heartbeats, especially while imaging the right coronary artery.^{170,186,187}

There are also ways to address motion artifacts after acquisition. A significant difference can be made in their appearance through the choice of reconstruction temporal window. Artifacts are usually improved in mid- to late-diastole at 70% of RR interval at low heart rates of < 60 beats per minute. At higher heart rates of >65 beats per minute, artifacts are typically improved in end systole or early diastole at 30-40% of the RR interval.^{170,188} A given coronary artery can sometimes be well visualized at different phases of the RR interval, which necessitates the use of multiple

reconstructions for assessment. For instance, the right coronary artery is typically best visualized at 40% of the RR interval, the left anterior descending coronary artery at 60-70% and the left circumflex coronary artery at 50%.¹⁷⁰

Another post-acquisition tool that decreases motion artifacts on helical ECG-triggered images is called ECG editing. Depending on the type of arrhythmia present, a post-acquisition ECG-editing feature can be used to choose the best RR segment for the reconstruction. In fact, data may be chosen from a different phase of each RR interval. If there is a problem with ECG-gating such as triggering from an abnormal T wave (see fig. 28 a-c, p.106), a new appropriate ECG position can be chosen through placement of new synchronization markers. In Figures 28d and 28f (p. 106), another example of ECG editing is visualized where synchronization markers from premature ventricular contractions were removed and thus, aberrant data eliminated.¹⁸⁹ However, ECG editing cannot fix ventricular tachycardia.¹⁷⁰

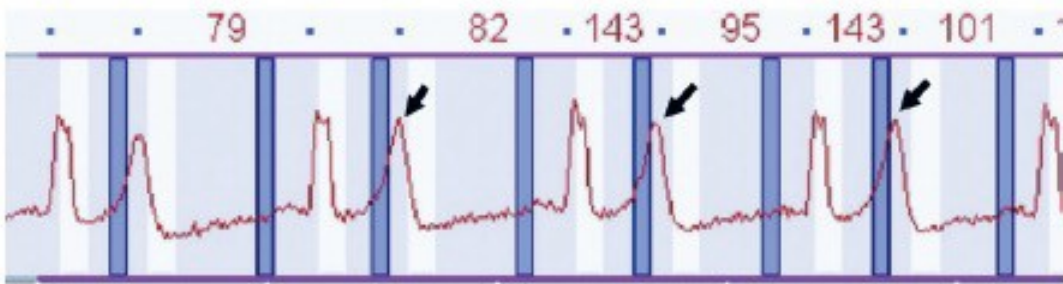
In conclusion, cardiac motion artifacts can be improved by lowering the heart rate; monitoring its variability and decreasing the duration of data acquisition; managing the position of the data window in a cardiac cycle; making a single-heartbeat scan of the heart; or applying motion-correction algorithms and performing electrocardiographic editing.



a.



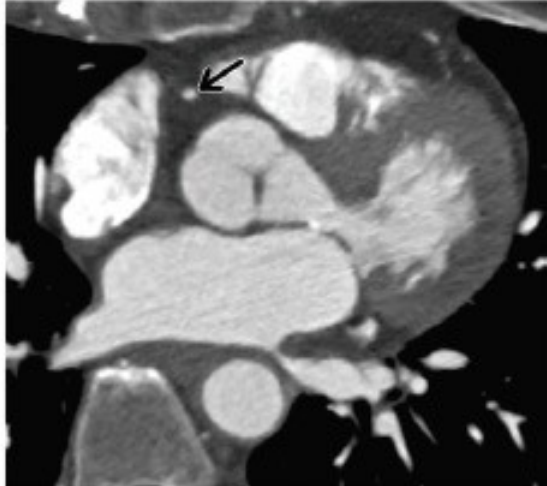
c.



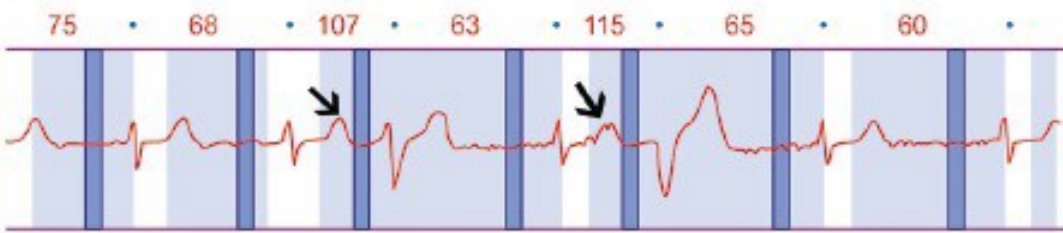
b.



d.



f.



e.

Figure 28. ECG editing performed in two patients. (a-c) Cardiac CT performed in a patient experiencing chest pain: (a) substantial blurring of the aortic root and the right coronary artery (arrows) seen on axial CT image; (b) ECG tracing showed inadequate triggering from extensively tall T waves (arrows); Cardiac phases utilized in data reconstruction are depicted by blue bars, and the heart rate for that given RR interval is represented by the numbers. After performing ECG editing, synchronization markers at tall T waves were deleted; (c) Axial CT image shows no motion artifacts after ECG editing; (d-f) Cardiac CT of a new patient; (d) Blurring of the right coronary artery (arrow) visualized at the axial CT image that was reconstructed at 70% of RR interval; (e) ECG tracing depicts faulty triggering during the ectopic beats caused by the premature ventricular contractions (arrows). ECG editing was performed, and the synchronization markers at the premature ventricular contractions were deleted; (f) After ECG editing, axial CT image presents no motion artifacts (arrow = right coronary artery). Reprinted from *RadioGraphics*, Kalisz, K. et al. *Artifacts at Cardiac CT: Physics and Solutions*, 2016 Nov-Dec;36(7):2064-2083. Copyright (2018), with permission from the Radiological Society of North America (RSNA®).¹⁷⁰

3.2.3.1.2. Respiratory motion

Patient respiration during image acquisition leads to motion artifacts similar to cardiac motion. Various scanner technologies and parameters lead to divergent image acquisition times and subsequently, different breath-holding durations. Sometimes, for even the shortest scanning duration, respiration may not be suspended by dyspneic patients. Respiratory motion artifacts usually occur at the end of acquisition, when patients can no longer hold their breath.¹⁷⁰

To prevent respiratory motion artifacts, it is essential to reduce image-acquisition time, especially for dyspneic patients. This implies favouring the fastest gantry rotation duration and selecting the longest z-axis coverage per rotation. One mean to reduce respiratory artifacts is to perform a single-heartbeat dual-source acquisition in high-pitch mode.^{170,190}

To improve compliance during image acquisition, patients should receive instruction on appropriate breath-holding techniques. For instance, breath should be held after breathing in. To

prepare the patient and familiarize the technician with the patient's capacities, it is advised to practice some breath holds beforehand. This practice can identify patients who do not close their glottis while holding their breath, a factor that leads to exhalation and diaphragmatic motion artifacts. It also gives the technician a sense of what heart rate variations to expect during breath holding. If there are major heart rate variations during practice, it can be beneficial to start breath holding a few cycles before image acquisition to stabilize the heart rate.^{191,192} Acutely dyspneic patients can be offered oxygen supplementation.^{171,193} To improve the compliance of such complex patients, the anatomic area to be scanned can be reduced or the thickness of the sections can be increased, which can decrease scanning duration, although sometimes this can be at the expense of diagnostic accuracy.¹⁷⁰

3.2.3.2. Metal or streak artifacts

Imaging metallic objects with a CT scanner can give multiple artifacts. The attenuation of metallic objects is above the range of the usual Hounsfield units and thus cannot be accurately reconstructed, leading to bright and dark streaks.

Another kind of artifact, called undersampling, can be produced by sharp-edged and small objects. This is due to a too-wide interval between projections utilized in reconstruction of a CT image, which leads to view aliasing, with fine bright lines projecting from the edges of the object.¹⁹⁴ Undersampling is more visible in metallic sharp-edged small objects, although it can be detected in other small sharp entities. The higher the atomic number of the object, the more important the artifact. When imaging the heart, metallic stents, surgical clips, pacemakers and defibrillators produce undersampling or blooming artifacts.¹⁷⁰ In comparison to metallic coronary stents, the new bioresorbable stents made of polymers do not produce blooming artifacts. In chapter 2, figure 21 (p.88), blooming artifacts can be observed with metallic stents, which are attenuated by the "sharp" reconstruction algorithm. Figure 22 (p.89) illustrates the absence of blooming artifacts with a bioresorbable stent.

3.2.4. Cardiac CT radiation

Advancements in CCTA technology have increased its use. However, this increase in use of CCTA has a price: increased radiation exposure for the patient population. Fortunately, improvements to this technology have decreased the radiation dose.¹⁹⁵⁻¹⁹⁷ Radiation exposure can be reduced by many techniques, including use of acquisition modes with high-pitch helical prospectively-triggered ECG-gated acquisitions, or use of iterative reconstruction algorithms.¹⁹⁸⁻²⁰⁰ Hausleiter et al.²⁰¹ estimated the radiation dose of coronary CT together with commonly used strategies of dose reduction in the PROTECTION I study. They found that median doses of coronary CT vary significantly between hospitals and CT systems. Following 1965 CCTA examinations that were conducted at 50 study sites, the mean estimated radiation dose was 12 mSv, which was also represented by 600 chest x-rays.²⁰¹ The available strategies to reduce radiation were not commonly used at the time of the study. In a recent publication, Stocker et al.¹⁹⁷ evaluated the radiation dose and dose-sparing strategies of more advanced coronary CT scans in the PROTECTION VI study. In this extensive international radiation survey, the authors concluded that in the last decade the radiation exposure was reduced. They also found an inter-hospital fluctuation in the radiation exposure suggesting that further training of the personnel is required for more optimal use of contemporary coronary scan protocols. Also, among conclusions of their 2017 survey, the authors', mention that if an imaging study is considered useful, patients should not get discouraged by the radiation doses of the coronary CTAs. Indeed, the life-time cancer risk changes only slightly when a 60-year-old patient (median age in their survey) undergoes imaging with 5 mSv.¹⁹⁷

3.3. CT imaging of coronaries

In this section, computed tomography imaging of coronary arteries and coronary stents will be discussed.

3.3.1. CT imaging of native coronary arteries

Four-slice CT was used in the first coronary angiography studies with computed tomography.⁵⁵ There has been progressive improvement in coronary stenosis detection since the invention of the four-slice CT. In comparison to conventional angiography, four-slice MSCT has been shown to correctly detect 81% of significant stenosis of >50% reduction of vessel diameter, and to accurately diagnose 97% of healthy or non-significantly diseased coronary segments of ≤50% reduction of vessel diameter.²⁰² Moreover, in comparison to conventional coronary angiography, 85% sensitivity and 76% specificity for diagnosis of significant stenosis were reported by Achenbach et al.²⁰³ Presence of non-assessable segments of up to 30% were mainly due to motion artifacts, extensive acquisition window and low spatial resolution.^{55,203}

Advancements made in CT imaging technology have resulted in better temporal and spatial resolution, which in turn has led to improved diagnostic accuracy and fewer non-assessable segments.²⁰⁴ Reported sensitivity of the 16-slice CT in the literature ranged from 63% to 95%, while specificity ranged from 86% to 98%.²⁰⁵⁻²¹² Early studies describing the 64-slice CT reported that its diagnostic accuracy was very good and its negative predictive value was remarkable (96-99%) for detection of significant (>50%) coronary stenosis, in selected patient populations.²¹³⁻²¹⁶ The literature has also shown that the sensitivity and specificity of the 64-slice CT are excellent, ranging from 73% to 99% and 95% to 97%, respectively.²¹³⁻²¹⁶

In a two-center study (including the CHUM) published by Chartrand-Lefebvre et al.²¹⁷ in 2007, the diagnostic accuracy of 16-slice retrospective ECG-gated CCTA was evaluated with respect to conventional angiography in 26 consecutive patients. To assess stenosis, 283 coronary segments were used for post-processing. When compared to conventional angiography, significant stenoses were detected with fairly high sensitivity, specificity and positive predictive values of 80%, 100% and 100%, respectively. Negative predictive value was also remarkable at 98%. However, 26% of segments were not optimally assessable due to calcifications and stepladder artifacts. Thus, the authors concluded that in a selected population with low coronary calcifications and low pretest probability, the 16-slice CCTA is a valuable modality for detection of coronary stenoses, as opposed to conventional angiography.²¹⁷

At present, coronary artery stenosis diagnosis with CT remains a challenge, mostly due to residual cardiac movements that appear as artifacts despite ECG-gating. The post-64-slice era of MDCT has offered several approaches to address this challenge. In one approach, the number of detector elements in MDCT were increased, which led to larger z-axis volume coverage.¹⁸⁰ Other approaches have focused on improving detector sensitivity, use of an iterative reconstruction algorithm (which makes continuous iterative adjustments until the best compromise between assumed and real images is found²¹⁸⁻²²²), and dual-source CT^{223,224} (see box #15, p.103), which images the entire heart in one beat.¹⁸⁰

3.3.2. CT imaging of coronary stents at present

As with native coronary arteries, studies using 64-slice MDCT have demonstrated improved intrastent stenosis detection performance in metallic stents, in comparison to previous generations of CT systems. Based on three meta-analyses done by Sun et al. (5 studies in total, 340 patients, 459 metallic stents),²²⁵ Kumbhani et al. (14 studies, 895 patients, 1447 metallic stents)²²⁶ and Carrabba et al. (9 studies, 598 patients, 978 metallic stents),²²⁷ 64-slice MDCT sensitivity in assessable intrastent segments ranged from 85% to 91%, specificity from 91% to 95%, positive predictive value from 68% to 90% and negative predictive value from 94% to 98%. Kumbhani et al. also reported that when non-assessable intrastent segments are included in stenosis detection analysis, specificity and positive predictive value are reduced by about 10% to 15% respectively, while sensitivity and negative predictive value remain close to constant.^{55,226}

The diagnostic accuracy of 64-slice MDCT for intrastent restenosis is comparable with new CT technology such as the 320-slice and double-energy MDCT.⁵⁵ In the aforementioned MDCT modalities, the sensitivity, specificity, positive and negative predictive values in detection of intrastent restenosis were 94%, 87%, 62% and 99% respectively, as reported in a recent study of 444 patients (729 stents).⁵⁵

In 2010, in a consensus report from the American College of Cardiology, the American College of Radiology, the Society of Cardiovascular Computed Tomography and the American Heart Association on appropriate use of CCTA for detection of coronary artery disease in asymptomatic patients, the investigated metallic stent was required to be in the left main coronary artery or to have a diameter of ≥ 3 mm.²²⁸ These criteria preclude imaging metallic stents of smaller diameter due to the high incidence of blooming and beam-hardening artifacts, which do not occur in bioresorbable stents (as discussed in chapter 2, figs. 21 and 22, pp. 88-89).

As an *avant-goût* for the following chapter on BRS and coronary plaque imaging, in a recent study published by Collet et al., diagnostic accuracy of CCTA in detection of coronary intrastent obstructions under BRS was compared with conventional coronary angiography and IVUS as references. A total of 238 patients (258 lesions), post 3-year follow-up in the ABSORB II study (discussed in chapter 2, section 5.3), were treated with BRS. Collet et al. determined that when conventional angiography was used as a reference, the intrastent diagnostic accuracy of CCTA in detection of significant stenosis (vessel diameter $\geq 50\%$) showed a sensitivity of 80% (95% Confidence Interval: 28% to 99%) and a specificity of 100% (95% Confidence Interval: 98% to 100%). In conclusion, detection of intrastent coronary stenosis in BRS stents is evaluated with good accuracy by modern CCTA modalities, as compared to conventional angiography.²²⁹

Chapter 4 – Imaging coronary plaque

Presentation and objectives:

This chapter will focus on imaging vulnerable coronary plaque with invasive (IVUS, OCT) and, more extensively, with non-invasive (CT scan) technologies. Imaging of plaque under coronary stents will be discussed. Most importantly, recent studies on bioresorbable stents with measurements of underlying coronary plaque, this being the main focus of the present thesis, will be analyzed.

4.1. Imaging coronary lumen and plaque

The epidemiology and pathophysiology of CAD are discussed in chapter 1. In complement to that discussion, there are many coronary disease risk-assessment algorithms that have good sensitivity and specificity, such as for example the Framingham Risk Score, which is the most widely accepted clinical assessment for measuring 10-year risk for clinical cardiovascular events. However, none of these clinical assessment tools can predict the biomechanical factors leading to vulnerable plaque rupture. Current and emerging imaging techniques allow visualization of the atherosclerotic plaque and represent good tools for characterization of the pathological processes of vulnerable plaque rupture.¹³⁶

4.1.1. Coronary CT imaging in action

Details of intravascular coronary imaging with IVUS and OCT were discussed in chapter 2, sections 2.6.2 and 2.6.3. The present section will focus for the most part on CCTA coronary imaging.

As Shaw et al. state,²³⁰ patients with angina and CAD pretest probability of coronary stenosis ranging from low to moderate are good candidates to have a first-line multidetector CCTA diagnostic assessment. In these patients, CCTA has good negative predictive value, providing a safe assessment for ruling out disease.²³⁰ As shown in large prospective multicenter studies, even though measurement of the degree of coronary stenosis in patients with CAD can be challenging due to coronary calcification blooming artifacts, CCTA remains nevertheless an accurate test with fairly good sensitivity compared to invasive angiography.^{231,232} Coronary artery calcification (CAC) scanning is often completed with CCTA, which is a risk stratification algorithm that produces measurements of disease burden and predicts the probability of subsequent coronary events.²³³ However, if the CAC score or CAD pretest probability is high, diagnostic conventional x-ray coronary angiography becomes the assessment of choice over CCTA and other noninvasive tests.¹³⁶

4.1.2. CT-based plaque composition and morphology imaging

As discussed in chapter 1, features of plaque vulnerability including large necrotic core, thin-cap fibroatheroma, positive remodeling, neovascularization, and microcalcifications can be evaluated by IVUS, OCT and CCTA. CCTA imaging offers an overview of coronary anatomy and allows determination of the extent of luminal stenosis, plaque composition and morphology. The major histological predictors of plaque rupture are fibrous cap thickness and size of the necrotic core²³⁴ which are imaged by, respectively, OCT and IVUS. Thickness of the fibrous cap cannot be measured by CCTA due to insufficient spatial resolution, which in current scanners is approximately 400 μm .^{235,236} CCTA, however, allows plaque stratification into calcified, partially calcified (less than 50%), or noncalcified plaque categories. The volume of noncalcified plaques is often underestimated and the volume of calcified plaques overestimated by CCTA due to blooming artifacts.²³⁷ When compared to IVUS, noncalcified plaques of >1mm of intimal thickness are visualized by CCTA with a sensitivity of about 90%, as has been demonstrated in an ex vivo human model study.²³⁸ Further in vivo studies are needed to confirm CCTA sensitivity.

Low attenuation plaques have been generally identified with a cutoff of <30 HU, fibrous plaques at between 30 and 150 HU and calcified plaques at >220.^{136,239} It is, however, ambitious to establish absolute CT attenuation values for different plaque features, due to variables such as wall thickness, necrotic core size, intraluminal contrast density, reconstruction algorithms, and slice thickness.^{136,240,241}

As compared to stable atheromas in patients with chronic stable angina, unstable atheromas found in patients with acute coronary syndrome (ACS) often have low attenuation components, spotty calcifications, a higher remodeling index and are larger in size, as imaged by CT.^{136,239,242} Positive remodeling is characterized by the outward compensatory expansion of the vessel wall as the plaque grows, which is often associated with a considerable lipid core and macrophages within.³⁹ Positive remodeling is defined as an increase of >10% in the cross-sectional area (or diameter) as compared to the adjacent reference site, while spotty calcification is usually determined to be <3mm in all axes.^{127,264,239,243,244} Spotty calcifications are small granulations

within the plaque that appear with inflammatory processes. They act on the stress mechanisms within the plaque and can make it more unstable.²⁴⁵

Another plaque vulnerability marker, the CT napkin-ring sign, is defined as a low attenuation area, which seems to correspond histopathologically to a lipid-rich necrotic core abutting the vessel lumen, and which is enveloped by a high-attenuation ring corresponding to fibrous plaque content²⁴⁶ (fig. 30, below). Plaque vulnerability features such as positive remodeling, low attenuation content and the napkin-ring sign constitute prognostic CT indicators of potential MI.^{247,248} It has also been demonstrated that, as opposed to nonischemic lesions, such high-risk plaque components have a 3 to 5 times greater prevalence in FFR-positive plaques²⁴⁹ (box #18, p.117).

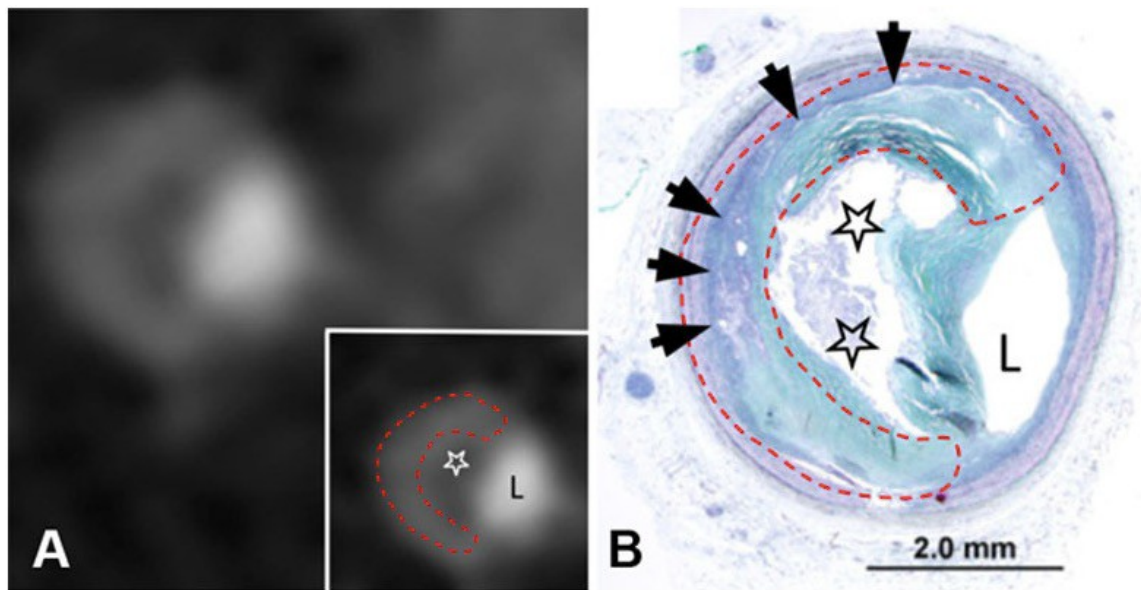


Figure 30. Non-invasive atherosclerotic plaque imaging.

Napkin-ring sign present in the coronary artery cross-section captured by the contrast-enhanced computed tomography (A) with corresponding histology (B) displaying advanced fibroatheroma. The low attenuation region (white star) on computed tomography corresponds to necrotic core (black star) on histology. Adjacent lumen is labeled (L). Region outlined by dashed red line on

computed tomography indicates the high-attenuation circumferential outer rim, which represents fibrous plaque tissue (black arrow) on histology.

Adapted from "Imaging Atherosclerosis"; Tarkin J.M. et al. *Circulation Research* 2016 Feb 19;118(4):750-69. doi: 10.1161/CIRCRESAHA.115.306247; Copyright (2018) with permission from Open Access article from Creative Common Public Domain¹³⁶ (license source: <https://creativecommons.org/licenses/by/4.0/>)

Box # 18

FFR and FFR_{CT}

The fractional flow reserve (FFR) is a current invasive standard of reference technique that determines the ischemic potential of a coronary lesion through intracoronary pressure measurements.^{244,250} Hemodynamically-significant stenoses are assessed through measurement of the ratio of mean distal coronary artery pressure to aortic pressure at maximal adenosine-induced coronary vasodilation.^{251,252} FFR is invasive since it requires the introduction of an intracoronary wire to measure the trans-lesional pressure gradient.

Recently, a non-invasive trans-lesional pressure gradient assessment technique called FFR_{CT} was developed which uses CCTA datasets and computational fluid dynamics algorithms.²⁵² Utilizing sophisticated algorithms, FFR_{CT} assessment can draw 3D pressure maps correlating with the physiological impact of luminal stenoses along the coronary tree²⁵² (see fig. 31 below).

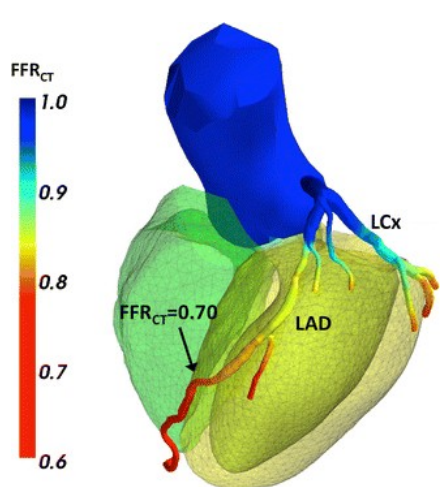


Figure 31. Computational simulation of FFR volume rendering of the left coronary artery tree. An ischemia of the distal left anterior descending coronary branch is depicted in red, noting the FFR_{CT} value of 0.70. Reprinted by permission from Springer Nature, *Int. J. Cardiovasc Imaging, Plaque assessment by coronary CT*, Szilveszter et al. (Copyright 2018).

Coenen et al. have demonstrated that FFR_{CT} has complementary value to CCTA as it increases the latter's diagnostic ability in identification of hemodynamically significant lesions, with higher specificity than CCTA alone (65.1% vs. 37.6%; p=0.001) and a moderately increased sensitivity of 87.3% vs. 81.3%.²⁵³

4.1.3. CT-based intrastent plaque imaging

Literature that reports CT-based imaging of atheromatous plaque under coronary stents is not extensive and reporting on bioresorbable stents even more limited. The majority of studies with bioresorbable stents will be described in this subsection.

CCTA has been determined to be an alternative to conventional coronary angiography for stent imaging and in-stent restenosis detection.^{204,254} For instance, it was found by Schuijf et al. that 16-slice CT assessed patency of 65 metallic stents with 78% sensitivity and 100% specificity, and assessed intimal hyperplasia (or coronary plaque component) in peri-stent stenosis with 75% sensitivity and 96% specificity.²⁵⁵

A recent study by Collet et al. addressed the accuracy (evaluation of how close the measurement is to the true value) and precision (or reproducibility of the measurements) of non-invasive CT lumen assessment under BRS as compared to assessment by OCT, a higher-resolution intravascular modality.²⁵⁶ In this study, 35 patients of the ABSORB cohort B trial underwent OCT within ±180 days of CCTA, which was planned at 18 months. After CT evaluation, the minimal

lumen area of the BRS-scaffolded segment was underestimated in CCTA assessment by 9.8% with accuracy of 0.39 mm² and precision of 1.0 mm². Evaluations of non-scaffolded segments were concluded with similar values. To summarize, in BRS-scaffolded or non-scaffolded segments, CCTA was determined to have good accuracy in assessing coronary lumen area when compared to OCT, a higher-resolution modality.²⁵⁶

Further parameters that can be measured with CCTA include numerous lumen and plaque measurements of BRS-scaffolded and adjacent segments. Some measurements that I have considered and/or performed automatically or semi-automatically during my master’s project can be found in table II below.

Parameters measured	Specifications
Lumen diameter	Minimum, average and maximum
External (vessel) diameter	Minimum, average and maximum
Lumen area	
Vessel area	
Lesion length	
Predictors of plaque instability ^{136,239,243,244,257,258}	
Remodeling index	<p>Remodeling can be considered a physiological response of the artery to lumen stenosis; it is a marker of high-risk plaque.</p> <p>= External lesion area (or diameter) / External reference area (or diameter)</p>

	Remodeling index >1.10 is a predictor of plaque vulnerability
Plaque composition analysis from -1000 HU to +3000 HU	
Low attenuation plaque	Composition of < 30 HU (hypoattenuation) suggests fatty unstable plaque
Fibrous plaques	Determined between 30 and 150 HU
Calcified plaques	Determined to be at >220 HU Spotty calcifications are predictors of plaque vulnerability

Table 2. BRS CCTA imaging: Assessment parameters of the intrastent lumen and arterial walls.

Copyright © 2018 [E. Zdanovich]

4.1.4. Clinical studies of BRS involving CT imaging

As discussed in chapter 2, blooming artifacts make it difficult to image coronary plaque under metallic stents. Further, in vitro and in vivo studies with CT-based BRS imaging are scarce.

An in vitro study performed by Gassenmaier et al. demonstrated that BRS offer excellent in-stent lumen visibility.²⁵⁹ The study was performed on 27 stents (1 BRS and other stents made of metal, such as either cobalt-chromium, platinum-chromium or stainless steel) implanted into plastic tubes with contrast. Out of 27 stents, 20 were made of cobalt-chromium alloy, four of stainless steel, one of stainless steel and PTFE, one of platinum-chromium alloy, and one was a poly-L-lactide BRS. These stents were imaged by dual-source CT at 0° z-axis for all stents and with a stent orientation of 90° to the z-axis. Fifteen stents from various companies had a diameter of 3.0 mm,

while the remaining 12 stents from two companies (Orsiro and Integrity) were imaged in six different diameters ranging from 2.25 mm to 4.0 mm. Collimation of CT acquisitions was 96 x 0.6 mm with a tube voltage of 120 kVp (kilovolt peak – see box #19 below), and a current of 340 mAs.

Box # 19

Kilovolt peak

Kilovolt peak (kVp) is the highest voltage expressed in the x-ray tube. It reflects the peak energy of the x-ray photon.²⁶⁰

The Gassenmaier et al. study results determined that in-stent lumen visibility in metallic stents was $\leq 80\%$ (i.e. 80% of the lumen diameter measured by the manufacturer was visible with CT) while in-stent lumen visibility in BRS was 100%.²⁵⁹ The authors also concluded that, in contrast to metallic stents, BRS produce no blooming artifacts and are radiolucent to CCTA, with the exception of two platinum markers at BRS extremities. Therefore, BRS radiolucency allows complete lumen visibility and assessment.²⁵⁹

There are several limitations to this study. First, not all tubes corresponded to the desired diameter of the stents after inflation. Therefore, some tubes were heated for the purpose of expansion. No visible changes of lumen diameter in these heated tubes were noticed, however, possible alterations of diameters cannot be eliminated from consideration. Second, a patient's increased heart rate or arrhythmia can cause motion artifacts, but heartbeat was not simulated in this study. Third, assessments of lumen diameter were performed by a single observer with a fixed window width of 1500 HU. Hence, errors and variability of results are not excluded with various window parameters. Finally, as this is an in vitro study, it does not account for the fact that in an in vivo study, the upper body surrounding the stented coronary can influence in-stent lumen visualization.²⁵⁹

Table 3 (below) illustrates the majority of in vivo studies performing quantitative CCTA analyses of DESolve and ABSORB BRS-stented coronary arteries and assessment of BRS patency. Some of the studies mentioned will subsequently be discussed in more detail.

Minimal luminal diameter (mm)	Minimal luminal area (mm ²)	Mean luminal area (mm ²)	Average lumen volume (mm ³)	Diameter stenosis (%)	Area stenosis (%)
A n/a	3.6 ± 0.9	5.2 ± 1.3	n/a	19 ± 9	34 ± 15
B n/a	3.5 ± 1.0	5.1 ± 1.4	n/a	n/a	22.7 ± 22.4
C n/a	3.10 (2.10-3.80) & 3.25 (2.20-4.30) p=0.21	4.47 (3.36-5.58) & 4.29 (3.38-5.73) p=0.11	72.12 at 18 mo 73.85 at 60 mo	n/a	31.6 (25.6-45.8) & 33.3 (13.2-40.7) p=0.25
D 2.9 ± 0.5	5.1 ± 2.3	6.7 ± 2.5	n/a	15.9 ± 10	n/a
E 3.09 ± 0.53	n/a	n/a	n/a	n/a	24.8 ± 17.8
F n/a	3.20 (2.80-4.20) & 4.00 (3.10-4.90) p=0.002	4.94 (3.83-6.30) & 5.76 (4.41-6.45) p=0.019	n/a	n/a	23.2 (11.42- 32.55) & 16.9 (3.33-29.91) p=0.357

Table 3. CT-based parameters measured in BRS-stented coronary arteries in recent studies.

A) An 18-month CT study by Serruys et al. (Lancet 2009) with 25 patients.⁷⁶

B) A study by Nieman et al. in J. Am Coll Cardiol 2013 (ABSORB trial cohort) – a quantitative CT analysis was performed on 61 patients within 18 months post-BRS implantation.²⁶¹

C) A study by Onuma et al. (JACC CardiovascInterv 2013) conducted with the ABSORB A cohort. CT angiography was performed at 18 months and again at 5 years. Comparison data presented for 18 patients.²⁶²

D) A 12-month CT study was done by Verheye et al. (JACC CardiovascInterv 2014) on 12 patients with DESolve stent.²⁶³

E) In this study by Marchese et al. (Minerva Cardioangiol 2016), a follow-up by CT angiography was performed at 1 year on 22 patients with a total of 25 BRSstents.²⁶⁴

F) Data is presented from a study by Onuma et al. (Eur Heart J. Cardiovasc Imaging 2017) in which 39 ABSORB Cohort B trial patients with bioresorbable stents underwent CCTA imaging at 18 months (25 patients) and 72 months (18 patients).²⁶⁵ Studies from A to E showed good BRS patency, while in study F there was one in-scaffold total occlusion. Copyright © 2018 [E Zdanovich].
n/a = not available; SD = standard deviation; values are reported as mean ± SD or as median with (interquartile range) where applicable; mo = months.

A study by Nieman et al.²⁶¹ investigated the performance of BRS by CCTA at 18 months (see table 3.B above). Seventy-one patients from the ABSORB trial had a CCTA scan. The ABSORB trial was a multicenter nonrandomized efficacy-safety single-arm study. Beyond the CT angiographic data presented in table III.B, clinical outcome was considered acceptable. Three non-Q-wave MI and 5 ischemia-driven target lesion revascularizations occurred at 18-month follow-up, with no cardiac deaths. The rate of major undesirable cardiac events was 7.9% (8 patients). By 18 months, angiographic patency was good. A limitation of this study is its non-randomized design.²⁶¹

The ABSORB Cohort A trial was a single-arm, prospective, open-label study with clinical endpoints and assessment with multiple imaging modalities (IVUS, OCT, and CT), involving 30 patients in four centers. All patients had a single *de novo* coronary artery lesion treated with a BRS (ABSORB scaffold).^{76,266} Clinical results of the ABSORB A trial are described in chapter 2, section 5.3. Twenty-five of the 30 patients (in three out of the four centers) underwent angiographic CT patency assessment after 18-mo follow-up, then 18 patients after 60-mo follow-up, using 6 different

scanners from 4 vendors. At 18 months, all BRS were patent at CT, with the exception of one patient whose CT was not interpretable because of severe motion artifacts.⁷⁶ At 60 months, the 18 BRS assessed with CT were patent.²⁶² More details of BRS stent patency results are illustrated in table 3 (A and C)(p. 122).

The 18-mo and 60-mo follow-up CT studies from the ABSORB A trials had a number of limitations. First, they involved a small number of patients. Second, they included only patients with single and simple anatomic lesions, thus limiting the generalizability of study results. Finally, not all patients of the ABSORB A trial underwent CT angiographic patency assessment.

In a subsequent 2017 study, Onuma et al. investigated the multicenter single-arm ABSORB Cohort B trial patients that were diagnosed with *de novo* non-complex lesions and treated with the second generation BRS.^{265,267} Patients were offered an optional CCTA investigation at 18 months and their consent was requested a second time for another optional CCTA at 72 months. Overall, Cohort B consisted of 101 patients out of whom 39 had CCTA assessments at both 18 and 72 months, and thus had paired angiographic data (see table 3.F, p.122). One scaffold was found to be occluded. Limitations of this study are similar to the limitations of Onuma's 2013 publication. Despite these limitations, this study has succeeded in demonstrating a significant longitudinal enlargement of in-scaffold lumen (see table 3.F, p.122).²⁶⁵

Overall, the stent patency of the aforementioned studies was good with only one occluded BRS stent in one out of the six studies. Moreover, one study even mentions significant in-scaffold enlargement over time.

4.1.5. CT-prediction of intrastent stenosis with plaque markers

In a recent study by Tesche et al.,²⁶⁸ a retrospective plaque analysis was performed on 74 patients who had undergone dual-source coronary CT within 3 months prior to stenting with metallic stents (28 BMS, 46 DES). During the follow-up, 21 of 74 stented lesions showed in-stent restenosis (ISR). Stent types were not specified. Following multivariate logistic regression analysis (adjusted

for dyslipidemia), 3 CT markers including non-calcified plaque volume, lesion length and remodeling index, were reported to have predictive values for in-stent restenosis (see table 4, below). A multivariate regression model is a single regression model in which two or more independent (or predictor) variables are used to predict (or estimate) a single dependant outcome or variable.^{269,270}

In ROC analysis, combining all three markers gave incremental predictive value (area under the curve of 0.89, $p < 0.0001$) with sensitivity = 90% and specificity = 84%. In conclusion, this study showed that non-calcified plaque volume, lesion length and remodeling index are predictive markers for in-stent restenosis. The study also determined that non-calcified plaque has good specificity and acceptable sensitivity for prediction of future in-stent stenosis, whereas lesion length and remodeling index have acceptable sensitivity and specificity.²⁶⁸

Vulnerability markers	OR (p-value)	SN (%)	SP (%)	AUC from ROC analysis (p-value)
NCPV	1.08 (p=0.045)	65	80	0.72 (p=0.001)
Lesion length	1.38 (p=0.0024)	74	74	0.77 (p<0.0001)
Remodeling index	1.13 (p=0.0019)	71	78	0.79 (p<0.0001)

Table 4. CT-based vulnerability markers of in-stent restenosis.²⁶⁸

N.B. OR = odds ratio; SN = sensitivity; SP = specificity; ROC = receiver-operating characteristics analysis; NCPV = non-calcified plaque volume; AUC = Area under the ROC curve.

There are several limitations to this study. The number of participating patients was not high, therefore larger studies are required to confirm this study's results. Furthermore, only one intrastent lesion was investigated per implanted stent per patient, in cases where there were many atheromatous lesions per implanted stent. The researchers did not perform correlation of their CCTA results with invasive imaging techniques since IVUS assessment was done in only six patients out of 21 with in-stent restenosis and OCT was not normally practiced in their institution.²⁶⁸

During my master's degree, I learned how to measure intrastent plaque vulnerability markers (see figs. 32 and 33, pp.126-128). Some of these markers, including lipid plaque volume and low-attenuation plaque, will be discussed as part of the core scientific work conducted by our team, to be detailed in chapter 5.

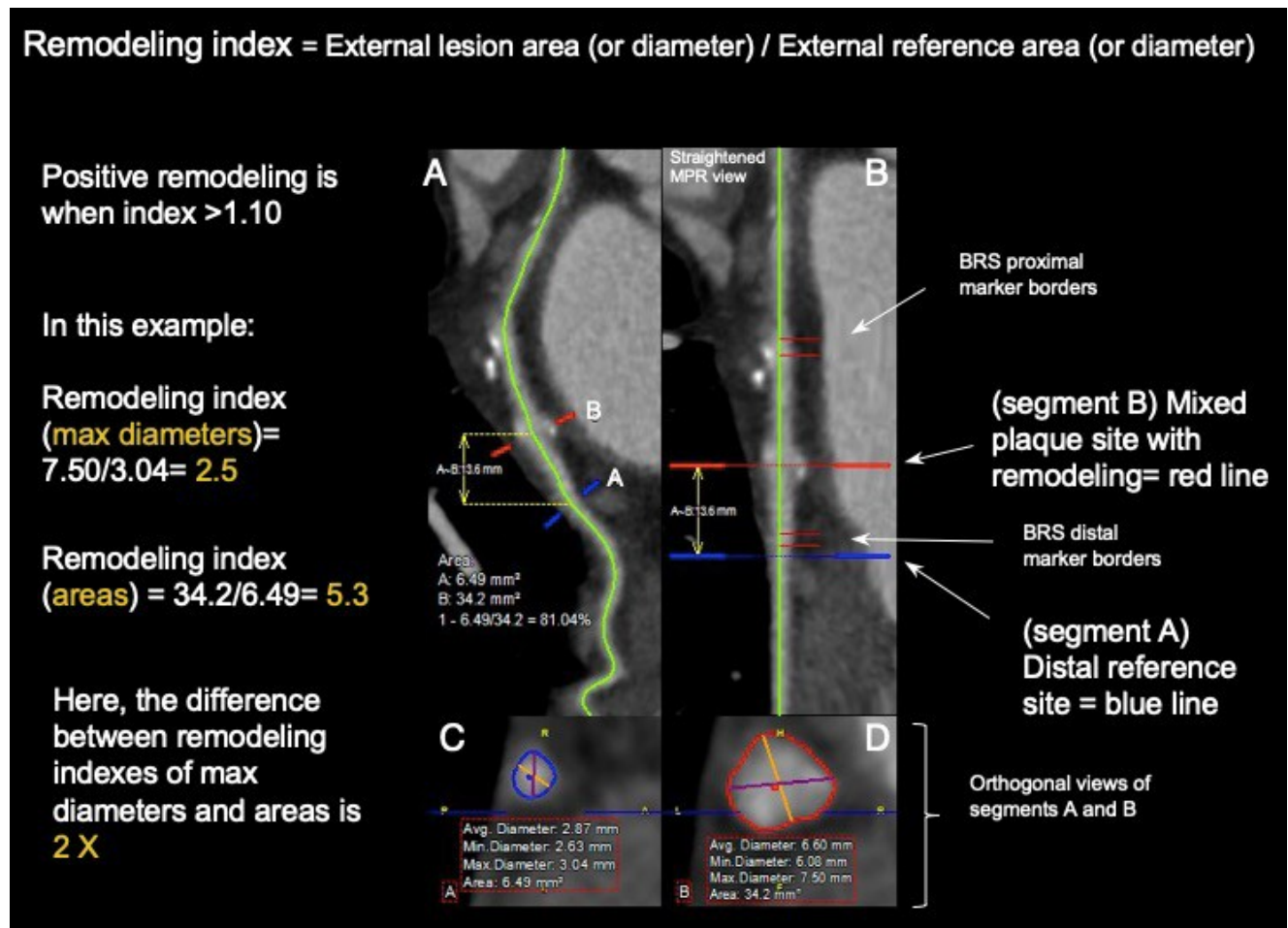


Figure 32. Calculating remodeling index of BRS-scaffolded coronary artery based on CCTA imaging.

This figure illustrates an example of remodeling index calculation using either maximal diameters or areas. As a reminder, remodeling index = external lesion area (or diameter) / external reference area (or diameter). Panel A depicts the curvilinear MPR view and panel B the straightened multi-planar review (MPR) view of the stented coronary with the blue line marking the healthy juxta-stent reference segment (segment A) and the red line indicating a segment with mixed plaque and positive remodeling located in the middle of the scaffolded region (segment B). The borders of the BRS platinum markers are delineated by two red lines. A cross-section of segment A is depicted in panel C and a cross-section of segment B in panel D, which offer the minimum, average and maximum diameters and areas of these segments' outer coronary walls. As illustrated in this figure, based on the aforementioned formula, the remodeling indexes based on maximal diameters and areas are calculated giving 2.5 and 5.3 units, respectively. In this example, both indexes are higher than 1.1²⁵⁸, which is the cut-off for positive remodeling, indicating that segment B has well-established positive remodeling. This example also shows that for the same segments, remodeling index calculations arrived at numbers around two times higher using areas than using diameters. Copyright © 2017 [E. Zdanovich]

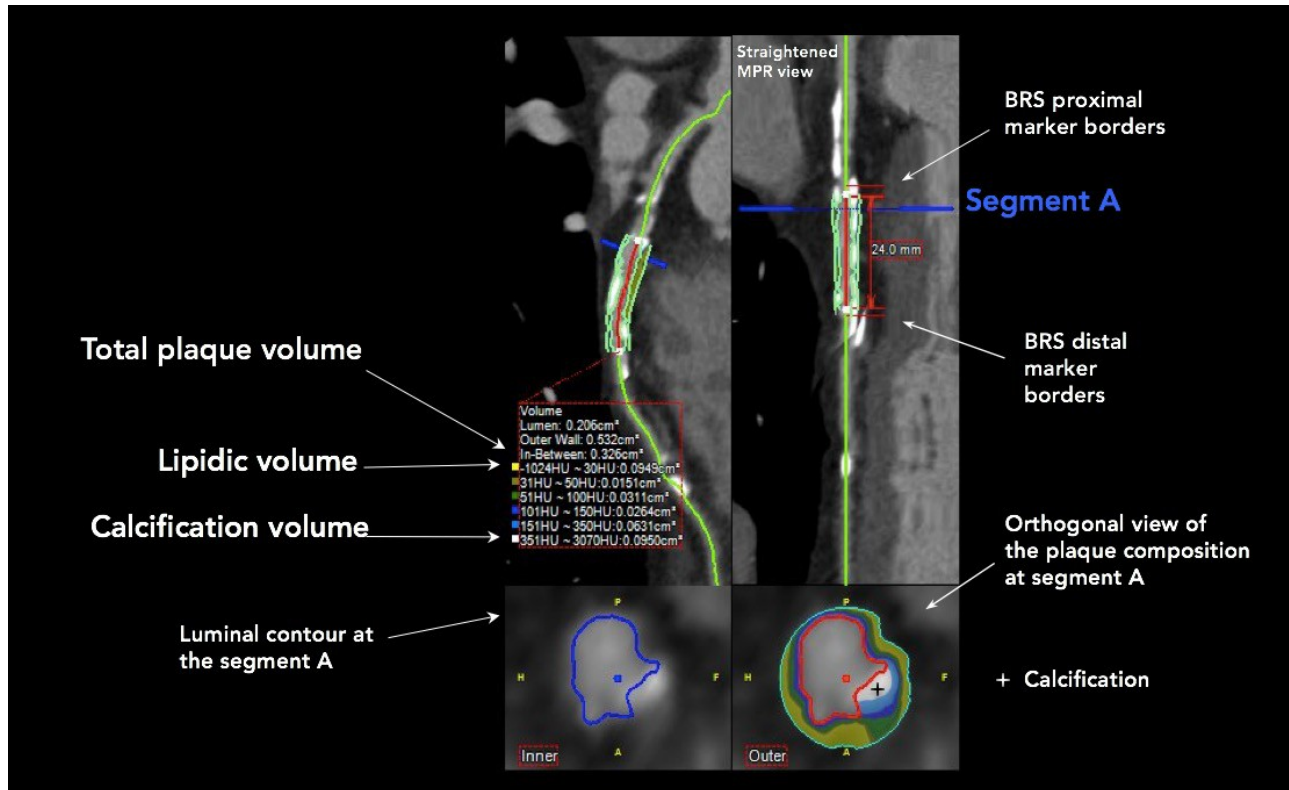


Figure 33. CCTA BRS imaging: plaque volume assessment with TeraRecon software (Aquarius Intuition version 4.4.12, TeraRecon Headquarters, Forster City, CA, USA).

Figure 37 continued: For the first time, the BRS scaffold allows in-stent plaque imaging with CCTA without need for blooming artifact reduction. In window A, a curvilinear MPR view of the stented artery can be visualized with the stratified composition volumes of its scaffolded portion. Low attenuation plaque appears in yellow and calcification in white. In window B, a straightened MPR view of the same portion of artery as the curvilinear MPR with a blue marker line called “Segment A”, which marks the position in the scaffolded segment of the two cross-sectional views illustrated in windows C and D. Window C depicts the contour of the lumen in blue. Window D illustrates the contour of the lumen traced in red, with the prevalent stratified compositions of the plaque in white, indicating calcification (marked with a cross) and other colours depicted in window A. Copyright © 2017 [E. Zdanovich]

4.1.6. IVUS and CT studies of intra- and juxta-BRS plaque

4.1.6.1. IVUS studies of intra- and juxta-BRS plaque imaging

Most studies that assessed intra- and juxta-bioresorbable stent plaque parameters used IVUS imaging. The follow-up range of these studies varies from 6 months to 5 years and their results are contradictory. In this subsection, the results of IVUS studies including plaque dimensions will be presented.

In 2011, Brugaletta et al.²⁷¹ published a study assessing longitudinal changes of plaque under BRS. In this study, 15 patients from the multicenter single-arm ABSORB Cohort B1 trial underwent virtual histology IVUS (see section 2.6.2) for analysis of plaque parameters under the stent, at baseline and at 6 months post-implantation. The authors found that the area of plaque under bioresorbable stents significantly increased from baseline to 6-month follow-up (see table 5, p.130).²⁷¹

Some limitations of this study should be taken into consideration. Virtual histology IVUS is a technique with an inherently high variability, which is not ideal for obtaining precise results in a study with a small number of patients, like this one.

Subsequently, in 2012, Ormiston et al.²⁶⁷ published another study with the ABSORB Cohort B1 trial patients investigating plaque progression under and juxta- bioresorbable stents. Serial-paired IVUS assessments were performed on 33 patients and showed that intra-, under- and juxta-stent plaque areas significantly increased by 6-month and 2-year follow-up (see table 5, below). No BRS thrombosis events were observed in this study. The two-year major adverse cardiac event rate was 6.8%.²⁶⁷

Study	ABSORB Cohort	No of patients	Region of interest	Units	Baseline	6-mo FU	1-year FU	2-year FU	3-year FU	4-year FU	5-year FU
Brugaletta 2011	B1	15	Intrastent	% change	↓ 30.2 % (p=0.005)	↓					
Ormiston 2012	B1	33	Intrastent	mm ²	0.51 ± 0.76 (p<0.001)	↓	0.25 ± 0.67 (p=0.03)	↓			
			Intra and juxta-stent	mm ²	0.57 ± 0.76 (p<0.001)	↓	0.41 ± 0.63 (p<0.001)	↓			
Serruys 2014	B2	44	Intrastent	mm ²	-0.57 ± 1.29 (p=0.007)		↓	0.58 ± 1.05 (p<0.001)	↓		
			Intra and juxta-stent	mm ²	-0.58 ± 1.08 (p<0.001)		↓	0.31 ± 0.93 (p=0.01)	↓		
Serruys 2016	B1	45	Intrastent	% change				↓	-9.86% (p = 0.0005)		↓
	B2	56	Intrastent	% change			↓	-1.69% (p=0.051)	↓	-10.01% (p = 0.0001)	↓

Table 5. IVUS assessment of plaque area changes under bioresorbable stents.^{92,267,271,272}

Baseline = post-implantation; mo = month; FU = follow-up; arrows indicate time points.

In a single-arm multicenter trial study published in 2014, Serruys et al. used IVUS to assess Absorb BRS in the ABSORB Cohort B2 (56 patients) at 12 and 36 months. Paired IVUS assessments in 44 patients (45 lesions) showed that from post-implantation to 1-year follow-up, the mean intrastent plaque area and total plaque area (intra- and juxta-stent) significantly decreased (see table 5, above). However, between the 1- and 3-year follow-ups, intrastent plaque and total plaque areas significantly increased.²⁷²

In a subsequent study, Serruys et al. further investigated plaque progression under bioresorbable stent with IVUS. This time, both the B1 and B2 cohorts from the ABSORB trial were included in the study. For cohort B1 (45 patients), IVUS assessments were performed at 6, 24 and 60 months, whereas cohort B2 (56 patients) underwent assessments at 12, 36 and 60 months. In cohort B1,

a highly significant decrease in intrastent plaque area occurred between 24 and 60 months. Similarly, intrastent plaque in B2 cohort had a near-significant decrease between 12 and 36 months and a highly significant decrease between 36 and 60 months (see table 5, p.130).⁹²

A limitation of this study should be noted. At 60-month follow-up, invasive imaging was not performed for half of the patients, since ethics committees in France and Germany did not grant approval for this assessment. It is likely that this was due to the invasive and controversial nature of the assessment, as bioresorbable stents are resorbed by 60 months. Therefore, the nonavailability of 60-month data could have affected the results.⁹²

In summary, the results of the clinical studies described above are contradictory, and further studies of plaque imaging under bioresorbable stents are needed.

In a retrospective study by Garcia-Garcia et al.,²⁷³ total plaque volume was analyzed by IVUS in two versions of Absorb BRS. The authors investigated version 1.0 (30 patients from Absorb cohort A²⁷³) and version 1.1 (45 patients from Absorb Cohort B²⁷⁴). This study showed that from post-implantation to 2-year follow-up, the Absorb BRS 1.1 had a significantly higher increase in total plaque volume than the previous model, the Absorb BRS 1.0 ($p=0.0499$). In addition, from the 1- to 3-year follow-up, the intrastent region of the Absorb BRS 1.1 showed a non-significant reduction of 2.2% in total plaque volume.²⁷³ Campos et al. state that variations in scaffold design differently affect vessel walls. Further studies are needed to understand the mechanisms of vessel wall response under scaffolds.²⁷⁵

4.1.6.2. CT studies of intra- and juxta-BRS plaque imaging

The next study, by Campos et al.,²⁷⁵ investigated plaque under BRS with CCTA. Campos et al. investigated whether plaque parameters change only in scaffolded segments or if the change is also seen in other coronary segments within the same patient. Thirty patients from a single-arm ABSORB Cohort A trial were included in this prospective study.²⁷⁶ The patients, who all had single *de novo* lesions of diameter stenosis >50% in native coronaries of 3.0 mm in diameter, underwent

a PCI intervention with a first generation ABSORB bioresorbable stent (version 1.0) of either 12 or 18 mm in length. Eighteen patients (18 BRS) with ACC/AHA lesion classifications of type B1 (9 patients, 50%) and B2 (9 patients, 50%) underwent CCTA at 18-month and 5-year follow-up. Four centers participated in total, with scanners used to perform CCTA varying from 64- to 256- to 320-slice CT. By following the modified 17-segment American Heart Association model,²⁷⁷ only major epicardial vessels were analyzed, including proximal and mid segments of the right coronary artery, left circumflex and left anterior descending coronaries. As a comparator to the intrastent regions, four inpatient nonintervened native coronary segments, including the two most proximal segments of the nonintervened arteries, were used in the analysis. The objective of this study was to perform an inpatient comparison of paired segments of the intrastent region and nonintervened segments for various parameters such as plaque volume, plaque burden and percent change in plaque atheroma volume.²⁷⁵

Percent atheroma volume and normalized total atheroma volume were part of imaging endpoints. Normalization for segment lengths was performed to allow equal inpatient weighting between different segments of the coronary tree and equal interpatient weighting, therefore organizing the atheroma parameters between patients for more standardized calculation of the atheroma volumes.²⁷⁸ Below are the formulas used by Campos et al.²⁷⁵:

Plaque burden per unit length or total plaque index is defined as follows²⁷⁹:

$$\text{Total plaque index (mm}^2\text{)} = \frac{\text{segmental plaque volume (mm}^3\text{)}}{\text{Segment length (mm)}}$$

$$\text{Percent atheroma volume} = \frac{\text{total vessel volume} - \text{total lumen volume}}{\text{total vessel volume}} * 100\%$$

Normalized total atheroma volume = total vessel – lumen volume * mean segment length in population.

The comparison of continuous variables between the two different follow-up points was performed with t-test statistical analysis.

Some of the results of this study are as follows. At baseline, the mean lesion length was 9.1 ± 3.6 mm. Out of 72 analyzable nonintervened segments, 1 segment was excluded due to the presence of motion artifacts at 18-month follow-up. The mean BRS length was 11.9 ± 1.9 mm and the mean nonintervened segment length was 22.6 ± 11.7 mm.²⁷⁵

Plaque burden and atheroma volume in the scaffolded segments did not show significant changes between the 18-month and 5-year follow-up time points. On the other hand, significant longitudinal increase in the mean plaque burden and total atheroma volume was observed in the control segments, $+2.7 \pm 6.5\%$ and $+8.0 \pm 22.8 \text{ mm}^3$, both $p < 0.01$, respectively.²⁷⁵

When mean serial changes between scaffolded and control segments were compared, analysis showed a significant difference ($p < 0.03$) in the evolution of percent atheroma volume. No significant difference was shown for mean serial changes between scaffolded and control segments for normalized total atheroma volume ($p = 0.10$).²⁷⁵

Campos et al. attributed the decrease in plaque burden to release of rapamycin and rapalogs, such as everolimus, that coat BRS struts, which inhibits *mammalian target of rapamycin* (mTOR) cellular complex, resulting in prevention of macrophage and lipid accumulation in a plaque.²⁸⁰ Moreover, everolimus on its own, through local autophagic and lipophagic responses, reduces the number of macrophages and lipid particles in a plaque.²⁸¹

There are some limitations to this study. It assessed patients as a first-in-human trial, with some patients presenting low clinical and anatomical complexity. Also, the sample size of this study was small. Therefore, these findings should be considered as hypothesis-generating. As a result, no definitive statement can be made about the efficacy of Absorb BRS in plaque regression. Finally, progression/regression studies show that when percent atheroma volume is large at the baseline, its chance of regression is higher than with smaller atheromas.²⁷⁵ Considering this finding, one can conclude that plaques have stronger potential for regression at the scaffolded segments.²⁷⁵

This study by Campos et al. has opened new possibilities for further research, as is the case with my master's project, in which, in addition to intrastent plaque volume, we have also investigated longitudinal change in plaque volume in the proximal and distal edges of the stent along with the plaque composition in the intrastent and juxta-stent.

In summary, there is discordance in studies as to whether plaque under the stent is increasing or decreasing at a given time point. Therefore, more studies are needed to investigate this discordance and the mechanisms of plaque evolution, in order to improve scaffold design.

Chapter 5 – The essence of my work

The title of my master's project is: "Coronary bioresorbable stents: Non-invasive quantitative evaluation of intra- and juxta-stent plaque composition – A computed tomography longitudinal study." This chapter is presented as an article that we would like to publish.

5.1. Introduction and hypothesis

Coronary bioresorbable stents (BRS) are made of a bioresorbable polymer that, unlike metal, progressively degrades and disappears within 2-3 years.⁸⁰ In contrast to metallic stents, BRS do not produce significant artifacts on computed tomography (CT).^{141,259,282} They can be identified on CT by platinum indicators located at each end of the stent, while the rest of the stent is radiolucent.²⁵⁹ Therefore, this novel scaffold platform allows CT assessment of intrastent atherosclerotic plaque without obstruction by metallic artifacts. In addition, CT evaluation of BRS can be performed on stent sizes of less than 2.5 mm in diameter.²⁸³

CT assessment of native coronary plaque has been available for many years. Qualitatively, it is possible to image calcified and non-calcified coronary plaque and luminal narrowing.²⁸⁴ Quantitatively, CT allows measurement of plaque volumes^{285,286} and, since a large lipid core²⁸⁷ is one of the features of vulnerable plaque, to observe evolution in plaque composition after lipid-lowering therapy²⁸⁸ through Hounsfield Unit (HU) analysis.

Non-calcified lipidic plaque or, in HU analysis, low attenuation plaque (LAP), is known for its potential to rupture.²⁸⁹ Low attenuation, remodelling index of >1.1 and spotty calcifications are predictors of plaque instability and are thus described as high-risk features or vulnerability markers.^{136,258} Studies have shown that LAP volume is greater in patients who had acute coronary events in the first year post-intervention.²³⁹

Understanding plaque evolution provides us with the potential to improve our understanding of the development of coronary artery disease (CAD), which could help us prevent and treat cardiovascular events. By identifying patients with high risk plaque, early treatment could be initiated, and plaque size and composition monitored.²⁸⁴ The increased ability of CT to assess intrastent plaque within bioresorbable stents offers a novel non-invasive model for assessment of atherosclerotic plaque evolution after percutaneous coronary intervention.

PRIMARY OBJECTIVE OF THE STUDY:

The aim of our study was to demonstrate the feasibility of non-invasive CT evaluation of the volume and composition of intrastent coronary plaque as well as plaque at stent edges.

5.2. Methods

5.2.1. Study design

This is a prospective cohort study that recruited consecutive patients with BRS for a 256-slice ECG-synchronized CT assessment at 1 and 12 months after stent implantation. We decided to choose 1-month follow-up to collect the data close to the post-implantation such that it could be compared with a more longitudinal follow-up time as 12 months. At 12 months, BRS is almost in the middle of its lifespan still providing good support to coronary artery (see chapter 2 for more information).

5.2.2. Ethical considerations

The Institutional Review Board of the *Centre Hospitalier de l'Université de Montréal* (CHUM) approved the protocol. All subjects provided written informed consent.

5.2.3. Study patients

The present study is nested in the ReABSORB registry which is a dual-centre, prospective, nonrandomized, observational registry of patients treated with an everolimus-eluting BRS (ABSORB™, version 1.1) at either the Centre Hospitalier de l'Université de Montréal in Montreal (CHUM) or the Cité-de-la-Santé Hospital in Laval, Quebec.¹⁰⁵ Twenty-seven consecutive patients (36 BRS) (mean age 59.7 +/- 8.6 years old; 17 males, 59.3 +/- 8.9 years old; 10 females, 60.5 +/- 8.3 years old) from the ReABSORB registry were prospectively

enrolled in the present study. A consenting adult population, defined as aged 18 years and older, was part of the criteria for inclusion. Exclusion criteria were renal impairment and adverse reaction to contrast agents.¹⁰⁵

5.2.3.1. Novel implantation protocol

BRS implantation was performed at the cardiologist's discretion with no mandated technique.¹⁰⁵ Nonetheless, the following procedure was recommended: (1) to select appropriate BRS size and adequate vessel preparation, vessel sizing was performed with QCA, OCT or IVUS; (2) a balloon at least 5 mm shorter than the chosen BRS length was deployed in a procedure called predilation preparation, where balloon diameter correspond in a 1:1 ratio with reference vessel diameter; (3) Slow deployment of BRS, respecting reference vessel diameter, was conducted in 2-atm increments every 5 seconds until the BRS was completely deployed at a maximum pressure of 12-18 atm; and (4) to prevent BRS non-appositions, postdilation was to be performed with a noncompliant balloon with ≥ 0.25 -0.5mm higher diameter than the BRS.¹⁰⁵

5.2.3.2. CT study patients

Two CT scans were planned for each patient, at 1 and 12 months after stent implantation. Twenty-seven patients (35 stents) had a CT scan at 1-month post-intervention. Among these 27 patients, 21 patients (26 stents) were scanned a second time at approximately 12 months post-intervention. Six patients did not have the second scan: hypersensitivity to contrast agent (1 patient), study withdrawal (3 patients), incarceration (1 patient) and loss to follow-up (1 patient).

5.2.4. CT imaging

5.2.4.1. Patient preparation

Prior to scan, patients received 0.4 mg nitro-glycerin sublingually and 25-75 mg metoprolol PO if their heart rate was >60 beats per minute (bpm), unless contraindicated.

5.2.4.2. CT acquisition protocol

A 256-slice ECG-gated CT scanner (Brilliance iCT, Philips Healthcare, Best, The Netherlands) was used to perform all examinations. Prospective ECG-gating was used for heart rates ≤ 70 bpm and retrospective ECG-gating for higher heart rates.

5.2.4.3. Contrast administration protocol

Patients received one of the following contrast agents (see Table 8): iopamidol (370 mg/mL, Isovue 370, Bracco Imaging, Montreal, Canada); iodixanol (320 mg/mL, Visipaque 320, GE Healthcare Canada Inc., Mississauga, Ontario, Canada); or iohexol (350 mg/mL, Omnipaque 350, GE Healthcare Canada Inc., Mississauga, Ontario, Canada). Contrast agent was administered with a power injector at a flow rate of 5 mL/s. About 60 to 80 ml of contrast was administered according to patient BMI.

5.2.4.4. CT image reconstruction and post-processing

Axial reconstruction was done using a medium-smooth kernel (XCB, Philips Healthcare, Cleveland, OH, USA) with a slice thickness of 0.8 mm. Iterative reconstruction (IR) was performed with a hybrid statistical algorithm (Philips iDose, Philips Healthcare, Level 3). Post-processing of images was performed by TeraRecon (Aquarius Intuition version 4.4.12, TeraRecon Headquarters, Forster City, CA, USA).

5.2.4.5. Radiation dose

Effective radiation dose was obtained by multiplying total dose-length product (DLP) with a conversion coefficient of $0.014 \text{ mSv /cm}^{-1} \cdot \text{mGy}^1$.

5.2.5. CT imaging analysis

For coronary intrastent and edge plaque analysis, 3 coronary locations were defined as pre-stent, intrastent and post-stent zones (see fig. 34 below). Each of these zones were then divided into blocks of 5 mm in length, along the long axis of the arteries. Pre-stent and post-stent zones are each represented by one block. The intrastent zone ranged from one to five blocks, depending on the length of the stent. Intrastent block count began at the platinum indicator of the proximal stent edge and ended close to the indicator of the distal edge.

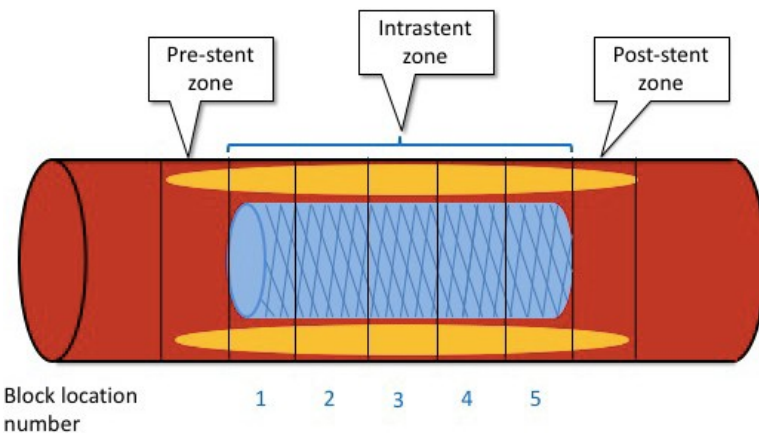


Figure 34. Pre-, intra- and post-stent zone composition in 5-mm blocks (vertical rectangles). Pre-stent zone is the most proximal, while post-stent zone is the most distal. Bioresorbable stents have 2 platinum indicators located at each extremity of the stent in intrastent blocks numbered 1 and 5. 2016 © [Omar Arfa et Evguenia Zdanovich]

The coronary segments were described according to nomenclature established by the American College of Cardiology / American Heart Association guidelines for coronary angiography in 1999.²⁹⁰

Plaque analysis included total plaque volume (mm^3), absolute LAP volume (mm^3) and relative LAP volume (%) per block plaque volume in the pre-, intra- and post-stent zones. LAP was defined as plaque component with CT attenuation of <30 Hounsfield units (HU). Relative LAP volume was defined as absolute LAP volume / total plaque volume (%). LAP volume was detected automatically by software in 5-mm length coronary blocks following manually-traced vessel contours (see fig. 35, p.142). Image postprocessing was performed by a trained operator using semi-automated software (Aquarius iNtuition 4.4.12, TeraRecon Inc., Foster City, CA, USA). Comparison was made between 1-mo and 12-mo post-BRS implantation. Care was taken for plaque analysis to be performed at the same location in a given coronary artery for the 1- and 12-mo scans.

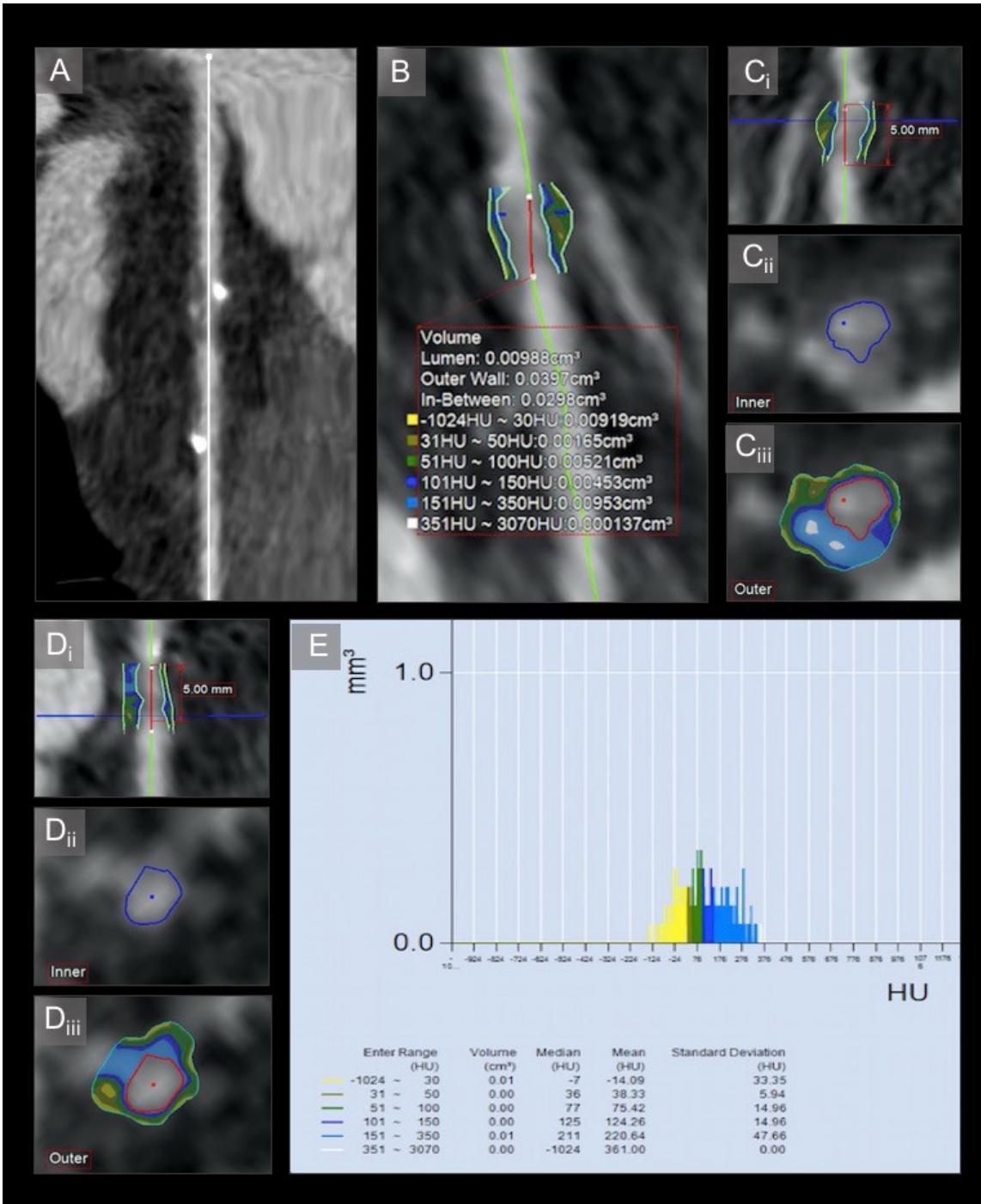


Figure 35. Volumetric plaque analysis. (A) Straightened MPR, stenosis at the proximal edge of the BRS in middle left anterior descending coronary artery (more details in Figure 36, p. 146). (B) Volumetric analysis of plaque HU-stratification. (Ci) Position in plaque of axial slice presented in views Cii and Ciii. (Cii) Axial view of lumen in Ci slice. (Ciii) Axial view of mixed plaque with LAP and two spotty

calcifications. (Di) Position in plaque of axial slice presented in views Dii and Diii. (Dii) Axial view of lumen in Di slice. (Diii) Axial view of LAP plaque. (E) Histogram of plaque composition stratification. LAP (9.19 mm³) represents one third of total plaque volume (29.8 mm³). 2018 © [Omar Arfa and Evguenia Zdanovich]

5.2.6. Statistical analysis

Data are expressed as mean \pm standard deviation or median [interquartile range] for continuous variables and frequency (%) for categorical variables. The mixed effects models were used to assess changes in total plaque volume and absolute or relative LAP volumes, and these account for the correlation between repeated measurements (mixed procedures in SAS software, version 9.4; SAS Institute, Cary, NC). Assessed coronary artery vessels and stented regions were divided into 3 zones (pre-stent, intra-stent, and post-stent). The intra-stent zone was further divided in 3 equidistant thirds using piecewise linear regression. P-values of <0.05 were considered statistically significant. Multiple comparisons were adjusted with Bonferroni correction in the ANOVA post hoc analysis.²⁹¹

5.3. Results

5.3.1. Study patients

The 27 patients had a total of 36 stented coronary artery segments: 25 (69%) of these segments were on the left coronary artery, and 11 (31%) on the right coronary artery (see table 6 below). All BRS could be assessed with CT at both 1-mo and 12-mo follow-up. One patient demonstrated intrastent stenosis in the LAD at 12-mo scan. This stenosis was subsequently dilated using an everolimus-eluting metallic stent (see fig. 36, p.146). The other 35 implanted stents were patent at the 1-mo and 12-mo CT scans.

Patient demographics and scanning parameters are described in tables 7 and 8 (pp.147-148). Based on ACC / AHA classification of coronary lesions,¹¹⁵ most lesions were classified as low- (class A, 31%) to moderate-risk (class B, 66%) before BRS implantation (see table 9, p.149). Most BRS had a length of 18 (47 %) or 28 (47 %) mm, with a mean length of 22.4 ± 5.6 mm (see table 10, p.150).

Table 6. Stent distribution parameters

N patients at 1st scan*	27 (100)
N patients at 2nd scan	21 (78)
Total n of stents	36 [§]
N of stents at 1st scan	35 (97)
N stents at 2nd scan	26 (72)
Time interval (days) (min-max)**:	
From BRS implantation to 1st scan	35.8 ± 38.4 (7-188)
From BRS implantation to 2nd scan	393.7 ± 45.3 (247-453)
From 1st to 2nd scan	356.7 ± 68.6 (185-446)
N of coronary segments stented by BRS among the whole group of patients***	36
<u>Left coronary artery:</u>	
Proximal LAD	7 (19)
Mid LAD	12 (33)
Distal LAD	1 (3)
First diagonal	1 (3)
Proximal Cx	1 (3)
Mid Cx	1 (3)
Distal Cx	1 (3)

1st obtuse marginal	1 (3)
<u>Right coronary artery:</u>	
Proximal RCA	2 (6)
Mid RCA	6 (17)
Distal RCA	2 (6)
PDA	1 (3)
N of stented segments / patient	1.3 ± 0.6 (1-3)
Stent length (mm)	22.4 ± 5.6 (12-28)
Stent diameter (mm)	3.2 ± 0.4 (2.5-3.5)

* Categorical variables are reported as n (%)

** Continuous variables are reported as (mean ± SD) (min-max)

*** Coronary segments were defined as per the American College of Cardiology / American Heart Association guidelines for coronary angiography.²⁹²

§ One stent imaging was only performed at 12-mo as one patient had a second BRS implanted after his 1-mo scan of his first BRS. Thus, there are 35 stents at 1-mo scan but a total of 36 stents for both scans.

LAD = left anterior descending coronary artery; Cx = circumflex coronary artery; RCA = right coronary artery; PDA = posterior descending coronary artery; SD = standard deviation.

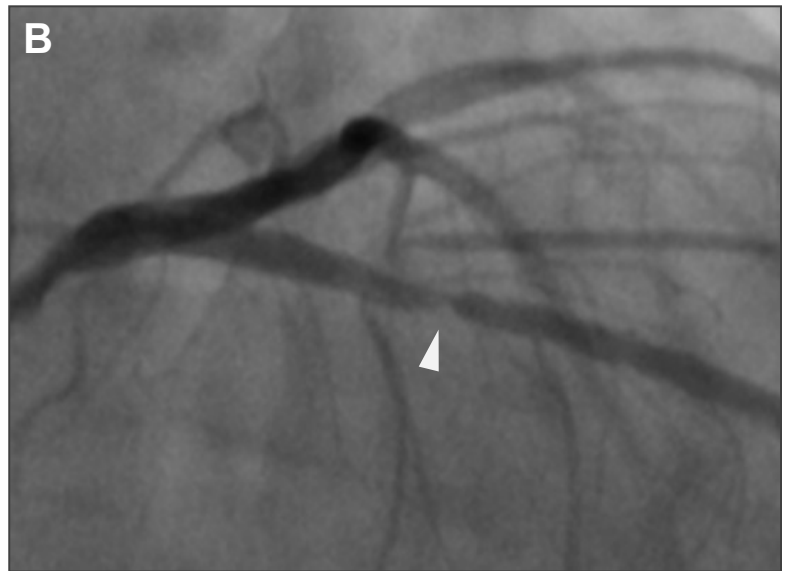
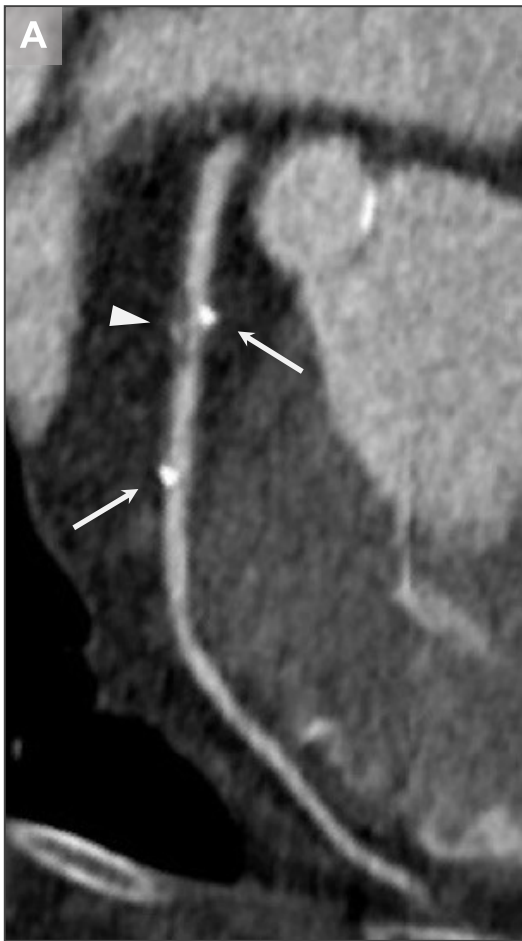


Figure 36. Intrastent stenosis.

A) ECG-gated 256-slice coronary CT angiography 14 months after BRS implantation in a 61-yo woman. An edge and intrastent mixed plaque with severe stenosis and positive remodeling is shown (arrowhead). Proximal and distal platinum indicators of BRS (2.5 x 18 mm) are also visible (arrows).

B) Conventional coronary angiography. Severe intrastent stenosis is also shown. The patient underwent stenting with an everolimus-eluting metallic stent in the same session.

Table 7. Patient demographics**(N patients= 27)**

Male gender *	17 (63)
Age (years) **	59.7 ± 8.5 (41-77)
BMI (kg/m ²)	27.0 ± 5.7 (18-43)

Risk factors:

Dyslipidemia	13 (48)
Diabetes	2 (7)
Hypertension	16 (59)
Smoking history	11 (41)
TIA / stroke	1 (5)

PCI indications:

Stable angina	7 (32)
Unstable angina	6 (27)
NSTEMI	5 (23)

* Categorical variables are reported as n (%)

** Continuous variables are reported as (mean ± SD) (min-max)

Table 8. Scan parameters

	1-mo	12-mo
Prospective ECG gating *	26 (96)	19 (95)
Retrospective ECG-gating	1 (4)	1 (5)
100 kV Voltage	0	6 (29)
120 kV Voltage	27 (100)	15 (71)
Current (mA)(min-max)**	828.9 ± 125.9 (551-1199)	775.4 ± 109.6 (496-1000)
DLP scan (mGy•cm)	413.9 ± 220.9 (226-1456)	372.8 ± 217.4 (164-1214)
Effective dose scan *** (mSv)	5.8 ± 3.1 (3-20)	5.2 ± 3.0 (2-17)
Z-coverage (mm)	152.7 ± 19.5 (125-192)	166.4 ± 21.2 (125-191)
Prescan metoprolol *	16 (59)	14 (88)
Prescan nitroglycerin *	24 (92)	19 (100)
Contrast type *:		
Iodixanol (320 mg I/mL)	12 (46)	6 (30)
Iopamidol (370 mg I/mL)	11 (42)	13 (65)
Iohexol (350 mg I/mL)	3 (12)	1 (5)

* Categorical variables are reported as n (%);

** Continuous variables are reported as (mean ± SD) (min-max);

*** The effective radiation dose = total DLP•conversion coefficient k, where

$k = 0.014 \text{ mSv} \cdot \text{mGy}^{-1} \cdot \text{cm}^{-1}$; n = number of patients, SD = standard deviation; mg I/mL = mg of iodine per milliliter.

Table 9. Pre-implantation lesion characteristics as assessed on conventional angiography (N stents= 29)

Lesion length (mm)*	13.2 ± 4.6 (8-24)
Calcifications	2 (7)
Lesion type***	
A	9 (31)
B1	11 (38)
B2	8 (28)
C	1 (3)
Vessel angulation**	
< 45°	26 (90)
45°-90°	3 (10)
Bifurcations	5 (17)

* Continuous variables are reported as (mean ± SD) (min-max);

** Categorical variables are reported as n (%);

*** Based on ACC / AHA classification of coronary lesions.

Lesion type A is discrete, concentric with smooth contours and absence of thrombus. Lesion type B is tubular, eccentric with some thrombus potentially present, where subtype B1 is determined by one type B characteristic and subtype B2 by ≥ 2 characteristics.

Lesion type C is diffuse and high risk, and is present in tortuous and extremely angulated coronary segments.¹¹⁵

Table 10. Description of the different sizes of BRS in our study (36 stents total)

Scaffold design	BRS diameter (mm)	BRS length (mm)		
		12	18	28
Small	2.5	0	4	2
	3.0	0	6	5
Medium	3.5	2	7	10

Numbers in the matrix represent number of stents.

5.3.2. CT plaque analysis

Plaque analysis was performed on a per-block basis. There were 177 (88%, 177/201) assessable blocks at 1-mo post-implantation out of a total of 201 blocks. For matched comparison at 12-mo, 132 (66%, 132/201) blocks were assessable out of 201 blocks for a total of 309 block assessments (77%, 309/402) for both scans. Ninety-three (23%, 93/402) blocks were non-assessable for longitudinal imaging analysis. Reasons for non-assessability of the 93 blocks were: absence of a second scan (6 patients, 11 stents, 51 blocks); absence of a first scan (1 patient, 1 stent, 7 blocks); stent overlap (4 patients, 10 stents, 21 blocks); image artifacts that were non-BRS non-blooming mostly due to motion and breathing (8 patients, 8 stents, 9 blocks); and blocks shorter than 5 mm (4 patients, 4 stents, 5 blocks).

5.3.2.1. Plaque volume analyses

Plaque volume using the 5mm-long blocks model of segmentation:

Table 11 below shows mean plaque volume of the pre-, intra- and post-stent blocks after 1- and 12-month follow-up, according to the 5mm-long model of plaque segmentation. Intrastent

block location is divided from proximal to distal blocks. There is a slight decrease in plaque volume from 1-mo to 12-mo follow-up in all locations, although this was not significant. More distal plaque shows greater decrease in volume in comparison to more proximal plaque, at 1-mo and 12-mo follow-up.

Table 11. Plaque volume at 1- and 12-month follow-up by block location
(pre-, intra 1-, 2-, 3-, 4-, 5-, and post-stent blocks).

Block location ¹	Plaque volume (mean ± SD, mm ³) (# blocks) at 1-mo scan	Plaque volume (mean ± SD, mm ³) (# blocks) at 12-mo scan	Volume variation (%) between scans	p-value
Pre-stent	30.38 ± 11.83 (28)	26.06 ± 10.81 (18)	-14	0.803
Intrastent 1	31.85 ± 12.06 (33) 0.018	31.63 ± 12.67 (25) 0.011 0.017	-1	0.627
Intrastent 2	32.11 ± 12.95 (34) 0.008	30.23 ± 11.25 (26) 0.031	-6	0.722
Intrastent 3	29.58 ± 10.72 (30)	27.32 ± 11.51 (24)	-8	0.567
Intrastent 4	31.53 ± 12.01 (14)	29.23 ± 15.81 (12)	-7	0.286
Intrastent 5	26.26 ± 5.67 (9)	22.00 ± 6.94 (7)	-16	0.324
Post-stent	24.24 ± 11.08 (29)	22.73 ± 10.13 (20)	-6	0.748

Legend for Table XI:

¹A total of 27 patients, 36 stents and 309 blocks were analyzed.

Note: Intrastent blocks are enumerated (1 to 5) from proximal to distal edge of stent. Some stents are only 1-,2-,3-, or 4-blocks long (see stent dimensions in Table 10, p.150). = intra-group p-values represented in blue bubbles. P-values are obtained by ANOVA analysis with Bonferroni correction.

Plaque volume using the tertiles model of segmentation:

Table 12 below demonstrates plaque volume in pre-, intra- and post-stent locations at 1- and 12-month scans. Intrastent plaque is classified into proximal, median and distal tertiles. There is no significant change in plaque volume from 1-mo to 12-mo follow-up in all locations.

Table 12. Plaque volume at 1- and 12-month follow-up by plaque location
(pre-, 1st, 2nd, and 3rd intrastent tertiles, and post-stent plaque)

Plaque location ¹	Plaque volume (mean ± SE, mm ³) at 1-mo scan	Plaque volume (mean ± SE, mm ³) at 12-mo scan	Volume variation (%) between scans	p-value
Pre-stent	29.9 ± 2.2	27.7 ± 2.2	-7	0.307
Proximal intrastent tertile	31.7 ± 2.4	32.0 ± 2.9	1	0.920
Middle intrastent tertile	31.5 ± 2.3	29.7 ± 2.4	-6	0.272
Distal intrastent tertile	29.1 ± 1.8	26.7 ± 2.4	-8	0.155
Post-stent	24.0 ± 2.0	23.0 ± 2.0	-4	0.915

¹A total of 27 patients, 36 stents and 309 blocks were analyzed. Nomenclature: there are 3 intrastent tertiles. The first tertile lies distally adjacent to the pre-stent block. The last (3rd) tertile lies proximally adjacent to the post-stent block. P-values are obtained by spline regression multivariate analysis.

5.3.2.2. LAP volume analysis

LAP volume using the 5mm-long blocks model of segmentation:

Table 13 below shows mean LAP volume of pre-, intra- and post-stent blocks after 1- and 12-month follow-up, according to the 5mm-long model of plaque segmentation. There is no significant change in LAP volume from 1-mo to 12-mo follow-up in all locations.

Table 13. Absolute LAP volume at 1- and 12-month follow-up by block location
(pre-, intra 1-, 2-, 3-, 4-, 5-, and post-stent blocks).

Block location ¹	LAP volume (mean ± SD, mm ³) (# blocks) at 1-mo scan	LAP volume (mean ± SD, mm ³) (# blocks) at 12-mo scan	Volume variation (%) between scans	Inter-follow-up p-value
Pre-stent	7.88 ± 4.66 (28)	6.09 ± 2.61 (18)	-23	0.139
Intrastent 1	8.09 ± 5.74 (33)	8.13 ± 4.29 (25)	0.5	0.866
Intrastent 2	7.77 ± 4.87 (34)	7.47 ± 5.26 (26)	-4	0.861
Intrastent 3	6.38 ± 2.70 (30)	6.85 ± 4.37 (24)	7	0.336
Intrastent 4	7.14 ± 2.52 (14)	7.68 ± 4.84 (12)	8	0.385
Intrastent 5	6.30 ± 3.04 (9)	5.76 ± 2.14 (7)	-9	0.995
Post-stent	6.35 ± 3.93 (29)	6.16 ± 4.13 (20)	-3	0.997

¹A total of 27 patients, 36 stents and 309 blocks were analyzed

Note: Intrastent blocks are enumerated from proximal to distal edge of stent. Some stents are only 1-,2-,3- or 4-blocks long (see stent dimensions in Table 10, p.150). P-values are obtained by ANOVA analysis with Bonferroni correction.

LAP volume using the tertiles model of segmentation:

Table 14 below demonstrates LAP volume in pre-, intra- and post-stent locations after 1- and 12-month scans, using the tertile model of segmentation for intrastent plaque. There is no significant change in LAP volume from 1-mo to 12-mo follow-up in all locations.

Table 14. Absolute LAP volume at 1- and 12-month follow-up by plaque location (pre-, 1st, 2nd, and 3rd intrastent tertiles, and post-stent blocks).

Plaque location ¹	LAP volume (mean ± SE, mm ³) at 1-mo scan	LAP volume (mean ± SE, mm ³) at 12-mo scan	Volume variation (%) between scans	p-value
Pre-stent	7.7 ± 0.8	6.6 ± 0.7	-13	0.305
Proximal intrastent tertile	8.0 ± 1.1	7.6 ± 0.9	-6	0.600
Middle intrastent tertile	7.4 ± 0.8	7.2 ± 0.9	-2	0.827
Distal intrastent tertile	6.4 ± 0.6	7.0 ± 1.0	8	0.527
Post-stent	6.3 ± 0.7	6.2 ± 0.9	-2	0.749

¹A total of 27 patients, 36 stents and 309 blocks were analyzed. Nomenclature: there are 3 intrastent tertiles. The first tertile lies distally adjacent to the pre-stent block. The last (3rd) tertile lies proximally adjacent to the post-stent block. P-values are obtained by spline regression multivariate analysis.

5.3.2.3. Relative LAP (%) analysis

Relative LAP volume using the 5mm-long blocks model of segmentation:

Table 15 below shows mean ratio of LAP volume over total plaque volume (%) in the pre-, intra- and post-stent blocks after 1- and 12-month follow-up, according to the 5mm-long model of plaque segmentation. There is no significant change in relative LAP volume from 1-mo to 12-mo follow-up in all locations.

Table 15. Relative LAP volume at 1- and 12-month follow-up by block location

(pre-, intra 1-, 2-, 3-, 4-, 5-, and post-stent blocks).

Block location ¹	% LAP volume (mean ± SD, %) (# blocks) at 1-mo scan	% LAP volume (mean ± SD, %) (# blocks) at 12-mo scan	Volume variation (%) between scans	Inter-follow-up p-value
Pre-stent	27.08 ± 12.60 (28)	25.14 ± 9.29 (18)	-7	0.312
Intrastent 1	24.26 ± 12.32 (33)	25.73 ± 10.77 (25)	6	0.640
Intrastent 2	24.59 ± 11.17 (34)	23.67 ± 9.25 (26)	-4	0.606
Intrastent 3	23.14 ± 10.55 (30)	24.94 ± 10.62 (24)	8	0.450
Intrastent 4	24.60 ± 8.18 (14)	27.72 ± 10.69 (12)	13	0.198
Intrastent 5	24.55 ± 10.97 (9)	27.94 ± 10.68 (7)	14	0.389
Post-stent	27.88 ± 12.31 (29)	29.01 ± 13.89 (20)	4	0.715

¹A total of 27 patients, 36 stents and 309 blocks were analyzed Note: Intrastent blocks are enumerated from proximal to distal edge of stent. Some stents are only 1-,2-,3- or 4-blocks long (see stent dimensions in Table 10, p.150). P-values are obtained by ANOVA analysis with Bonferroni correction.

Relative LAP volume using the tertile model of segmentation:

Table 16 below demonstrates mean ratio of LAP volume over total plaque volume (%) in the pre- intra- and post-stent locations after 1- and 12-month scans, using the tertile model of segmentation for intrastent plaque. There is no significant change in relative LAP volume from 1-mo to 12-mo follow-up.

Table 16. Relative LAP volume at 1- and 12-month follow-up by plaque location (pre-, 1st, 2nd and 3rd intrastent tertiles, and post-stent blocks).

Plaque location ¹	% LAP volume (mean ± SE, mm ³) at 1-mo scan	% LAP volume (mean ± SE, mm ³) at 12-mo scan	Volume variation (%) between scans	p-value
Pre-stent	26.8 ± 2.3	25.2 ± 1.9	-6	0.541
Proximal intrastent tertile	23.3 ± 2.2	23.4 ± 2.1	0.4	0.936
Middle intrastent tertile	24.6 ± 2.0	23.6 ± 1.7	-4	0.594
Distal intrastent tertile	23.4 ± 1.8	26.9 ± 2.2	15	0.052
Post-stent	27.8 ± 2.3	28.8 ± 2.8	4	0.258

¹A total of 27 patients, 36 stents and 309 blocks were analyzed. Nomenclature: there are 3 intrastent tertiles. The first tertile lies distally adjacent to the pre-stent block. The last (3rd) tertile lies proximally adjacent to the post-stent block. P-values are obtained by spline regression multivariate analysis.

There was no interaction between time and zone or block in any aforementioned ANOVA analysis.

5.4. Discussion

The present study serves as a pilot and strongly supports the feasibility of noninvasive longitudinal assessment of intrastent plaque volume and composition after BRS implantation

using CT imaging. In our prospective cohort study of 27 consecutive ReABSORB registry patients, we used mixed effects models to determine changes in total plaque volume and absolute and relative LAP volumes. In respect to both block and tertile model analysis, our study has shown no significant difference in plaque or LAP volumes in pre-, intra- and post-stent zones between 1 and 12 months (see tables 11-13 and 16, pp.151-156).

Plaque volume and absolute LAP volume:

In our CT study, plaque volumes in pre-, intra- and post-stent were found to be similar at 1- and 12-month follow-up. There is no established consensus in the literature as to how plaque area or volume evolves over time under the bioresorbable stent. Studies of plaque assessment under and juxta bioresorbable stents have mostly used IVUS for assessment with follow-up ranging from 6 months to 5 years and reporting contradictory results.^{92,271,272,275} Further CT studies are required to infirm or confirm our results.

Relative LAP volume:

Our data demonstrated a 15 % relative LAP increases in the distal intrastent tertile over time that however did not reach clinical significance ($p=0.052$). In a study by Gogas et al., 101 ABSORB Cohort B trial patients with bioresorbable stents were investigated at 6-mo (45 patients) and 12-mo (56 patients) follow-up with virtual histology intravascular ultrasound (VH-IVUS) imaging. This study demonstrated that at 1 year post-implantation, there was a significant increase of 43.32% ($p < 0.05$) in relative fibrofatty tissue at the 5-mm distal edge of the stent.²⁹³

In a study by Pendyala et al. in which eight farm pigs were implanted with 18 DES stents, the authors found that superoxide production juxta-stent was 55% more prominent in the 4 distal millimeters than the 4 proximal millimeters.²⁹⁴ As superoxide production in intrastent tertiles

has not yet been examined in the literature, we hypothesize that, as with the distal juxta-stent region, superoxide production in the distal intrastent tertile will be more prominent. Additionally, an *in vitro* study by Su et al. has demonstrated that superoxide is also produced in bioresorbable PLLA fibers.²⁹⁵

As excessive superoxide can oxidize naturally-circulating LDL in the blood, Rodríguez et al.²⁹⁶ state that plaque formation increases with high oxidized LDL / LDL ratio. Therefore, we assume that an unusual increase in superoxide could be responsible for higher percentage LAP volumes in the distal intrastent tertile.

In comparison with the Campos et al.²⁷⁵ study discussed in chapter 4, which also focused on plaque assessment by CT scan under BRS, our study included a larger patient sample (27 vs. 18 patients), which has allowed us to perform a regression analysis comparing smaller variations in plaque components between two follow-ups. Moreover, our study investigates a newer model of Absorb stent, version 1.1 (vs. version 1.0—as in Campos et al. study.²⁷³

The Campos et al.²⁷⁵ study largely focused on comparing atheroma volume change over time from scaffolded coronary arteries to the neighbouring healthy portion of coronary artery, which can offer some insight as to the natural history of within-patient atherosclerosis. Our study, however, is largely interested in evaluation of total plaque volume change over time and changes in plaque components, with the goal of improved understanding of the mechanisms of plaque change.

Clinical relevance:

This is a proof-of-concept study which non-invasive imaging methodology could bring novel insight to the physiopathology of plaque progression and its components under bioresorbable stents. Our study may be useful for the development of more efficient stents, for which intrastent plaque and plaque evolution could be investigated as a target for new stent technologies.

Strengths and limitations:

Our proof-of concept study is the first to analyze the relationship and progression of intra- and juxta-BRS plaque and LAP volumes by CT scan.

Our data did not show any significant difference in plaque or LAP volumes in pre-, intra- and post-stent zones between 1 and 12 months. This could be related to the insufficient power due to our small sample size. Moreover, in most of our study patients a novel BRS implantation protocol was used, in comparison to other studies (see methods section, subsection *Novel implantation protocol*). This implantation protocol was developed in order to promote more optimal stent apposition. It could however have influenced the plaque progression mechanism and the generalizability of our results compared to previous studies with different protocols.¹⁰⁵ Moreover, as in the Campos et al. study,²⁷⁵ in our study the recruited patients had relatively low plaque complexity with regards to ACC/AHA lesion type evaluation, which can also compromise the generalisability of our study to the true population of patients.

Conclusion and Perspectives

Our study is unique in demonstrating the feasibility of repeated non-invasive quantitative analysis of intrastent and juxta-stent coronary plaque with CT scan, and may allow the assessment of region-related mechanism of vulnerable plaque formation under- and juxta-BRS stent. The method we used could be applied to evaluation of various scaffold designs or to the pharmacological profile of bioresorbable stents.

In summary, BRS stents are promising as they are reported to confer better coronary vasomotion and offer CT imaging radiolucency, in contrast to metallic stents. Early clinical outcomes of BRS stents were found to be similar to the DES. Nevertheless, at two and three years after BRS implantation, studies report an increased incidence of device-related adverse events and scaffold thrombosis as compared to metallic stents. This is likely at least in part due to the implantation technique, which still needs to be refined.¹⁰⁵

Recent studies by Stone et al.¹⁰⁴ and Haddad et al.¹⁰⁵ have determined that target lesion failure, MACE event-free survival rate, and stent thrombosis were dependent on surgical technique including adequately sizing the vessel before implantation or using the predilation-sizing-postdilation BRS implantation technique.

After performing an in vitro study, Zhao et al.¹¹⁷ suggested that a solution to BRS scaffold thrombosis was to coat the scaffold with nanoparticles covered in a non-proliferative agent.

Further studies are needed to improve current bioresorbable stents and to address adverse clinical events.

Some take-home messages are:

- Unlike metallic stent scaffolds, the BRS scaffold is made of resorbable polymers, which do not cause blooming artifacts on CT imaging.
- BRS can be identified on CT imaging by two small platinum markers, one at each end of the implanted stent.
- BRS radiolucency helps the diagnosis of intrastent stenosis and, for the first time, offers the opportunity of in-stent plaque assessment on CT imaging.
- CT allows a noninvasive quantitative assessment of intrastent plaque volume and attenuation over time in patients with BRS.
- Our study proposes two statistical analyses to answer our main questions that are the assessment of: 1) the change in total plaque, absolute and relative LAP volumes over time by spline using mixed effect modeling; and 2) the inter-group change in the plaque volume between pre-, intra- and post-stent blocks by conducting ANOVA *post hoc* analysis with Bonferroni correction.²⁹¹

Bibliography

1. Yahagi K, Kolodgie FD, Otsuka F, et al. Pathophysiology of native coronary, vein graft, and in-stent atherosclerosis. *Nat Rev Cardiol* 2016;13:79-98.
2. Laslett LJ, Alagona P, Jr., Clark BA, 3rd, et al. The worldwide environment of cardiovascular disease: prevalence, diagnosis, therapy, and policy issues: a report from the American College of Cardiology. *J Am Coll Cardiol* 2012;60:S1-49.
3. Mack M, Gopal A. Epidemiology, Traditional and Novel Risk Factors in Coronary Artery Disease. *Heart Fail Clin* 2016;12:1-10.
4. Mozaffarian D, Benjamin EJ, Go AS, et al. Heart disease and stroke statistics--2015 update: a report from the American Heart Association. *Circulation* 2015;131:e29-322.
5. Joshi SD, Joshi SS, Athavale SA. Origins of the coronary arteries and their significance. *Clinics (Sao Paulo, Brazil)* 2010;65:79-84.
6. Dewey M. *Cardiac CT*: Springer-Verlag Berlin Heidelberg; 2011.
7. Zekic T. Cardiac involvement in eosinophilic granulomatosis with polyangiitis. *Rheumatol Int* 2018;38:705-6.
8. Parikh NI, Honeycutt EF, Roe MT, et al. Left and codominant coronary artery circulations are associated with higher in-hospital mortality among patients undergoing percutaneous coronary intervention for acute coronary syndromes: report From the National Cardiovascular Database Cath Percutaneous Coronary Intervention (CathPCI) Registry. *Circ Cardiovasc Qual Outcomes* 2012;5:775-82.
9. Shahoud JS, Tivakaran VS. *Cardiac Dominance*. StatPearls. Treasure Island (FL): StatPearls Publishing StatPearls Publishing LLC.; 2019.

10. O'Brien JP, Srichai MB, Hecht EM, Kim DC, Jacobs JE. Anatomy of the heart at multidetector CT: what the radiologist needs to know. *Radiographics* 2007;27:1569-82.
11. Tucker WD, Bhimji SS. *Anatomy, Blood Vessels*. StatPearls. Treasure Island (FL): StatPearls Publishing StatPearls Publishing LLC.; 2018.
12. Arterial wall. *WikiJournal of Medicine* 2014. (Accessed November 27, 2018,
13. Ross R, Glomset J, Harker L. Response to injury and atherogenesis. *Am J Pathol* 1977;86:675-84.
14. Ross R. The pathogenesis of atherosclerosis: a perspective for the 1990s. *Nature* 1993;362:801-9.
15. Libby P. Inflammation in atherosclerosis. *Nature* 2002;420:868-74.
16. Hansson GK, Libby P, Schonbeck U, Yan ZQ. Innate and adaptive immunity in the pathogenesis of atherosclerosis. *Circ Res* 2002;91:281-91.
17. Hansson GK. Inflammation, atherosclerosis, and coronary artery disease. *N Engl J Med* 2005;352:1685-95.
18. Fuster V, Badimon L, Badimon JJ, Chesebro JH. The pathogenesis of coronary artery disease and the acute coronary syndromes (1). *N Engl J Med* 1992;326:242-50.
19. Richardson PD, Davies MJ, Born GV. Influence of plaque configuration and stress distribution on fissuring of coronary atherosclerotic plaques. *Lancet* 1989;2:941-4.
20. Stary HC, Chandler AB, Dinsmore RE, et al. A definition of advanced types of atherosclerotic lesions and a histological classification of atherosclerosis. A report from the Committee on Vascular Lesions of the Council on Arteriosclerosis, American Heart Association. *Arterioscler Thromb Vasc Biol* 1995;15:1512-31.

21. Stary HC, Blankenhorn DH, Chandler AB, et al. A definition of the intima of human arteries and of its atherosclerosis-prone regions. A report from the Committee on Vascular Lesions of the Council on Arteriosclerosis, American Heart Association. *Arterioscler Thromb* 1992;12:120-34.
22. Virmani R, Kolodgie FD, Burke AP, Farb A, Schwartz SM. Lessons from sudden coronary death: a comprehensive morphological classification scheme for atherosclerotic lesions. *Arterioscler Thromb Vasc Biol* 2000;20:1262-75.
23. Kolodgie FD, Gold HK, Burke AP, et al. Intraplaque hemorrhage and progression of coronary atheroma. *N Engl J Med* 2003;349:2316-25.
24. Narula J, Nakano M, Virmani R, et al. Histopathologic characteristics of atherosclerotic coronary disease and implications of the findings for the invasive and noninvasive detection of vulnerable plaques. *J Am Coll Cardiol* 2013;61:1041-51.
25. Soloperto G, Casciaro S. Progress in atherosclerotic plaque imaging. *World journal of radiology* 2012;4:353-71.
26. Kataoka Y, Puri R, Hammadah M, et al. Spotty calcification and plaque vulnerability in vivo: frequency-domain optical coherence tomography analysis. *Cardiovasc Diagn Ther* 2014;4:460-9.
27. Shimizu T, Mintz GS, De Bruyne B, et al. Relationship between left main coronary artery plaque burden and nonleft main coronary atherosclerosis: results from the PROSPECT study. *Coron Artery Dis* 2018;29:397-402.
28. Wang Y, Qiu J, Luo S, et al. High shear stress induces atherosclerotic vulnerable plaque formation through angiogenesis. *Regenerative biomaterials* 2016;3:257-67.
29. Pant S, Deshmukh A, Gurumurthy GS, et al. Inflammation and atherosclerosis--revisited. *J Cardiovasc Pharmacol Ther* 2014;19:170-8.
30. Packard RR, Libby P. Inflammation in atherosclerosis: from vascular biology to biomarker discovery and risk prediction. *Clin Chem* 2008;54:24-38.

31. Ma T, Zhou B, Hsiai TK, Shung KK. A Review of Intravascular Ultrasound-based Multimodal Intravascular Imaging: The Synergistic Approach to Characterizing Vulnerable Plaques. *Ultrason Imaging* 2016;38:314-31.
32. Sinclair H, Bourantas C, Bagnall A, Mintz GS, Kunadian V. OCT for the identification of vulnerable plaque in acute coronary syndrome. *JACC Cardiovasc Imaging* 2015;8:198-209.
33. Virmani R, Burke AP, Kolodgie FD, Farb A. Pathology of the thin-cap fibroatheroma: a type of vulnerable plaque. *J Interv Cardiol* 2003;16:267-72.
34. Hong YJ, Jeong MH, Choi YH, et al. Comparison of Coronary Plaque Components between Non-Culprit Lesions in Patients with Acute Coronary Syndrome and Target Lesions in Patients with Stable Angina: Virtual Histology-Intravascular Ultrasound Analysis. *Korean Circ J* 2013;43:607-14.
35. Raffel OC, Merchant FM, Tearney GJ, et al. In vivo association between positive coronary artery remodelling and coronary plaque characteristics assessed by intravascular optical coherence tomography. *Eur Heart J* 2008;29:1721-8.
36. Reddy HK, Koshy SK, Wasson S, et al. Adaptive-outward and maladaptive-inward arterial remodeling measured by intravascular ultrasound in hyperhomocysteinemia and diabetes. *J Cardiovasc Pharmacol Ther* 2006;11:65-76.
37. Glagov S, Weisenberg E, Zarins CK, Stankunavicius R, Kolettis GJ. Compensatory enlargement of human atherosclerotic coronary arteries. *N Engl J Med* 1987;316:1371-5.
38. Pasterkamp G, Schoneveld AH, van der Wal AC, et al. Relation of arterial geometry to luminal narrowing and histologic markers for plaque vulnerability: the remodeling paradox. *J Am Coll Cardiol* 1998;32:655-62.
39. Varnava AM, Mills PG, Davies MJ. Relationship between coronary artery remodeling and plaque vulnerability. *Circulation* 2002;105:939-43.
40. Rathore S, Terashima M, Matsuo H, et al. Association of coronary plaque composition and arterial remodelling: a optical coherence tomography study. *Atherosclerosis* 2012;221:405-15.

41. Ehara S, Kobayashi Y, Yoshiyama M, et al. Spotty calcification typifies the culprit plaque in patients with acute myocardial infarction: an intravascular ultrasound study. *Circulation* 2004;110:3424-9.
42. Motoyama S, Kondo T, Sarai M, et al. Multislice computed tomographic characteristics of coronary lesions in acute coronary syndromes. *J Am Coll Cardiol* 2007;50:319-26.
43. Bluestein D, Alemu Y, Avrahami I, et al. Influence of microcalcifications on vulnerable plaque mechanics using FSI modeling. *J Biomech* 2008;41:1111-8.
44. Kelly-Arnold A, Maldonado N, Laudier D, Aikawa E, Cardoso L, Weinbaum S. Revised microcalcification hypothesis for fibrous cap rupture in human coronary arteries. *Proc Natl Acad Sci U S A* 2013;110:10741-6.
45. Salem BI, Lagos JA, Haikal M, Gowda S. The potential impact of the thrombolytic era on cardiac rupture complicating acute myocardial infarction. *Angiology* 1994;45:931-6.
46. Smilowitz NR, Feit F. The History of Primary Angioplasty and Stenting for Acute Myocardial Infarction. *Curr Cardiol Rep* 2016;18:5.
47. An international randomized trial comparing four thrombolytic strategies for acute myocardial infarction. The GUSTO investigators. *N Engl J Med* 1993;329:673-82.
48. Ohman EM, Califf RM, Topol EJ, et al. Consequences of reocclusion after successful reperfusion therapy in acute myocardial infarction. TAMI Study Group. *Circulation* 1990;82:781-91.
49. Indications for fibrinolytic therapy in suspected acute myocardial infarction: collaborative overview of early mortality and major morbidity results from all randomised trials of more than 1000 patients. Fibrinolytic Therapy Trialists' (FTT) Collaborative Group. *Lancet* 1994;343:311-22.
50. Phillips SJ, Kongtahworn C, Zeff RH, et al. Emergency coronary artery revascularization: a possible therapy for acute myocardial infarction. *Circulation* 1979;60:241-6.

51. Iqbal J, Gunn J, Serruys PW. Coronary stents: historical development, current status and future directions. *Br Med Bull* 2013;106:193-211.
52. Carroll DL, Malecki-Ketchell A, Astin F. Non-pharmacological interventions to reduce psychological distress in patients undergoing diagnostic cardiac catheterization: a rapid review. *Eur J Cardiovasc Nurs* 2017;16:92-103.
53. Manda YR BK. Cardiac Catheterization, Risks and Complications. In: StatPearls [Internet].
54. Barton M, Gruntzig J, Husmann M, Rosch J. Balloon Angioplasty - The Legacy of Andreas Gruntzig, M.D. (1939-1985). *Frontiers in cardiovascular medicine* 2014;1:15.
55. Chartrand-Lefebvre C. Mémoire de Maîtrise: "Réduction des artéfacts de tuteur coronarien au moyen d'un algorithme de reconstruction avec renforcement des bords – Étude prospective transversale en tomодensitométrie 256 coupes": Université de Montréal; 2015; 154 pages.
56. Umeda H, Iwase M, Kanda H, et al. Promising efficacy of primary gradual and prolonged balloon angioplasty in small coronary arteries: a randomized comparison with cutting balloon angioplasty and conventional balloon angioplasty. *Am Heart J* 2004;147:E4.
57. Cai YY, Chui CK, Ye XZ, Fan Z, Anderson JH. Tactile VR for hand-eye coordination in simulated PTCA. *Comput Biol Med* 2006;36:167-80.
58. Omeh DJ, Shlofmitz E. Restenosis. StatPearls. Treasure Island (FL): StatPearls Publishing StatPearls Publishing LLC.; 2019.
59. Kim MS, Dean LS. In-stent restenosis. *Cardiovasc Ther* 2011;29:190-8.
60. Percutaneous coronary intervention (PCI or angioplasty with stent). © 2018 Heart and Stroke Foundation of Canada., 2018. at <https://www.heartandstroke.ca/heart/treatments/surgery-and-other-procedures/percutaneous-coronary-intervention.>)
61. Buccheri D, Piraino D, Andolina G, Cortese B. Understanding and managing in-stent restenosis: a review of clinical data, from pathogenesis to treatment. *J Thorac Dis* 2016;8:E1150-e62.

62. Roguin A. Stent: the man and word behind the coronary metal prosthesis. *Circ Cardiovasc Interv* 2011;4:206-9.
63. Esser JF. *Studies in Plastic Surgery of the Face: I. Use of Skin from the Neck to Replace Face Defects. II. Plastic Operations About the Mouth. III. The Epidermic Inlay.* *Ann Surg* 1917;65:297-315.
64. Fontos G. [Drug-eluting coronary stents]. *Orv Hetil* 2006;147:2059-66.
65. Pioneering medical devices – the Palmaz-Schatz stent. European Society of Cardiology, 2018. (Accessed May 21st, 2019, at <https://www.escardio.org/Congresses-&-Events/ESC-Congress/Congress-resources/Congress-news/pioneering-medical-devices-the-palmaz-schatz-stent>.)
66. Vassanelli C, Menegatti G, Molinari J, Loschiavo I, Zardini P. [Coronary recanalization: rationale for stents]. *Cardiologia* 1994;39:53-7.
67. Kinga David KB, Deborah Samek, Peter Bogaty, Laurie Lambert. Le fichier MED-ÉCHO du Québec est-il la source de données appropriée pour dénombrer les interventions coronariennes percutanées (ICP)?: l’Institut national d’excellence en santé et en services sociaux (INESSS) et l’Institut canadien d’information sur la santé (ICIS); Septembre 2011.
68. Premarket approval application (PMA) for the Absorb GT1™ Bioresorbable Vascular Scaffold (BVS) System. 2016. (Accessed 09 March, 2017, at http://www.accessdata.fda.gov/cdrh_docs/pdf15/P150023a.pdf.)
69. Stone GW, Grines CL, Cox DA, et al. Comparison of angioplasty with stenting, with or without abciximab, in acute myocardial infarction. *N Engl J Med* 2002;346:957-66.
70. Rechenmacher F, Steigerwald K, Laufer B, et al. The integrin ligand c(RGDf(NMe)Nal) reduces neointimal hyperplasia in a polymer-free drug-eluting stent system. *ChemMedChem* 2014;9:1413-8.

71. Comparison of drug-eluting intracoronary stents. © 2019 UpToDate, 2019. (Accessed May 21st, 2019, at <https://www.uptodate.com/contents/comparison-of-drug-eluting-intracoronary-stents>.)
72. Byrne RA, Serruys PW, Baumbach A, et al. Report of a European Society of Cardiology-European Association of Percutaneous Cardiovascular Interventions task force on the evaluation of coronary stents in Europe: executive summary. *Eur Heart J* 2015;36:2608-20.
73. Serruys PW, Onuma Y, Ormiston JA, et al. Evaluation of the second generation of a bioresorbable everolimus drug-eluting vascular scaffold for treatment of de novo coronary artery stenosis: six-month clinical and imaging outcomes. *Circulation* 2010;122:2301-12.
74. Koenigsberger M, Sauser R, Beny JL, Meister JJ. Role of the endothelium on arterial vasomotion. *Biophys J* 2005;88:3845-54.
75. Rizik DG, Hermiller JB, Simonton CA, Klassen KJ, Kereiakes DJ. Bioresorbable vascular scaffolds for the treatment of coronary artery disease: what have we learned from randomized- controlled clinical trials? *Coron Artery Dis* 2017;28:77-89.
76. Serruys PW, Ormiston JA, Onuma Y, et al. A bioabsorbable everolimus-eluting coronary stent system (ABSORB): 2-year outcomes and results from multiple imaging methods. *Lancet* 2009;373:897-910.
77. Brugaletta S, Heo JH, Garcia-Garcia HM, et al. Endothelial-dependent vasomotion in a coronary segment treated by ABSORB everolimus-eluting bioresorbable vascular scaffold system is related to plaque composition at the time of bioresorption of the polymer: indirect finding of vascular reparative therapy? *Eur Heart J* 2012;33:1325-33.
78. Hofma SH, van der Giessen WJ, van Dalen BM, et al. Indication of long-term endothelial dysfunction after sirolimus-eluting stent implantation. *Eur Heart J* 2006;27:166-70.
79. Serruys PW, Onuma Y, Dudek D, et al. Evaluation of the second generation of a bioresorbable everolimus-eluting vascular scaffold for the treatment of de novo coronary artery stenosis: 12-month clinical and imaging outcomes. *J Am Coll Cardiol* 2011;58:1578-88.

80. Brie D, Penson P, Serban MC, et al. Bioresorbable scaffold - A magic bullet for the treatment of coronary artery disease? *Int J Cardiol* 2016;215:47-59.
81. Serruys PW, Garcia-Garcia HM, Onuma Y. From metallic cages to transient bioresorbable scaffolds: change in paradigm of coronary revascularization in the upcoming decade? *Eur Heart J* 2012;33:16-25b.
82. How Aspirin Works. Corgenix, 2018. (Accessed 21 February 2018, at [https://www.aspirinworks.com/aspirin-resistance/how-aspirin-works/.](https://www.aspirinworks.com/aspirin-resistance/how-aspirin-works/))
83. 2017. (Accessed 31 January, 2018, at [http://www.heart.org/idc/groups/heart-public/@wcm/@hcm/documents/downloadable/ucm_493120.pdf.](http://www.heart.org/idc/groups/heart-public/@wcm/@hcm/documents/downloadable/ucm_493120.pdf))
84. Byrne RA, Stone GW, Ormiston J, Kastrati A. Coronary balloon angioplasty, stents, and scaffolds. *Lancet* 2017;390:781-92.
85. Sotomi Y, Onuma Y, Collet C, et al. Bioresorbable Scaffold: The Emerging Reality and Future Directions. *Circ Res* 2017;120:1341-52.
86. Health Canada approves Abbott Absorb stent. published 18th July 2016. (Accessed 23rd February 2018, at [https://cardiovascularnews.com/health-canada-approves-abbott-absorb-stent/.](https://cardiovascularnews.com/health-canada-approves-abbott-absorb-stent/))
87. Rzeszutko L, Depukat R, Dudek D. Biodegradable vascular scaffold ABSORB BVS - scientific evidence and methods of implantation. *Postepy Kardiologii Interwencyjnej* 2013;9:22-30.
88. Muramatsu T, Onuma Y, Garcia-Garcia HM, et al. Incidence and short-term clinical outcomes of small side branch occlusion after implantation of an everolimus-eluting bioresorbable vascular scaffold: an interim report of 435 patients in the ABSORB-EXTEND single-arm trial in comparison with an everolimus-eluting metallic stent in the SPIRIT first and II trials. *JACC Cardiovasc Interv* 2013;6:247-57.
89. Absorb GT1 product design elements 2006-2016. (Accessed 09 March, 2017, at [https://www.vascular.abbott/int/products/coronary-intervention/absorb-bioresorbable-scaffold-dissolving-stent.html#product-overview.](https://www.vascular.abbott/int/products/coronary-intervention/absorb-bioresorbable-scaffold-dissolving-stent.html#product-overview))

90. Ormiston JA, Serruys PW. Bioabsorbable coronary stents. *Circ Cardiovasc Interv* 2009;2:255-60.
91. Kereiakes DJ, Onuma Y, Serruys PW, Stone GW. Bioresorbable Vascular Scaffolds for Coronary Revascularization. *Circulation* 2016;134:168-82.
92. Serruys PW, Ormiston J, van Geuns RJ, et al. A Polylactide Bioresorbable Scaffold Eluting Everolimus for Treatment of Coronary Stenosis: 5-Year Follow-Up. *J Am Coll Cardiol* 2016;67:766-76.
93. Karanasos A, Simsek C, Gnanadesigan M, et al. OCT assessment of the long-term vascular healing response 5 years after everolimus-eluting bioresorbable vascular scaffold. *J Am Coll Cardiol* 2014;64:2343-56.
94. Brugaletta S, Radu MD, Garcia-Garcia HM, et al. Circumferential evaluation of the neointima by optical coherence tomography after ABSORB bioresorbable vascular scaffold implantation: can the scaffold cap the plaque? *Atherosclerosis* 2012;221:106-12.
95. Serruys PW, Chevalier B, Dudek D, et al. A bioresorbable everolimus-eluting scaffold versus a metallic everolimus-eluting stent for ischaemic heart disease caused by de-novo native coronary artery lesions (ABSORB II): an interim 1-year analysis of clinical and procedural secondary outcomes from a randomised controlled trial. *Lancet* 2015;385:43-54.
96. Serruys PW, Chevalier B, Sotomi Y, et al. Comparison of an everolimus-eluting bioresorbable scaffold with an everolimus-eluting metallic stent for the treatment of coronary artery stenosis (ABSORB II): a 3 year, randomised, controlled, single-blind, multicentre clinical trial. *Lancet* 2016;388:2479-91.
97. Chevalier B, Cequier A, Dudek D, et al. Four-year follow-up of the randomised comparison between an everolimus-eluting bioresorbable scaffold and an everolimus-eluting metallic stent for the treatment of coronary artery stenosis (ABSORB II Trial). *EuroIntervention* 2018;13:1561-4.
98. Puricel S, Cuculi F, Weissner M, et al. Bioresorbable Coronary Scaffold Thrombosis: Multicenter Comprehensive Analysis of Clinical Presentation, Mechanisms, and Predictors. *J Am Coll Cardiol* 2016;67:921-31.

99. Ellis SG, Kereiakes DJ, Metzger DC, et al. Everolimus-Eluting Bioresorbable Scaffolds for Coronary Artery Disease. *N Engl J Med* 2015;373:1905-15.
100. Moreno R, Garcia E, Teles R, et al. Randomized comparison of sirolimus-eluting and everolimus-eluting coronary stents in the treatment of total coronary occlusions: results from the chronic coronary occlusion treated by everolimus-eluting stent randomized trial. *Circ Cardiovasc Interv* 2013;6:21-8.
101. Ali ZA, Serruys PW, Kimura T, et al. 2-year outcomes with the Absorb bioresorbable scaffold for treatment of coronary artery disease: a systematic review and meta-analysis of seven randomised trials with an individual patient data substudy. *Lancet* 2017;390:760-72.
102. Kereiakes DJ, Ellis SG, Metzger C, et al. 3-Year Clinical Outcomes With Everolimus-Eluting Bioresorbable Coronary Scaffolds: The ABSORB III Trial. *J Am Coll Cardiol* 2017;70:2852-62.
103. Absorb IV Randomized Controlled Trial. U.S. National Library of Medicine 25 June 2014. (Accessed 17 March 2018, at <https://clinicaltrials.gov/ct2/show/NCT02173379>.)
104. Stone GW, Ellis SG, Gori T, et al. Blinded outcomes and angina assessment of coronary bioresorbable scaffolds: 30-day and 1-year results from the ABSORB IV randomised trial. *Lancet* 2018;392:1530-40.
105. Haddad K, Tanguay JF, Potter BJ, Matteau A, Gobeil F, Mansour S. Longer Inflation Duration and Predilation-Sizing-Postdilation Improve Bioresorbable Scaffold Outcomes in a Long-term All-Comers Canadian Registry. *Can J Cardiol* 2018;34:752-8.
106. Dudek D, Onuma Y, Ormiston JA, Thuesen L, Miquel-Hebert K, Serruys PW. Four-year clinical follow-up of the ABSORB everolimus-eluting bioresorbable vascular scaffold in patients with de novo coronary artery disease: the ABSORB trial. *EuroIntervention* 2012;7:1060-1.
107. Diletti R, Farooq V, Girasis C, et al. Clinical and intravascular imaging outcomes at 1 and 2 years after implantation of absorb everolimus eluting bioresorbable vascular scaffolds in small vessels. Late lumen enlargement: does bioresorption matter with small vessel size? Insight from the ABSORB cohort B trial. *Heart* 2013;99:98-105.

108. Ali ZA, Gao R, Kimura T, et al. Three-Year Outcomes With the Absorb Bioresorbable Scaffold: Individual-Patient-Data Meta-Analysis From the ABSORB Randomized Trials. *Circulation* 2018;137:464-79.
109. POINTS TO CONSIDER ON MULTIPLICITY ISSUES IN CLINICAL TRIALS The European Agency for the Evaluation of Medicinal Products published on 19th September 2002. (Accessed 23rd February 2018, at http://www.ema.europa.eu/docs/en_GB/document_library/Scientific_guideline/2009/09/WC500003640.pdf.)
110. Kang SH, Gogas BD, Jeon KH, et al. Long-term safety of bioresorbable scaffolds: insights from a network meta-analysis including 91 trials. *EuroIntervention* 2018;13:1904-13.
111. Stone GW, Abizaid A, Onuma Y, et al. Effect of Technique on Outcomes Following Bioresorbable Vascular Scaffold Implantation: Analysis From the ABSORB Trials. *J Am Coll Cardiol* 2017;70:2863-74.
112. Colombo A, Giannini F. Encouraging data from ABSORB IV pave the way to new scaffolds. *Lancet* 2018;392:1490-1.
113. Mallat J. Understanding the null hypothesis (H0) in non-inferiority trials. *Crit Care* 2017;21:101.
114. Hahn S. Understanding noninferiority trials. *Korean J Pediatr* 2012;55:403-7.
115. Ellis SG, Vandormael MG, Cowley MJ, et al. Coronary morphologic and clinical determinants of procedural outcome with angioplasty for multivessel coronary disease. Implications for patient selection. Multivessel Angioplasty Prognosis Study Group. *Circulation* 1990;82:1193-202.
116. Goel MK, Khanna P, Kishore J. Understanding survival analysis: Kaplan-Meier estimate. *International journal of Ayurveda research* 2010;1:274-8.

117. Zhao J, Mo Z, Guo F, Shi D, Han QQ, Liu Q. Drug loaded nanoparticle coating on totally bioresorbable PLLA stents to prevent in-stent restenosis. *Journal of biomedical materials research Part B, Applied biomaterials* 2018;106:88-95.
118. Abbott Will End Sales of Absorb Bioresorbable Stent. *Diagnostic and Interventional Cardiology*, 2017. (Accessed April 3rd, 2019, at <https://www.dicardiology.com/article/abbott-will-end-sales-absorb-bioresorbable-stent>.)
119. Onuma Y, Serruys PW, Ormiston JA, et al. Three-year results of clinical follow-up after a bioresorbable everolimus-eluting scaffold in patients with de novo coronary artery disease: the ABSORB trial. *EuroIntervention* 2010;6:447-53.
120. Abizaid A, Ribamar Costa J, Jr., Bartorelli AL, et al. The ABSORB EXTEND study: preliminary report of the twelve-month clinical outcomes in the first 512 patients enrolled. *EuroIntervention* 2015;10:1396-401.
121. Porto I, Selvanayagam JB, Van Gaal WJ, et al. Plaque volume and occurrence and location of periprocedural myocardial necrosis after percutaneous coronary intervention: insights from delayed-enhancement magnetic resonance imaging, thrombolysis in myocardial infarction myocardial perfusion grade analysis, and intravascular ultrasound. *Circulation* 2006;114:662-9.
122. Muschart X, Slimani A, Jamart J, et al. The different mechanisms of periprocedural myocardial infarction and their impact on in-hospital outcome. *J Invasive Cardiol* 2012;24:655-60.
123. Lindsey JB, Kennedy KF, Stolker JM, et al. Prognostic implications of creatine kinase-MB elevation after percutaneous coronary intervention: results from the Evaluation of Drug-Eluting Stents and Ischemic Events (EVENT) registry. *Circ Cardiovasc Interv* 2011;4:474-80.
124. Park DW, Kim YH, Yun SC, et al. Frequency, causes, predictors, and clinical significance of peri-procedural myocardial infarction following percutaneous coronary intervention. *Eur Heart J* 2013;34:1662-9.
125. Park DW, Kim YH, Yun SC, et al. Impact of the angiographic mechanisms underlying periprocedural myocardial infarction after drug-eluting stent implantation. *Am J Cardiol* 2014;113:1105-10.

126. Okamura T, Onuma Y, Garcia-Garcia HM, et al. 3-Dimensional optical coherence tomography assessment of jailed side branches by bioresorbable vascular scaffolds: a proposal for classification. *JACC Cardiovasc Interv* 2010;3:836-44.
127. Okamura T, Serruys PW, Regar E. Cardiovascular flashlight. The fate of bioresorbable struts located at a side branch ostium: serial three-dimensional optical coherence tomography assessment. *Eur Heart J* 2010;31:2179.
128. Ojeda S, Pan M, Suarez de Lezo J, et al. Patency of coronary side branches covered by an everolimus-eluting bioresorbable vascular scaffold: clinical outcomes and computed tomography scan follow-up. *EuroIntervention* 2016;11:e1283-90.
129. Onuma Y, Grundeken MJ, Nakatani S, et al. Serial 5-Year Evaluation of Side Branches Jailed by Bioresorbable Vascular Scaffolds Using 3-Dimensional Optical Coherence Tomography: Insights From the ABSORB Cohort B Trial (A Clinical Evaluation of the Bioabsorbable Everolimus Eluting Coronary Stent System in the Treatment of Patients With De Novo Native Coronary Artery Lesions). *Circ Cardiovasc Interv* 2017;10.
130. Ormiston JA, Webber B, Ubod B, Darremont O, Webster MW. An independent bench comparison of two bioresorbable drug-eluting coronary scaffolds (Absorb and DESolve) with a durable metallic drug-eluting stent (ML8/Xpedition). *EuroIntervention* 2015;11:60-7.
131. Angiogram vs. Angioplasty (and stents). 2012. (Accessed 09 March, 2017, at [http://nevadacardiology.com/angiogram-vs-angioplasty-and-stents/.](http://nevadacardiology.com/angiogram-vs-angioplasty-and-stents/))
132. Fujii K, Carlier SG, Mintz GS, et al. Stent underexpansion and residual reference segment stenosis are related to stent thrombosis after sirolimus-eluting stent implantation: an intravascular ultrasound study. *J Am Coll Cardiol* 2005;45:995-8.
133. Liu X, Doi H, Maehara A, et al. A volumetric intravascular ultrasound comparison of early drug-eluting stent thrombosis versus restenosis. *JACC Cardiovasc Interv* 2009;2:428-34.
134. Chamie D, Garcia-Garcia H, Costa RA, Onuma Y, Abizaid A, Serruys PW. Role of invasive imaging in acute and long-term assessment of bioresorbable scaffold technology. *Catheter Cardiovasc Interv* 2016;88:38-53.

135. Johnson PM, Patel J, Yeung M, Kaul P. Intra-coronary imaging modalities. *Curr Treat Options Cardiovasc Med* 2014;16:304.
136. Tarkin JM, Dweck MR, Evans NR, et al. Imaging Atherosclerosis. *Circ Res* 2016;118:750-69.
137. Brugaletta S, Gomez-Lara J, Serruys PW, et al. Serial in vivo intravascular ultrasound-based echogenicity changes of everolimus-eluting bioresorbable vascular scaffold during the first 12 months after implantation insights from the ABSORB B trial. *JACC Cardiovasc Interv* 2011;4:1281-9.
138. Sotomi Y, Ishibashi Y, Suwannasom P, et al. Acute Gain in Minimal Lumen Area Following Implantation of Everolimus-Eluting ABSORB Biodegradable Vascular Scaffolds or Xience Metallic Stents: Intravascular Ultrasound Assessment From the ABSORB II Trial. *JACC Cardiovasc Interv* 2016;9:1216-27.
139. Mintz GS. Clinical utility of intravascular imaging and physiology in coronary artery disease. *J Am Coll Cardiol* 2014;64:207-22.
140. Tatsugami F, Higaki T, Sakane H, et al. Diagnostic accuracy of in-stent restenosis using model-based iterative reconstruction at coronary CT angiography: initial experience. *Br J Radiol* 2018;91:20170598.
141. Tan S, Soulez G, Diez Martinez P, et al. Coronary Stent Artifact Reduction with an Edge-Enhancing Reconstruction Kernel - A Prospective Cross-Sectional Study with 256-Slice CT. *PLoS One* 2016;11:e0154292.
142. Brief history of CT. (Accessed August 2nd 2017, at <http://www.imaginis.com/ct-scan/brief-history-of-ct>.)
143. The Nobel Prize in Physiology or Medicine 1979 - Perspectives: With a Little Help from My Friends. 2014. (Accessed March 19th, 2018, at https://www.nobelprize.org/nobel_prizes/medicine/laureates/1979/perspectives.html.)

144. David A. Dowe, Massimo Fioranelli, Paolo Pavone. Imaging Coronary Arteries: Springer-Verlag Italia; 2013.
145. Paolo Pavone, Massimo Fioranelli, David A. Dowe. CT evaluation of coronary artery disease: Springer-Verlag Italia; 2009.
146. Tobias Schwarz, Saunders J. Veterinary Computed Tomography: Wiley- Blackwell; 2011.
147. Brenner DJ, Georgsson MA. Mass screening with CT colonography: should the radiation exposure be of concern? *Gastroenterology* 2005;129:328-37.
148. Ter-Pogossian MM. Basic principles of computed axial tomography. *Semin Nucl Med* 1977;7:109-27.
149. M. F. Reiser, C. R. Becker, K. Nikolaou, G. Glazer. Multislice CT: Springer-Verlag Berlin Heidelberg; 2009.
150. Ramjattan NAM, A. N. Coronary CT Angiography. In: StatPearls, ed. Last Update: December 16, 2017.
151. Axial, Lateral and Temporal Resolution. Drs. Atif Qasim and Amresh Raina. (Accessed 8 March, 2018, at <http://www.echocardiographer.org/Echo%20Physics/Axresolution.html>.)
152. Taguchi K, Anno H. High temporal resolution for multislice helical computed tomography. *Med Phys* 2000;27:861-72.
153. Desjardins B, Kazerooni EA. ECG-gated cardiac CT. *AJR Am J Roentgenol* 2004;182:993-1010.
154. Leschka S, Scheffel H, Husmann L, et al. Effect of decrease in heart rate variability on the diagnostic accuracy of 64-MDCT coronary angiography. *AJR Am J Roentgenol* 2008;190:1583-90.
155. Leschka S, Wildermuth S, Boehm T, et al. Noninvasive coronary angiography with 64-section CT: effect of average heart rate and heart rate variability on image quality. *Radiology* 2006;241:378-85.

156. Giesler T, Baum U, Ropers D, et al. Noninvasive visualization of coronary arteries using contrast-enhanced multidetector CT: influence of heart rate on image quality and stenosis detection. *AJR Am J Roentgenol* 2002;179:911-6.
157. Bley TA, Ghanem NA, Foell D, et al. Computed tomography coronary angiography with 370-millisecond gantry rotation time: evaluation of the best image reconstruction interval. *J Comput Assist Tomogr* 2005;29:1-5.
158. Chartrand-Lefebvre C, Cadrin-Chenevert A, Bordeleau E, et al. Coronary computed tomography angiography: overview of technical aspects, current concepts, and perspectives. *Can Assoc Radiol J* 2007;58:92-108.
159. Coles DR, Smail MA, Negus IS, et al. Comparison of radiation doses from multislice computed tomography coronary angiography and conventional diagnostic angiography. *J Am Coll Cardiol* 2006;47:1840-5.
160. Earls JP, Berman EL, Urban BA, et al. Prospectively gated transverse coronary CT angiography versus retrospectively gated helical technique: improved image quality and reduced radiation dose. *Radiology* 2008;246:742-53.
161. Ghostine S, Caussin C, Daoud B, et al. Non-invasive detection of coronary artery disease in patients with left bundle branch block using 64-slice computed tomography. *J Am Coll Cardiol* 2006;48:1929-34.
162. Husmann L, Valenta I, Gaemperli O, et al. Feasibility of low-dose coronary CT angiography: first experience with prospective ECG-gating. *Eur Heart J* 2008;29:191-7.
163. Labounty TM, Leipsic J, Min JK, et al. Effect of padding duration on radiation dose and image interpretation in prospectively ECG-triggered coronary CT angiography. *AJR Am J Roentgenol* 2010;194:933-7.
164. Lee AM, Engel LC, Shah B, et al. Coronary computed tomography angiography during arrhythmia: Radiation dose reduction with prospectively ECG-triggered axial and retrospectively ECG-gated helical 128-slice dual-source CT. *J Cardiovasc Comput Tomogr* 2012;6:172-83 e2.

165. Lin E, Alessio A. What are the basic concepts of temporal, contrast, and spatial resolution in cardiac CT? *J Cardiovasc Comput Tomogr* 2009;3:403-8.
166. Wykrzykowska JJ, Arbab-Zadeh A, Godoy G, et al. Assessment of in-stent restenosis using 64-MDCT: analysis of the CORE-64 Multicenter International Trial. *AJR Am J Roentgenol* 2010;194:85-92.
167. Cui X, Li T, Li X, Zhou W. High-definition computed tomography for coronary artery stents imaging: Initial evaluation of the optimal reconstruction algorithm. *Eur J Radiol* 2015;84:834-9.
168. Voxel. Farlex Partner Medical Dictionary © 2012. (Accessed March 22, 2018, at <https://medical-dictionary.thefreedictionary.com/voxel>.)
169. Gerber AJ, Peterson BS. What is an image? *J Am Acad Child Adolesc Psychiatry* 2008;47:245-8.
170. Kalisz K, Bueth J, Saboo SS, Abbara S, Halliburton S, Rajiah P. Artifacts at Cardiac CT: Physics and Solutions. *Radiographics* 2016;36:2064-83.
171. Choi HS, Choi BW, Choe KO, et al. Pitfalls, artifacts, and remedies in multi- detector row CT coronary angiography. *Radiographics* 2004;24:787-800.
172. Achenbach S, Ropers D, Holle J, Muschiol G, Daniel WG, Moshage W. In-plane coronary arterial motion velocity: measurement with electron-beam CT. *Radiology* 2000;216:457-63.
173. Hofman MB, Wickline SA, Lorenz CH. Quantification of in-plane motion of the coronary arteries during the cardiac cycle: implications for acquisition window duration for MR flow quantification. *J Magn Reson Imaging* 1998;8:568-76.
174. Mao S, Lu B, Oudiz RJ, Bakhsheshi H, Liu SC, Budoff MJ. Coronary artery motion in electron beam tomography. *J Comput Assist Tomogr* 2000;24:253-8.
175. Chartrand-Lefebvre C. Stepladder artifact in coronary computed tomography angiography. *Catheter Cardiovasc Interv* 2007;69:922; author reply 3.

176. Mao SS, Oudiz RJ, Bakhsheshi H, Wang SJ, Brundage BH. Variation of heart rate and electrocardiograph trigger interval during ultrafast computed tomography. *Am J Card Imaging* 1996;10:239-43.
177. Gramer BM, Diez Martinez P, Chin AS, et al. 256-slice CT angiographic evaluation of coronary artery bypass grafts: effect of heart rate, heart rate variability and Z-axis location on image quality. *PLoS One* 2014;9:e91861.
178. Sun G, Li M, Jiang XS, et al. 320-detector row CT coronary angiography: effects of heart rate and heart rate variability on image quality, diagnostic accuracy and radiation exposure. *Br J Radiol* 2012;85:e388-94.
179. Qin J, Liu LY, Fang Y, et al. 320-detector CT coronary angiography with prospective and retrospective electrocardiogram gating in a single heartbeat: comparison of image quality and radiation dose. *Br J Radiol* 2012;85:945-51.
180. Hsiao EM, Rybicki FJ, Steigner M. CT coronary angiography: 256-slice and 320-detector row scanners. *Curr Cardiol Rep* 2010;12:68-75.
181. Dual Source CT Imaging. Spirit Link GmbH 2007-2018. (Accessed April 19, 2018, at [http://www.dsct.com/index.php/the-technology/introduction/dual-source-ct-imaging/.](http://www.dsct.com/index.php/the-technology/introduction/dual-source-ct-imaging/))
182. Flohr TG, McCollough CH, Bruder H, et al. First performance evaluation of a dual-source CT (DSCT) system. *Eur Radiol* 2006;16:256-68.
183. Attenuation. Miller-Keane Encyclopedia and Dictionary of Medicine, Nursing, and Allied Health, Seventh Edition., 2003. (Accessed March 06, 2018, at <https://medical-dictionary.thefreedictionary.com/attenuation.>)
184. Attenuation Correction. Copyright Rector and Visitors of the University of Virginia, 2013. (Accessed March 06, 2018, at <https://www.med-ed.virginia.edu/courses/rad/petct/Attenuation.html>)
185. McKetty MH. The AAPM/RSNA physics tutorial for residents. X-ray attenuation. *Radiographics* 1998;18:151-63; quiz 49.

186. Leipsic J, Labounty TM, Hague CJ, et al. Effect of a novel vendor-specific motion-correction algorithm on image quality and diagnostic accuracy in persons undergoing coronary CT angiography without rate-control medications. *J Cardiovasc Comput Tomogr* 2012;6:164-71.
187. Takayanagi T, Sano T, Kondo T, et al. [Clinical usefulness of low tube current scanning with full reconstruction and automatic patient motion correction (APMC) reconstruction in a prospective ECG-gated coronary CT angiography using 320-row area detector CT]. *Nihon Hoshasen Gijutsu Gakkai zasshi* 2015;71:237-45.
188. Herzog C, Arning-Erb M, Zangos S, et al. Multi-detector row CT coronary angiography: influence of reconstruction technique and heart rate on image quality. *Radiology* 2006;238:75-86.
189. Lesser JR, Flygenring BJ, Knickelbine T, Longe T, Schwartz RS. Practical approaches to overcoming artifacts in coronary CT angiography. *J Cardiovasc Comput Tomogr* 2009;3:4-15.
190. Kropil P, Rojas CA, Ghoshhajra B, et al. Prospectively ECG-triggered high-pitch spiral acquisition for cardiac CT angiography in routine clinical practice: initial results. *J Thorac Imaging* 2012;27:194-201.
191. Halliburton SS, Abbara S. Practical tips and tricks in cardiovascular computed tomography: patient preparation for optimization of cardiovascular CT data acquisition. *J Cardiovasc Comput Tomogr* 2007;1:62-5.
192. Horiguchi J, Shen Y, Hirai N, et al. Timing on 16-slice scanner and implications for 64-slice cardiac CT: do you start scanning immediately after breath hold? *Acad Radiol* 2006;13:173-6.
193. Enzweiler CN, Kivelitz DE, Wiese TH, et al. Coronary artery bypass grafts: improved electron-beam tomography by prolonging breath holds with preoxygenation. *Radiology* 2000;217:278-83.
194. Barrett JF, Keat N. Artifacts in CT: recognition and avoidance. *Radiographics* 2004;24:1679-91.

195. Galiwango P, Chow BJ. Cardiac computed tomography and risks of radiation exposure: how low can we go? *Can J Cardiol* 2011;27:536-7.
196. Heydari B, Leipsic J, Mancini GB, et al. Diagnostic performance of high-definition coronary computed tomography angiography performed with multiple radiation dose reduction strategies. *Can J Cardiol* 2011;27:606-12.
197. Stocker TJ, Deseive S, Leipsic J, et al. Reduction in radiation exposure in cardiovascular computed tomography imaging: results from the PROspective multicenter registry on radiaTion dose Estimates of cardiac CT angIOgraphy iN daily practice in 2017 (PROTECTION VI). *Eur Heart J* 2018;39:3715-23.
198. Matsutani H, Sano T, Kondo T, et al. [Comparison of radiation dose reduction of prospective ECG-gated one beat scan using 320 area detector CT coronary angiography and prospective ECG-gated helical scan with high helical pitch (FlashScan) using 64 multidetector-row CT coronary angiography]. *Nihon Hoshasen Gijutsu Gakkai zasshi* 2010;66:1548-54.
199. Machida H, Tanaka I, Fukui R, et al. Current and Novel Imaging Techniques in Coronary CT. *Radiographics* 2015;35:991-1010.
200. Kalra MK, Sodickson AD, Mayo-Smith WW. CT Radiation: Key Concepts for Gentle and Wise Use. *Radiographics* 2015;35:1706-21.
201. Hausleiter J, Meyer T, Hermann F, et al. Estimated radiation dose associated with cardiac CT angiography. *JAMA* 2009;301:500-7.
202. Nieman K, Oudkerk M, Rensing BJ, et al. Coronary angiography with multi-slice computed tomography. *Lancet* 2001;357:599-603.
203. Achenbach S, Giesler T, Ropers D, et al. Detection of coronary artery stenoses by contrast-enhanced, retrospectively electrocardiographically-gated, multislice spiral computed tomography. *Circulation* 2001;103:2535-8.
204. Cademartiri F, La Grutta L, Palumbo A, et al. Non-invasive visualization of coronary atherosclerosis: state-of-art. *J Cardiovasc Med (Hagerstown)* 2007;8:129-37.

205. Nieman K, Cademartiri F, Lemos PA, Raaijmakers R, Pattynama PM, de Feyter PJ. Reliable noninvasive coronary angiography with fast submillimeter multislice spiral computed tomography. *Circulation* 2002;106:2051-4.
206. Ropers D, Baum U, Pohle K, et al. Detection of coronary artery stenoses with thin-slice multi-detector row spiral computed tomography and multiplanar reconstruction. *Circulation* 2003;107:664-6.
207. Martuscelli E, Romagnoli A, D'Eliseo A, et al. Accuracy of thin-slice computed tomography in the detection of coronary stenoses. *Eur Heart J* 2004;25:1043-8.
208. Mollet NR, Cademartiri F, Nieman K, et al. Multislice spiral computed tomography coronary angiography in patients with stable angina pectoris. *J Am Coll Cardiol* 2004;43:2265-70.
209. Hoffmann U, Moselewski F, Cury RC, et al. Predictive value of 16-slice multidetector spiral computed tomography to detect significant obstructive coronary artery disease in patients at high risk for coronary artery disease: patient-versus segment-based analysis. *Circulation* 2004;110:2638-43.
210. Kuettner A, Beck T, Drosch T, et al. Diagnostic accuracy of noninvasive coronary imaging using 16-detector slice spiral computed tomography with 188 ms temporal resolution. *J Am Coll Cardiol* 2005;45:123-7.
211. Mollet NR, Cademartiri F, Krestin GP, et al. Improved diagnostic accuracy with 16-row multi-slice computed tomography coronary angiography. *J Am Coll Cardiol* 2005;45:128-32.
212. Hoffmann MH, Shi H, Schmitz BL, et al. Noninvasive coronary angiography with multislice computed tomography. *JAMA* 2005;293:2471-8.
213. Leschka S, Alkadhi H, Plass A, et al. Accuracy of MSCT coronary angiography with 64-slice technology: first experience. *Eur Heart J* 2005;26:1482-7.
214. Raff GL, Gallagher MJ, O'Neill WW, Goldstein JA. Diagnostic accuracy of noninvasive coronary angiography using 64-slice spiral computed tomography. *J Am Coll Cardiol* 2005;46:552-7.

215. Leber AW, Knez A, von Ziegler F, et al. Quantification of obstructive and nonobstructive coronary lesions by 64-slice computed tomography: a comparative study with quantitative coronary angiography and intravascular ultrasound. *J Am Coll Cardiol* 2005;46:147-54.
216. Mollet NR, Cademartiri F, van Mieghem CA, et al. High-resolution spiral computed tomography coronary angiography in patients referred for diagnostic conventional coronary angiography. *Circulation* 2005;112:2318-23.
217. Bordeleau E, Lamonde A, Prenovault J, et al. Accuracy and rate of coronary artery segment visualization with CT angiography for the non-invasive detection of coronary artery stenoses. *Int J Cardiovasc Imaging* 2007;23:771-80.
218. Min JK, Swaminathan RV, Vass M, Gallagher S, Weinsaft JW. High-definition multidetector computed tomography for evaluation of coronary artery stents: comparison to standard-definition 64-detector row computed tomography. *J Cardiovasc Comput Tomogr* 2009;3:246-51.
219. Beister M, Kolditz D, Kalender WA. Iterative reconstruction methods in X-ray CT. *Phys Med* 2012;28:94-108.
220. Kim M, Lee JM, Yoon JH, et al. Adaptive iterative dose reduction algorithm in CT: effect on image quality compared with filtered back projection in body phantoms of different sizes. *Korean journal of radiology* 2014;15:195-204.
221. Klink T, Obmann V, Heverhagen J, Stork A, Adam G, Begemann P. Reducing CT radiation dose with iterative reconstruction algorithms: the influence of scan and reconstruction parameters on image quality and CTDIvol. *Eur J Radiol* 2014;83:1645-54.
222. Hara AK, Paden RG, Silva AC, Kujak JL, Lawder HJ, Pavlicek W. Iterative reconstruction technique for reducing body radiation dose at CT: feasibility study. *AJR Am J Roentgenol* 2009;193:764-71.
223. Achenbach S, Ropers D, Kuettner A, et al. Contrast-enhanced coronary artery visualization by dual-source computed tomography--initial experience. *Eur J Radiol* 2006;57:331-5.

224. Dey D, Lee CJ, Ohba M, et al. Image quality and artifacts in coronary CT angiography with dual-source CT: initial clinical experience. *J Cardiovasc Comput Tomogr* 2008;2:105-14.
225. Sun Z, Davidson R, Lin CH. Multi-detector row CT angiography in the assessment of coronary in-stent restenosis: a systematic review. *Eur J Radiol* 2009;69:489-95.
226. Kumbhani DJ, Ingelmo CP, Schoenhagen P, Curtin RJ, Flamm SD, Desai MY. Meta-analysis of diagnostic efficacy of 64-slice computed tomography in the evaluation of coronary in-stent restenosis. *Am J Cardiol* 2009;103:1675-81.
227. Carrabba N, Schuijf JD, de Graaf FR, et al. Diagnostic accuracy of 64-slice computed tomography coronary angiography for the detection of in-stent restenosis: a meta-analysis. *J Nucl Cardiol* 2010;17:470-8.
228. Taylor AJ, Cerqueira M, Hodgson JM, et al. ACCF/SCCT/ACR/AHA/ASE/ASNC/NASCI/SCAI/SCMR 2010 appropriate use criteria for cardiac computed tomography. A report of the American College of Cardiology Foundation Appropriate Use Criteria Task Force, the Society of Cardiovascular Computed Tomography, the American College of Radiology, the American Heart Association, the American Society of Echocardiography, the American Society of Nuclear Cardiology, the North American Society for Cardiovascular Imaging, the Society for Cardiovascular Angiography and Interventions, and the Society for Cardiovascular Magnetic Resonance. *J Am Coll Cardiol* 2010;56:1864-94.
229. Collet C, Chevalier B, Cequier A, et al. Diagnostic Accuracy of Coronary CT Angiography for the Evaluation of Bioresorbable Vascular Scaffolds. *JACC Cardiovasc Imaging* 2018;11:722-32.
230. Shaw LJ, Hausleiter J, Achenbach S, et al. Coronary computed tomographic angiography as a gatekeeper to invasive diagnostic and surgical procedures: results from the multicenter CONFIRM (Coronary CT Angiography Evaluation for Clinical Outcomes: an International Multicenter) registry. *J Am Coll Cardiol* 2012;60:2103-14.
231. Miller JM, Rochitte CE, Dewey M, et al. Diagnostic performance of coronary angiography by 64-row CT. *N Engl J Med* 2008;359:2324-36.

232. Meijboom WB, Meijs MF, Schuijf JD, et al. Diagnostic accuracy of 64-slice computed tomography coronary angiography: a prospective, multicenter, multivendor study. *J Am Coll Cardiol* 2008;52:2135-44.
233. Hecht HS. Coronary artery calcium scanning: past, present, and future. *JACC Cardiovasc Imaging* 2015;8:579-96.
234. Finn AV, Nakano M, Narula J, Kolodgie FD, Virmani R. Concept of vulnerable/unstable plaque. *Arterioscler Thromb Vasc Biol* 2010;30:1282-92.
235. Achenbach S. Can CT detect the vulnerable coronary plaque? *Int J Cardiovasc Imaging* 2008;24:311-2.
236. Maurovich-Horvat P, Ferencik M, Voros S, Merkely B, Hoffmann U. Comprehensive plaque assessment by coronary CT angiography. *Nat Rev Cardiol* 2014;11:390-402.
237. Otsuka M, Bruining N, Van Pelt NC, et al. Quantification of coronary plaque by 64-slice computed tomography: a comparison with quantitative intracoronary ultrasound. *Invest Radiol* 2008;43:314-21.
238. van der Giessen AG, Toepker MH, Donnelly PM, et al. Reproducibility, accuracy, and predictors of accuracy for the detection of coronary atherosclerotic plaque composition by computed tomography: an ex vivo comparison to intravascular ultrasound. *Invest Radiol* 2010;45:693-701.
239. Motoyama S, Sarai M, Harigaya H, et al. Computed tomographic angiography characteristics of atherosclerotic plaques subsequently resulting in acute coronary syndrome. *J Am Coll Cardiol* 2009;54:49-57.
240. Suzuki S, Furui S, Kuwahara S, et al. Accuracy of attenuation measurement of vascular wall in vitro on computed tomography angiography: Effect of wall thickness, density of contrast medium, and measurement point. *Invest Radiol* 2006;41:510-5.

241. Achenbach S, Boehmer K, Pflederer T, et al. Influence of slice thickness and reconstruction kernel on the computed tomographic attenuation of coronary atherosclerotic plaque. *J Cardiovasc Comput Tomogr* 2010;4:110-5.
242. Hoffmann U, Moselewski F, Nieman K, et al. Noninvasive assessment of plaque morphology and composition in culprit and stable lesions in acute coronary syndrome and stable lesions in stable angina by multidetector computed tomography. *J Am Coll Cardiol* 2006;47:1655-62.
243. Psaltis PJ, Talman AH, Munnur K, et al. Relationship between epicardial fat and quantitative coronary artery plaque progression: insights from computer tomography coronary angiography. *Int J Cardiovasc Imaging* 2016;32:317-28.
244. Szilveszter B, Celeng C, Maurovich-Horvat P. Plaque assessment by coronary CT. *Int J Cardiovasc Imaging* 2016;32:161-72.
245. Hutcheson JD, Maldonado N, Aikawa E. Small entities with large impact: microcalcifications and atherosclerotic plaque vulnerability. *Curr Opin Lipidol* 2014;25:327-32.
246. Maurovich-Horvat P, Hoffmann U, Vorpahl M, Nakano M, Virmani R, Alkadhi H. The napkin-ring sign: CT signature of high-risk coronary plaques? *JACC Cardiovasc Imaging* 2010;3:440-4.
247. Otsuka K, Fukuda S, Tanaka A, et al. Napkin-ring sign on coronary CT angiography for the prediction of acute coronary syndrome. *JACC Cardiovasc Imaging* 2013;6:448-57.
248. Puchner SB, Liu T, Mayrhofer T, et al. High-risk plaque detected on coronary CT angiography predicts acute coronary syndromes independent of significant stenosis in acute chest pain: results from the ROMICAT-II trial. *J Am Coll Cardiol* 2014;64:684-92.
249. Park HB, Heo R, o Hartaigh B, et al. Atherosclerotic plaque characteristics by CT angiography identify coronary lesions that cause ischemia: a direct comparison to fractional flow reserve. *JACC Cardiovasc Imaging* 2015;8:1-10.

250. Fihn SD, Gardin JM, Abrams J, et al. 2012 ACCF/AHA/ACP/AATS/PCNA/SCAI/STS Guideline for the diagnosis and management of patients with stable ischemic heart disease: a report of the American College of Cardiology Foundation/American Heart Association Task Force on Practice Guidelines, and the American College of Physicians, American Association for Thoracic Surgery, Preventive Cardiovascular Nurses Association, Society for Cardiovascular Angiography and Interventions, and Society of Thoracic Surgeons. *J Am Coll Cardiol* 2012;60:e44-e164.
251. Pijls NH, De Bruyne B, Peels K, et al. Measurement of fractional flow reserve to assess the functional severity of coronary-artery stenoses. *N Engl J Med* 1996;334:1703-8.
252. Rajani R, Modi B, Ntalas I, Curzen N. Non-invasive fractional flow reserve using computed tomographic angiography: where are we now and where are we going? *Heart* 2017;103:1216-22.
253. Coenen A, Lubbers MM, Kurata A, et al. Fractional flow reserve computed from noninvasive CT angiography data: diagnostic performance of an on-site clinician-operated computational fluid dynamics algorithm. *Radiology* 2015;274:674-83.
254. Gilard M, Cornily JC, Rioufol G, et al. Noninvasive assessment of left main coronary stent patency with 16-slice computed tomography. *Am J Cardiol* 2005;95:110-2.
255. Schuijf JD, Bax JJ, Jukema JW, et al. Feasibility of assessment of coronary stent patency using 16-slice computed tomography. *Am J Cardiol* 2004;94:427-30.
256. Collet C, Sotomi Y, Cavalcante R, et al. Accuracy of coronary computed tomography angiography for bioresorbable scaffold luminal investigation: a comparison with optical coherence tomography. *Int J Cardiovasc Imaging* 2017;33:431-9.
257. Motoyama S, Sarai M, Harigaya H, et al. Computed tomographic angiography characteristics of atherosclerotic plaques subsequently resulting in acute coronary syndrome, *J Am Coll Cardiol* 2009; 54 :49-57.
258. Sabate M, Kay IP, de Feyter PJ, et al. Remodeling of atherosclerotic coronary arteries varies in relation to location and composition of plaque. *Am J Cardiol* 1999;84:135-40.
259. Gassenmaier T, Petri N, Allmendinger T, et al. Next generation coronary CT angiography: in vitro evaluation of 27 coronary stents. *Eur Radiol* 2014;24:2953-61.

260. KVP ACCURACY. 2015. (Accessed 2nd october, 2019, at <http://qcirradiography.weebly.com/kvp-accuracy/kvp-accuracy>.)
261. Nieman K, Serruys PW, Onuma Y, et al. Multislice computed tomography angiography for noninvasive assessment of the 18-month performance of a novel radiolucent bioresorbable vascular scaffolding device: the ABSORB trial (a clinical evaluation of the bioabsorbable everolimus eluting coronary stent system in the treatment of patients with de novo native coronary artery lesions). *J Am Coll Cardiol* 2013;62:1813-4.
262. Onuma Y, Dudek D, Thuesen L, et al. Five-year clinical and functional multislice computed tomography angiographic results after coronary implantation of the fully resorbable polymeric everolimus-eluting scaffold in patients with de novo coronary artery disease: the ABSORB cohort A trial. *JACC Cardiovasc Interv* 2013;6:999-1009.
263. Verheye S, Ormiston JA, Stewart J, et al. A next-generation bioresorbable coronary scaffold system: from bench to first clinical evaluation: 6- and 12-month clinical and multimodality imaging results. *JACC Cardiovasc Interv* 2014;7:89-99.
264. Marchese G, Petr R, Tousek P, Widimsky P, Kocka V. Bioresorbable vascular scaffolds in STEMI patients: multimodality imaging comparison in mid-term perspective. *Minerva Cardioangiol* 2016;64:411-8.
265. Onuma Y, Collet C, van Geuns RJ, et al. Long-term serial non-invasive multislice computed tomography angiography with functional evaluation after coronary implantation of a bioresorbable everolimus-eluting scaffold: the ABSORB cohort B MSCT substudy. *Eur Heart J Cardiovasc Imaging* 2017;18:870-9.
266. Sarno G, Bruining N, Onuma Y, et al. Morphological and functional evaluation of the bioresorption of the bioresorbable everolimus-eluting vascular scaffold using IVUS, echogenicity and vasomotion testing at two year follow-up: a patient level insight into the ABSORB A clinical trial. *Int J Cardiovasc Imaging* 2012;28:51-8.

267. Ormiston JA, Serruys PW, Onuma Y, et al. First serial assessment at 6 months and 2 years of the second generation of absorb everolimus-eluting bioresorbable vascular scaffold: a multi-imaging modality study. *Circ Cardiovasc Interv* 2012;5:620-32.
268. Tesche C, De Cecco CN, Vliegenthart R, et al. Coronary CT angiography-derived quantitative markers for predicting in-stent restenosis. *J Cardiovasc Comput Tomogr* 2016;10:377-83.
269. Hidalgo B, Goodman M. Multivariate or multivariable regression? *Am J Public Health* 2013;103:39-40.
270. MULTIVARIATE REGRESSION ANALYSIS | STATA DATA ANALYSIS EXAMPLES. UC REGENTS, 2018. (Accessed November 14th, 2018, at [https://stats.idre.ucla.edu/stata/dac/multivariate-regression-analysis/.](https://stats.idre.ucla.edu/stata/dac/multivariate-regression-analysis/))
271. Brugaletta S, Garcia-Garcia HM, Garg S, et al. Temporal changes of coronary artery plaque located behind the struts of the everolimus eluting bioresorbable vascular scaffold. *Int J Cardiovasc Imaging* 2011;27:859-66.
272. Serruys PW, Onuma Y, Garcia-Garcia HM, et al. Dynamics of vessel wall changes following the implantation of the absorb everolimus-eluting bioresorbable vascular scaffold: a multi-imaging modality study at 6, 12, 24 and 36 months. *EuroIntervention* 2014;9:1271-84.
273. Garcia-Garcia HM, Serruys PW, Campos CM, Onuma Y. Differential impact of five coronary devices on plaque size: insights from the ABSORB and SPIRIT trials. *Int J Cardiol* 2014;175:441-5.
274. Suwannasom P, Sotomi Y, Asano T, et al. Change in lumen eccentricity and asymmetry after treatment with Absorb bioresorbable vascular scaffolds in the ABSORB cohort B trial: a five-year serial optical coherence tomography imaging study. *EuroIntervention* 2017;12:e2244-e52.
275. Campos CM, Garcia-Garcia HM, Muramatsu T, et al. Impact of the Everolimus-eluting Bioresorbable Scaffold in Coronary Atherosclerosis. *Revista espanola de cardiologia (English ed)* 2016;69:109-16.

276. Ormiston JA, Serruys PW, Regar E, et al. A bioabsorbable everolimus-eluting coronary stent system for patients with single de-novo coronary artery lesions (ABSORB): a prospective open-label trial. *Lancet* 2008;371:899-907.
277. Austen WG, Edwards JE, Frye RL, et al. A reporting system on patients evaluated for coronary artery disease. Report of the Ad Hoc Committee for Grading of Coronary Artery Disease, Council on Cardiovascular Surgery, American Heart Association. *Circulation* 1975;51:5-40.
278. Papadopoulou SL, Neefjes LA, Garcia-Garcia HM, et al. Natural history of coronary atherosclerosis by multislice computed tomography. *JACC Cardiovasc Imaging* 2012;5:S28-37.
279. Rodriguez K, Kwan AC, Lai S, et al. Coronary Plaque Burden at Coronary CT Angiography in Asymptomatic Men and Women. *Radiology* 2015;277:73-80.
280. Martinet W, De Loof H, De Meyer GR. mTOR inhibition: a promising strategy for stabilization of atherosclerotic plaques. *Atherosclerosis* 2014;233:601-7.
281. Croons V, Martinet W, Herman AG, Timmermans JP, De Meyer GR. Selective clearance of macrophages in atherosclerotic plaques by the protein synthesis inhibitor cycloheximide. *J Pharmacol Exp Ther* 2007;320:986-93.
282. Tanabe K, Popma JJ, Kozuma K, et al. Multi-slice Computed Tomography Assessment of Everolimus-Eluting Absorb Bioresorbable Scaffold in Comparison with Metallic Drug-Eluting Stents from the ABSORB Japan randomized Trial. *EuroIntervention* 2017.
283. Wiebe J, Hoppmann P, Kufner S, et al. Impact of stent size on angiographic and clinical outcomes after implantation of everolimus-eluting bioresorbable scaffolds in daily practice: insights from the ISAR-ABSORB registry. *EuroIntervention* 2016;12:e137-43.
284. Maurovich-Horvat P, Ferencik M, Bamberg F, Hoffmann U. Methods of plaque quantification and characterization by cardiac computed tomography. *J Cardiovasc Comput Tomogr* 2009;3 Suppl 2:S91-8.

285. Brodoefel H, Burgstahler C, Heuschmid M, et al. Accuracy of dual-source CT in the characterisation of non-calcified plaque: use of a colour-coded analysis compared with virtual histology intravascular ultrasound. *Br J Radiol* 2009;82:805-12.
286. Chen Z, Boldeanu I, Nepveu S, et al. In vivo coronary artery plaque assessment with computed tomography angiography: is there an impact of iterative reconstruction on plaque volume and attenuation metrics? *Acta Radiol* 2017;58:660-9.
287. Sadeghi MM, Glover DK, Lanza GM, Fayad ZA, Johnson LL. Imaging atherosclerosis and vulnerable plaque. *J Nucl Med* 2010;51 Suppl 1:51S-65S.
288. Sato Y, Inoue F, Yoshimura A, et al. Regression of an atherosclerotic coronary artery plaque demonstrated by multislice spiral computed tomography in a patient with stable angina pectoris. *Heart Vessels* 2003;18:224-6.
289. Gardner CM, Tan H, Hull EL, et al. Detection of lipid core coronary plaques in autopsy specimens with a novel catheter-based near-infrared spectroscopy system. *JACC Cardiovasc Imaging* 2008;1:638-48.
290. Morey SS. ACC and AHA update guidelines for coronary angiography. American College of Cardiology. American Heart Association. *Am Fam Physician* 1999;60:1017-20.
291. McHugh ML. Multiple comparison analysis testing in ANOVA. *Biochem Med (Zagreb)* 2011;21:203-9.
292. Gibbons RJ, Chatterjee K, Daley J, et al. ACC/AHA/ACP-ASIM guidelines for the management of patients with chronic stable angina: a report of the American College of Cardiology/American Heart Association Task Force on Practice Guidelines (Committee on Management of Patients With Chronic Stable Angina). *J Am Coll Cardiol* 1999;33:2092-197.
293. Gogas BD, Serruys PW, Diletti R, et al. Vascular response of the segments adjacent to the proximal and distal edges of the ABSORB everolimus-eluting bioresorbable vascular scaffold: 6-month and 1-year follow-up assessment: a virtual histology intravascular ultrasound study from the first-in-man ABSORB cohort B trial. *JACC Cardiovasc Interv* 2012;5:656-65.

294. Pendyala LK, Matsumoto D, Shinke T, et al. Nobori stent shows less vascular inflammation and early recovery of endothelial function compared with Cypher stent. *JACC Cardiovasc Interv* 2012;5:436-44.

295. Su SH, Nguyen KT, Satasiya P, Greilich PE, Tang L, Eberhart RC. Curcumin impregnation improves the mechanical properties and reduces the inflammatory response associated with poly(L-lactic acid) fiber. *J Biomater Sci Polym Ed* 2005;16:353-70.

296. Rodriguez M, Ringstad L, Schafer P, et al. Reduction of atherosclerotic nanoplaque formation and size by Ginkgo biloba (EGb 761) in cardiovascular high-risk patients. *Atherosclerosis* 2007;192:438-44.

Appendices



Comité d'éthique de la recherche du CHUM
Pavillon R, 900 rue St-Denis, 3^e étage
Montréal (Québec) H2X 0A9

Le 31 mai 2016

Docteur Carl Chartrand-Lefebvre
Axe de recherche : cardio-métabolique

a/s: Evguenia Zdanovich

courriel: **secured**

Objet:	Autorisation de réaliser la recherche suivante:
	Évaluation quantitative de la morphologie de la plaque et de la lumière intrastent des tuteurs biorésorbables - Étude longitudinale par tomодensitométrie 256 coupes (REABSORB-CT)
	- Numéro identifiant multicentrique: MP-02-2016-6556
	- Numéro CÉR CHUM: 15.397

Docteur,

Il nous fait plaisir de vous autoriser à réaliser la recherche identifiée en titre dans notre établissement et/ou sous ses auspices.

Cette autorisation vous est accordée sur la foi des documents que vous avez déposés auprès de notre établissement, notamment la lettre du Comité d'éthique de la recherche (CÉR) du CHUM portant la date du 6 mai 2016 qui établit que votre projet de recherche a fait l'objet d'un examen scientifique et d'un examen éthique dont le résultat est positif.

Si ce CÉR vous informe pendant le déroulement de cette recherche d'une décision négative portant sur l'acceptabilité éthique de cette recherche, vous devrez considérer que la présente autorisation de réaliser la recherche dans notre établissement est, de ce fait, révoquée à la date que porte l'avis du CÉR évaluateur.

Cette autorisation suppose également que vous respectiez les modalités énoncées ci-après:

1. avoir un statut de chercheur confirmé et à jour, et si applicable, transmettre à la Direction adjointe scientifique - Développement académique - CRCHUM (Mme Julie LeBlanc) tous les documents demandés ou vous conformer à toutes les procédures requises au plus tard 30 jours suivant la date de la présente ;
2. avoir obtenu l'autorisation du bureau des contrats;
3. vous conformer aux demandes du CÉR évaluateur, notamment pour le suivi éthique continu de la recherche;

4. rendre compte au CÉR évaluateur et à la signataire de la présente autorisation du déroulement du projet, des actes de votre équipe de recherche, s'il en est une, ainsi que du respect des règles de l'éthique de la recherche;
5. respecter les moyens relatifs au suivi continu qui ont été fixés par le CÉR évaluateur;
6. conserver les dossiers de recherche pendant la période fixée par le CÉR évaluateur, après la fin du projet, afin de permettre leur éventuelle vérification;
7. respecter les modalités arrêtées au regard du mécanisme d'identification des participants à la recherche dans notre établissement, à savoir, la tenue à jour et la conservation de la liste à jour des sujets de recherche recrutés dans notre établissement. Cette liste devra nous être fournie sur demande.

La présente autorisation peut être suspendue ou révoquée par notre établissement en cas de non-respect des conditions établies. Le CÉR évaluateur en sera alors informé.

Vous consentez également à ce que notre établissement communique aux autorités compétentes des renseignements personnels qui sont nominatifs au sens de la loi en présence d'un cas avéré de manquement à la conduite responsable en recherche de votre part lors de la réalisation de cette recherche.

Je vous invite à entrer en communication avec moi pendant le déroulement de cette recherche dans notre établissement, si besoin est. Vous pouvez aussi solliciter l'appui de notre CÉR en vous adressant au secrétariat pour obtenir les conseils et le soutien voulu, aux coordonnées suivantes:

- par courriel: ethique.recherche.chum@ssss.gouv.qc.ca
- par téléphone: 514 890-8000, poste 14485.

En terminant, je vous demanderais de toujours mentionner dans votre correspondance au sujet de ce projet de recherche le numéro attribué à votre demande par notre établissement 15.397 ainsi que le numéro attribué au projet de recherche par le CÉR évaluateur MP-02-2016-6556. Par ailleurs, vous voudrez bien faire suivre cette lettre aux personnes mentionnées ci-dessous (en cc).

Nous vous prions d'accepter, Docteur, nos salutations distinguées.

secured information

Mme Lynda Ferlatte

Personne-ressource pour le Comité d'éthique de la recherche du CHUM,
instance mandatée pour autoriser la réalisation des recherches
au nom du Directeur du Centre de recherche du CHUM

c.c.:

- Président du CÉR évaluateur
- Président du CÉR de l'établissement
- Promoteur (le cas échéant)
- Chercheur à qui est adressée la lettre du CÉR évaluateur donnant le résultat de l'examen éthique (si cette personne est différente du chercheur à qui est adressée la présente lettre d'autorisation)



Comité d'éthique de la recherche du CHUM
Pavillon R, 900 rue St-Denis, 3^e étage
Montréal (Québec) H2X 0A9

Le 27 octobre 2018

Docteur Carl Chartrand-Lefebvre
Axe de recherche: cardio-métabolique

a/s: Mme Evguenia Zdanovich
courriel: **secured**

Objet:	MP-02-2016-6556, 15.397 - Approbation d'un formulaire (F9 - 37930)
	Évaluation quantitative de la morphologie de la plaque et de la lumière intrastent des tuteurs biorésorbables - Étude longitudinale par tomographie 256 coupes (REABSORB-CT)

Docteur,

La présente est pour vous informer que le formulaire F9 - 37930 que vous nous avez soumis est complet et conforme aux règles applicables. Il a donc été approuvé par le CÉR du CHUM qui agit à titre de CÉR évaluateur pour le projet en titre.

Vous souhaitant la meilleure des chances dans la poursuite de vos travaux, nous vous prions d'accepter, Docteur, nos salutations distinguées.

secured information

Me Marie-Josée Bernardi, avocate
Chef du Bureau de l'éthique
Présidente du Comité d'éthique de la recherche

Information and patient consent forms

TITRE DU PROJET DE RECHERCHE :

Évaluation quantitative de la morphologie de la plaque et de la lumière intrastent des tuteurs biorésorbables - Étude longitudinale REABSORB-CT par tomodensitométrie 256 coupes.

Titre court : REABSORB-CT

Protocole no : Version 03, 23 Mars 2016

Chercheurs principaux : Dr Carl Chartrand-Lefebvre, MD

Service de radiologie,

Hôpital Hôtel-Dieu, CHUM

Dr Samer Mansour, MD

Service de cardiologie,

Hôpital Hôtel-Dieu, CHUM

Co-chercheurs :

Dr Alexandre Semionov

Dr Gilles Soulez

Dr Claude Kauffmann

Dr Jeannot Potvin

Dr André Kokis

Dr Jean-Bernard Masson

Dr François Gobeil

Dr Vu Quan

Dr François Lemire

Dr François Reeves

Dr Claude Pilon

Dr Guy Leclerc

Dr Alain Rivard

Evguenia Zdanovich

No du projet au CÉR CHUM : 15.397

ORGANISME SUBVENTIONNAIRE : Le chercheur responsable du projet et l'établissement bénéficient également d'un financement par un organisme subventionnaire public provincial nommé RBIQ (Réseau de Bio-imagerie du Québec).

PRÉAMBULE :

Nous sollicitons votre participation à un projet de recherche, car votre cardiologue vous a installé un tuteur coronarien (stent, implant) biorésorbable à libération d'éverolimus Absorb® dans le cadre de vos soins cliniques. Cependant, avant d'accepter de participer à ce projet et de signer ce formulaire d'information et de consentement, veuillez prendre le temps de lire, de comprendre et de considérer attentivement les renseignements qui suivent.

Ce formulaire peut contenir des mots que vous ne comprenez pas. Nous vous invitons à poser toutes les questions que vous jugerez utiles au chercheur responsable et aux membres de son équipe de recherche et à leur demander de vous expliquer tout mot ou renseignement qui n'est pas clair.

NATURE ET OBJECTIFS DU PROJET DE RECHERCHE :

Le traitement des artères coronaires est effectué par l'implantation de tuteur coronarien en métal. Toutefois, ce type de tuteur médicamenté a des limitations à long terme. Le tuteur biorésorbable à libération d'éverolimus Absorb® est une nouvelle approche pour le traitement des artères coronaires qui nous permet l'arrêt de la double thérapie antiplaquettaire à long terme. Ce tuteur est approuvé en Europe et disponible au Canada en accès spécial.

L'objectif de ce registre est de recueillir les données médicales permettant d'évaluer l'expérience clinique de ce tuteur bioresorbable à libération d'everolimus Absorb® en situation aiguë et à long terme.

De plus, dans le cadre de l'étude REABSORB-CT, nous vous proposons d'évaluer, via la tomodensitométrie, certains paramètres de la perméabilité de votre implant coronarien, durant la période qui se situe entre 1 à 60 mois après votre implantation (notamment, à 1, 12, 36 et 60 mois).

L'étude REABSORB-CT vise à identifier le potentiel de reblocage dans vos artères coronariennes nourrissant le cœur. Comme vous savez peut-être déjà, même si ces blocages sont présents, il se peut que vous ne ressentiez aucun symptôme. Cependant, une progression de ces blocages pourrait entraîner de l'angine ou même un infarctus.

La recherche pour laquelle vous êtes sollicité vise donc à collecter des données sur la perméabilité à moyen et à long terme de l'implant dont vous êtes porteur et de comparer avec les données de la littérature. Or, l'objectif principal de cette étude est d'évaluer le potentiel de reblocage de votre implant coronarien à l'aide d'une méthode non invasive, soit la tomodensitométrie, plus souvent appelée *scanner (scan, CT scan)*.

La tomodensitométrie ou scanner hélicoïdal multidétecteurs est une technique non invasive récemment utilisée dans le diagnostic de la maladie coronarienne. Cette technique est basée sur l'utilisation de rayon X et nécessite l'injection intraveineuse (dans une veine du bras) de colorants iodés. Elle ne nécessite toutefois pas de ponction dans une artère ni l'introduction d'un cathéter dans les artères coronaires comme ce le serait lors d'une coronarographie conventionnelle. Nous pensons que cette technique pourrait être très utile dans la détection des rétrécissements ou des reblocage des implants coronariens. De plus, cet examen pourrait permettre la détection des rétrécissements des artères coronaires natives (n'ayant subi aucune intervention et ne portant aucun implant). L'utilisation de la tomodensitométrie pour l'évaluation des artères coronaires ou les implants coronariens a été récemment introduite en clinique, mais est beaucoup moins fréquemment utilisée qu'une coronarographie conventionnelle. Nous avons au CHUM un

appareil de tomodensitométrie haute performance contenant plusieurs détecteurs permettant des images de très haute résolution avec un minimum de radiation.

NOMBRE DE PARTICIPANTS ET DURÉE DE LA PARTICIPATION :

Tous les patients ayant subi une revascularisation coronarienne dans le cadre du projet REABSORB seront invités à participer à 1, à 12, à 36 et à 60 mois après leur chirurgie d'implantation coronarienne, jusqu'à un maximum de 60 patients pour un maximum de 4 visites au département de radiologie pour la participation individuelle.

NATURE DE LA PARTICIPATION DEMANDÉE :

En acceptant de participer à ce projet de recherche, vous nous autorisez à utiliser les informations contenues dans votre dossier médical concernant les soins que vous avez reçus lors de l'intervention utilisant le tuteur biorésorbable à libération d'everolimus et tout au long de votre participation à l'étude. Ces données peuvent comprendre votre date de naissance et votre sexe, les examens effectués et les médicaments administrés dans le cadre de la procédure.

De plus, on vous demandera de fournir des informations sur votre état de santé cardiaque 1, 6, 12, 36 et 60 mois après la procédure lors d'un appel téléphonique ou lors d'une visite avec votre cardiologue. Ces suivis visent l'évaluation de votre condition médicale. Nous vous demanderons la médication que vous prenez et la survenue d'évènements cardiovasculaires (crise cardiaque, angine, revascularisation, décès cardiaque) ou procédures cardiaques depuis l'implantation du tuteur bioresorbable.

Également, si vous acceptez de participer à cette étude, vous devrez vous soumettre à un examen par tomodensitométrie qui sera effectué au Département de Radiologie de l'Hôtel-Dieu du CHUM.

La tomodensitométrie est un examen supplémentaire que vous n'auriez pas nécessairement à subir si vous ne participiez pas à l'étude. Le scanner est couramment utilisé pour évaluer les organes

thoraciques ou abdominaux. C'est un examen de courte durée, entraînant très peu d'inconforts et très peu de risques.

Le projet est d'une durée de 60 mois. Tous les patients traités avec le tuteur bioresorbable à libération d'évérolimus et qui répondent aux critères d'inclusion et d'exclusion de l'étude peuvent participer à ce registre. Nous prévoyons recruter environ 60 patients au CHUM.

DÉROULEMENT DU PROJET DE RECHERCHE :

Le projet de recherche se déroulera de la façon suivante :

- Selon nos protocoles de routine, vous rencontrerez l'équipe médicale avant l'examen, et vous aurez à remplir un questionnaire pour vérifier si vous êtes allergique à l'iode, si vous avez des problèmes rénaux, ou si vous avez des contre-indications à certains médicaments.
- Ensuite nous prendrons vos signes vitaux : pression artérielle et fréquence cardiaque avant l'examen, pendant l'examen, et après l'examen.
- Après avoir vérifié si vous n'avez pas de contre-indications, il se peut que nous vous administrions une dose d'un médicament bêta-bloqueur (le plus souvent du métoprolol) pour ralentir le cœur, sachez que vous prenez probablement déjà ce type de médicament. Après avoir administré la dose de ce bêta-bloqueur (par la bouche), nous attendons environ une heure pour s'assurer qu'il fait effet. De plus, nous aurons peut-être à vous administrer une petite dose de nitroglycérine sous la langue, un autre médicament que vous avez déjà probablement pris pour votre maladie coronarienne. Il y a une attente nécessaire de 2 à 4 minutes après l'administration de la nitroglycérine.
- Nous procéderons à l'aide d'une piqûre sur votre bras à l'installation d'un soluté pour administrer l'iode.
- L'examen par tomographie assistée par ordinateur sera ensuite effectué, pendant lequel vous serez en constante observation par le personnel médical. Il est essentiel de bien collaborer et de

suivre les consignes. La prise des images se fait pendant que vous êtes sur la table du scanner. Cette prise des images elle-même ne prend que quelques secondes, pendant lesquelles il est important de ne pas bouger et de ne pas respirer. Si vous avez des questions, en tout temps quelqu'un pourra vous aider et vous assister.

- Lorsque l'examen sera complété, nous vous demanderons de rester encore 15 minutes pour vérifier vos signes vitaux et s'assurer que tout s'est bien passé.
- En tout, il faut compter environ de 1 heure à 2,5 heures de votre temps pour compléter l'examen, remplir le questionnaire, l'entretien avec le personnel et le médecin, la prise des images, et la surveillance. Le temps total peut varier, notamment, selon la nécessité ou non d'administrer le bêta-bloqueur, et selon l'achalandage en patients en tomodensitométrie (provenant des étages ou de l'urgence). Vous pourrez retourner chez vous par la suite.

Risques et inconvénients

La tomodensitométrie est un examen supplémentaire que vous n'auriez pas nécessairement à subir si vous ne participiez pas à l'étude. La tomodensitométrie est couramment utilisée pour évaluer les organes thoraciques ou abdominaux. C'est un examen de courte durée, entraînant très peu d'inconfort.

Les risques et les inconvénients reliés au scanner hélicoïdal multidétecteurs sont reliés surtout à l'administration du produit de contraste iodé. Les réactions au contraste iodé sont la majorité du temps absentes.

Ces réactions en effet ne surviennent que quelques fois, car le produit de contraste utilisé pour ces examens est un produit non-ionique d'osmolarité réduite qui diminue considérablement les réactions allergiques. La plupart du temps, lorsqu'elles surviennent, il s'agit d'effets secondaires mineurs.

- Parmi les effets secondaires mineurs non-allergiques, il y a par exemple : chaleur ($\leq 1\%$), nausées (1.2 %), goût métallique à la bouche ($\leq 1\%$).
- Parmi les effets secondaires mineurs de type allergique, on les retrouve dans moins de 1% : éternuements, rougeurs temporaires à la peau, démangeaisons temporaires, asthme léger.

Rarement des effets secondaires plus graves peuvent survenir (0.5%). Les effets secondaires majeurs de type allergique sont : problèmes respiratoires majeurs tels que dyspnée (difficulté à respirer) sévère, œdème aigu du poumon, œdème des voies respiratoires supérieures (la gorge) ($< 1\%$).

Le produit de contraste à l'iode peut aussi parfois causer une insuffisance rénale. Cette éventualité est rare (0.1 %) lors d'une injection intraveineux (tel que lors de l'examen par tomodensitométrie actuelle). Lorsqu'elle survient, il s'agit dans la majorité du temps d'un problème transitoire qui peut rarement devenir permanent.

Certaines conditions peuvent faire en sorte que vous ne pourriez pas subir la tomodensitométrie, selon les critères définis dans le protocole de recherche (critères d'exclusion).

Les principales contre-indications sont la présence d'une allergie sévère à l'iode et une insuffisance rénale sévère. Par contre, une allergie légère à l'iode et une insuffisance rénale légère sont des contre-indications relatives à l'administration de produits de contraste iodés; ce ne sont pas des contre-indications absolues, en ce sens qu'une préparation rénale ou en rapport avec l'allergie à l'iode peut vous être prescrit avant l'examen.

Un questionnaire est complété avant l'examen afin de savoir si vous êtes déjà connu pour une allergie à l'iode ou à un autre produit, ou pour un problème rénal. Dans certains cas, une préparation préalable peut être donnée au patient allergique ou au patient avec insuffisance rénale.

Enfin, si votre fréquence cardiaque (battements cardiaques) est élevée (égale ou supérieure à 60 battements par minute), il se peut que des bêta- bloqueurs (médicaments qui ralentissent les battements cardiaques) vous soient administrés (par la bouche), au département de radiologie, avant l'examen. Par contre, ceux-ci pourraient ne pas vous être prescrits, si vous avez de l'asthme sévère, ou avez une sténose sévère de la valve aortique, ou certaines arythmies. Il est également possible que de la nitroglycérine vous soit administrée avant l'examen. Elle pourrait ne pas être prescrite si vous avez pris du Viagra (Cialis, Levitra) dans les dernières 24h.

Un examen par tomodensitométrie comporte une exposition aux rayons X. Il y a un risque d'induction de cancer, bien que ce risque soit relativement faible. La tomodensitométrie cardiaque est réalisée au moyen d'une technologie nommée synchronisation prospective à l'ECG, qui diminue l'exposition aux rayons X. Un cache-thyroïde est placé devant la glande thyroïde, diminuant ainsi l'exposition de la glande aux radiations. Si l'examen est effectué chez une femme jeune, des cache-mammaires sont utilisés.

Si vous êtes enceinte, ou si vous allaitez, vous ne passerez pas de tomodensitométrie. Cet examen peut présenter des risques pour l'enfant à naître (radiations, administration d'iode). Si vous suspectez être enceinte, un test de grossesse sera fait pour s'assurer que vous n'êtes pas enceinte, avant la tomodensitométrie.

AVANTAGES:

Il se peut que vous retiriez un bénéfice personnel de votre participation à ce projet de recherche, mais on ne peut vous l'assurer. À tout le moins, les résultats obtenus contribueront à l'avancement des connaissances dans ce domaine.

PARTICIPATION VOLONTAIRE ET POSSIBILITÉ DE RETRAIT :

Votre participation à ce projet de recherche est volontaire. Vous êtes donc libre de refuser d'y participer. Vous pouvez également vous retirer de ce projet à n'importe quel moment, sans avoir à donner de raisons, en faisant connaître votre décision au chercheur responsable du projet ou à l'un des membres du personnel affecté au projet.

Votre décision de ne pas participer à ce projet de recherche ou de vous en retirer n'aura aucune conséquence sur la qualité des soins et des services auxquels vous avez droit ou sur votre relation avec le chercheur responsable du projet et les autres intervenants.

Le chercheur responsable du projet de recherche, le comité d'éthique de la recherche du CHUM ou l'organisme subventionnaire peuvent mettre fin à votre participation, sans votre consentement, si de nouvelles découvertes ou informations indiquent que votre participation au projet n'est plus dans votre intérêt, si vous ne respectez pas les consignes du projet de recherche ou s'il existe des raisons administratives d'abandonner le projet.

Si vous vous retirez ou êtes retiré(e) du projet, l'information déjà obtenue dans le cadre de ce projet sera conservée aussi longtemps que nécessaire pour assurer votre sécurité et aussi celles des autres participants de recherche et rencontrer les exigences réglementaires.

Toute nouvelle connaissance acquise durant le déroulement du projet qui pourrait affecter votre décision de continuer d'y participer vous sera communiquée sans délai verbalement et par écrit.

CONFIDENTIALITÉ :

Avec votre permission, votre médecin traitant sera averti de votre participation à ce projet de recherche.

Durant votre participation à ce projet, le chercheur responsable ainsi que son personnel recueilleront et consigneront dans un dossier de recherche les renseignements vous concernant. Seuls les renseignements nécessaires pour répondre aux objectifs scientifiques de ce projet seront recueillis.

Ces renseignements peuvent comprendre les informations contenues dans vos dossiers médicaux concernant votre état de santé passé et présent, vos habitudes de vie ainsi que les résultats de tous les tests, examens et procédures que vous aurez subis lors de l'intervention avec le tuteur Absorb® ainsi que les informations de suivi fournies lors des suivis téléphoniques ou des visites cliniques. Votre dossier peut aussi comprendre d'autres renseignements tels que votre nom, votre sexe, votre date de naissance et votre origine ethnique.

Tous les renseignements recueillis demeureront strictement confidentiels dans les limites prévues par la loi. Afin de préserver votre identité et la confidentialité des renseignements, vous ne serez identifié(e) que par un numéro de code. La clé du code reliant votre nom à votre dossier de recherche sera conservée par le chercheur responsable.

Le chercheur responsable fera parvenir à l'organisme subventionnaire ou à ses représentants, les données vous concernant. Ces données n'incluent pas votre nom ni votre adresse. L'organisme subventionnaire utilisera les données à des fins de recherche dans le but de répondre aux objectifs scientifiques du projet décrits dans le formulaire d'information et de consentement.

Les données en elles-mêmes ou combinées aux données provenant d'autres projets, pourront être partagées avec les organismes réglementaires canadiens ou d'autres pays ou avec les partenaires commerciaux de l'organisme subventionnaire. Ce transfert d'information implique que vos données pourraient être transmises dans d'autres pays que le Canada.

Cependant, l'organisme subventionnaire respectera les règles de confidentialité en vigueur au Québec et au Canada, et ce, dans tous les pays. Ces données seront conservées pendant 7 ans après la fin de l'étude par le chercheur responsable et l'organisme subventionnaire.

Également, les données du projet pourraient servir pour d'autres analyses de données reliées au projet ou pour l'élaboration de projets de recherches futurs.

Les données pourront être publiées dans des revues spécialisées ou faire l'objet de discussions scientifiques, mais il ne sera pas possible de vous identifier.

À des fins de surveillance et de contrôle, votre dossier de recherche ainsi que vos dossiers médicaux pourront être consultés par une personne mandatée par le comité d'éthique de la recherche du CHUM ou par l'établissement, par une personne mandatée par des organismes publics autorisés ainsi que par des représentants de l'organisme subventionnaire. Toutes ces personnes et ces organismes adhèrent à une politique de confidentialité.

À des fins de protection, notamment afin de pouvoir communiquer avec vous rapidement, vos noms et prénoms, vos coordonnées et la date de début et de fin de votre participation au projet seront conservés pendant un an après la fin du projet dans un répertoire à part maintenu par le chercheur responsable.

Vous avez le droit de consulter votre dossier de recherche pour vérifier les renseignements recueillis, et les faire rectifier au besoin, et ce, aussi longtemps que le chercheur responsable du projet ou l'établissement détiennent ces informations. Cependant, afin de préserver l'intégrité scientifique du projet, vous pourriez n'avoir accès à certaines de ces informations qu'une fois votre participation terminée.

COMMUNICATION DES RÉSULTATS GÉNÉRAUX :

Vous pourrez connaître les résultats généraux de cette étude si vous en faites la demande au chercheur principal à la fin de l'étude.

FINANCEMENT DU PROJET :

Le chercheur responsable du projet et l'établissement ont reçu un financement de l'organisme subventionnaire public provincial nommé RBIQ (Réseau de Bio-imagerie du Québec) pour mener à bien ce projet de recherche.

INDEMNISATION EN CAS DE PRÉJUDICE ET DROITS DU PARTICIPANT DE RECHERCHE :

Si vous deviez subir quelque préjudice que ce soit par suite à une procédure reliée à l'étude, vous recevrez tous les soins et services requis par votre état de santé, sans frais de votre part.

En acceptant de participer à cette étude, vous ne renoncez à aucun de vos droits ni ne libérez les chercheurs, l'établissement ou l'organisme subventionnaire de leurs responsabilités légales et professionnelles.

COMPENSATION :

Vous ne recevrez aucune compensation monétaire pour votre participation à ce projet de recherche et cette participation pourrait vous occasionner des coûts supplémentaires (stationnement, essence, repas, taxis).

Vous n'aurez à engager aucun frais pour l'ensemble des traitements et des examens qui seront exécutés à l'hôpital dans le cadre de votre participation à l'étude. L'hôpital n'est pas financièrement responsable pour le coût des médicaments nécessaires au traitement des effets secondaires reliés à cette étude. Vous devrez les assumer ou les réclamer au régime d'assurance-maladie de votre province ou à votre régime d'assurances privé s'ils sont couverts.

PERSONNES-RESSOURCES:

Si vous avez des questions concernant le projet de recherche ou si vous éprouvez un problème que vous croyez relié à votre participation au projet de recherche, vous pouvez communiquer avec le chercheur responsable, le cochercheur ou avec l'étudiante à la maîtrise aux numéros suivants (dans le but de confidentialité, les numéros ont été enlevés de mon mémoire de maîtrise):

- **Dr Carl Chartrand-Lefebvre (chercheur responsable), CHUM Hôtel-Dieu, Tel : (...) ...-....**
- **Evguenia Zdanovich (étudiante à la maîtrise), CHUM Hôtel-Dieu, Tél : (...) ...-....**
- **Dr Samer Mansour (cochercheur), CHUM Hôtel-Dieu, Tel : (...) ...-....**

En tout autre temps (soir, nuit, fin de semaine et jour férié), en cas d'urgence, pour rapporter des effets secondaires ou toute lésion liée à la recherche, vous devrez vous présenter à l'urgence de l'Hôtel-Dieu du CHUM au besoin et vous serez vu(e) par le médecin de garde en cardiologie. Vous devrez mentionner que vous participez à ce projet de recherche.

Pour toute question concernant vos droits en tant que participant impliqué dans ce projet de recherche ou si vous avez des plaintes ou des commentaires à formuler vous pouvez communiquer avec le commissaire local aux plaintes et à la qualité des services de l'Hôpital Hôtel-Dieu du CHUM au 514-890-8000, poste 12761.

SURVEILLANCE DES ASPECTS ÉTHIQUES DU PROJET DE RECHERCHE :

Le comité d'éthique de la recherche du CHUM a approuvé ce projet de recherche et en assure le suivi. De plus, il approuvera au préalable toute révision et toute modification apportée au formulaire d'information et de consentement et au protocole de recherche.

CONSENTEMENT

Avant de signer et dater le présent formulaire de consentement, j'ai reçu des explications complètes sur les méthodes et les moyens qui seront utilisés pour appliquer les procédures ainsi que sur les désagréments, les risques et les effets indésirables qui pourraient y être associés.

J'ai lu et j'ai eu suffisamment de temps pour comprendre pleinement les renseignements présentés ci-dessus concernant cette étude. J'ai eu l'occasion de poser toutes mes questions et on y a répondu à ma satisfaction. Je suis libre de poser d'autres questions à n'importe quel moment. J'accepte de plein gré de signer ce formulaire de consentement. Je recevrai un exemplaire de ce formulaire après l'avoir signé et daté. Un exemplaire sera également déposé à mon dossier médical. En conséquence, je comprends que cette information sera disponible à toute personne ou compagnie à qui je donnerai accès à mon dossier médical. En apposant ma signature sur ce formulaire, je ne renonce cependant à aucun de mes droits légaux ni ne libère le chercheur, l'hôpital ou l'organisme subventionnaire de leur responsabilité civile et professionnelle.

J'autorise le chercheur à informer mon médecin traitant de ma participation à ce projet et à lui transmettre toute information pertinente :

Oui Δ

Non Δ

Nom et adresse du médecin traitant :

.....

Nom du participant

.....

Signature

.....

Date de la signature

Signature de la personne qui a obtenu le consentement, si différente du chercheur

responsable du projet de recherche

J'ai expliqué au participant à la recherche les termes du présent formulaire d'information et de consentement et j'ai répondu aux questions qu'il m'a posées.

Nom et signature de la personne qui obtient le consentement

Date

Engagement du chercheur

Je certifie qu'on a expliqué au participant de recherche les termes du présent formulaire d'information et de consentement, que l'on a répondu aux questions que le participant de

recherche avait à cet égard et qu'on lui a clairement indiqué qu'il demeure libre de mettre un terme à sa participation, et datée au participant de recherche.

Je m'engage, avec l'équipe de recherche, à respecter ce qui a été convenu au formulaire d'information et de consentement et à en remettre une copie signée au participant de recherche.

.....

Nom du chercheur

.....

Signature

.....

Date de la signature


Protocole de volumétrie et de composition


Paramètre à mesurer :

- 1) la progression du volume de la plaque intrastent (mm^3) : variable continue.
- 2) la composition de la plaque (volumétrie (mm^3) des composantes selon leur atténuation différentielle en unités Hounsfield) (-1024 à 30, 31-50, 51-100, 101-150, 151-350 and 351-3070 HU) : variable catégorielle.
- 3) Évaluer si la composition à 1 mois dans les trois régions peut prédire la morphologie de la plaque (volume, diminution de la lumière etc.) à 12 mois.
 - on comparera par des segments regroupés de 5 mm

Mesures de volumes (composition par strates de HU et mm^3):


Selon le tutoriel de Caroline Brisson et le protocole d'Irina Boldeanu


1. Ouvrir le dossier du patient dans Aquarius iNtuition, TeraRecon. Si le dossier n'a pas été encore transféré dans Aquarius faire l'étape 2
2. Ouvrir le dossier dans IMPAX. Choisir la série dans la fenêtre « Description de la série » avec les paramètres suivants : préférentiellement, ALG : XCB; 0.8 mm; 78 % ou 75 %; No correction et id3. Ensuite, cliquer bouton droite de la souris sur les images de la série choisie, et cliquer « Transmettre » puis « Séries » puis dans la fenêtre « Transmission en cours » choisir « Aquarius_3D gateway server Terarecon » et cliquer « transmettre ». La transmission peut prendre du temps. Alors, rechercher le patient dans l'Aquarius Intuition dans l'onglet « Liste Patients ». Si le dossier du patient ne s'affiche pas dans la liste d'examen, alors attendre et ensuite, vérifier le bouton refresh  dans la barre d'outils d'Aquarius.
3. Choisir série + « charger »
4. Choisir reconstruction (scénario) « Cardiaque 4D» (pas Cardiaque 1 ou Cardiaque Tech)
5. Une pop-up fenêtre va s'ouvrir « Suppression Automatique de l'os/ Run automatic bone removal? », il faut cliquer « Oui »
6. Ensuite on choisit la coronaire qui nous intéresse dans les scénarios (workflows).

- On choisit la coronaire selon l'endroit où le stent a été posé. Pour ce faire, on peut aller dans Oacis, choisir l'onglet « documents », puis sous la rubrique « Spéc. de la visite » l'hémodynamie et puis le compte-rendu de l'intervention.
7. Dans, l'Aquarius, pour avoir seulement 4 fenêtres de gauche (et pas les 6 fenêtres au total), on peut double-cliquer sur la fenêtre CPR / MPR.
 8. Si l'axe médiane n'est pas créé :
 - Se mettre en vue « CPR » - en cliquant sur le bouton « CPR » dans la barre du menu à haut.
 - on peut faire « Shift » + clique gauche sur le vaisseau d'intérêt dans la fenêtre de droite (3D VR) pour créer l'axe médiane.
 - i. Bien important d'ajuster l'axe médiane pour qu'elle ne passe pas à travers des calcifications ou autres parties du vaisseau que la lumière (sinon tous les calculs vont être faussés) (aussi, la distance entre les billes peut varier si l'axe médian n'est pas bien choisi).
 - ii. Pour changer l'emplacement de l'axe médian, on peut faire « Shift » + clic gauche sur les points verts qui sont situés sur la ligne médiane et puis on tire l'axe vers la gauche ou vers la droite pour créer un nouveau parcours.
 - iii. On peut créer nos propres points verts sur l'axe médian en tenant la touche « Shift » et en cliquant avec la touche gauche de la souris sur l'axe à l'endroit où on veut incérer un point vert et ensuite en relâchant la souris.
 9. Afin de prendre les bonnes photos on doit faire les étapes 10, 11, 12, 13, 14 et 15.
 10. Pour avoir toute information être affichée en anglais, on va dans le bouton « Preference »  à haut à droit et on choisit l'onglet « Général » et puis, on choisit la langue anglaise.
 11. Pour cacher l'information du patient, on clique sur bouton « i A » à côté de la liste de patients dans la barre du menu à haut et on choisit « Cacher les informations du patient ».
 12. Ou on peut cacher toutes les annotations en cliquant sur bouton « i A » à côté de la liste de patients dans la barre du menu à haut et en décochant « Annotation ».
 13. Dans la vue MPR, on clique-droit sur « MPR droit »-- c'est plus facile à travailler ainsi.
 14. Dans les deux fenêtres de bas, pour agrandir les proportions à 80% de l'image, on clique sur la roulette de la souris et on drag vers le haut.
 15. Dans la fenêtre sMPR, agrandir la région d'intérêt en cliquant sur la roulette et en tirant vers le haut et réfocuser la région par un clique-droit.
 - N.B. C'est réglé par défaut que les deux fenêtres de CPR/MPR bougent ensemble. Parfois, c'est difficile de prendre des belles photos ainsi. Donc, on peut enlever ce


lien en cliquant avec la touche droite de la souris sur la fenêtre CPR de gauche et en décochant le choix « Link CPR windows » dans le menu qui apparaît.

Par la suite :

16. Si l'on veut, on clique-droit sur la ligne verte et choisir « Afficher les repères de grille ».
17. Pour trouver la bille proximale du stent et en tournant l'artère à droite-gauche, repérer le bord distal de la bille et y mettre un marqueur en cliquant sur la grille et en choisissant « Marquer ici ».
18. En suivant la même procédure qu'à l'étape 17, mettre aussi un marqueur près du bord proximal de la bille distale.
19. Vérifier si le patient a plusieurs stents (en regardant dans Oacis ou WebCardio), et mettre les marqueurs sur toutes les billes avant de commencer à mesurer.
20. Vérifier la distance entre les deux billes. Ça devrait être environ la longueur marquée dans le rapport de l'angioplastie.
21. Maintenant, on clique sur le bouton Distance  qui est situé à haut dans le panel d'outils. Puis, on clique sur la ligne médiane à côté du premier marqueur et on glisse vers le bas pour avoir 5 mm au total.
22. Dans la fenêtre MPR/CPR, on fait sortir le menu avec le clic droit, et dans le menu on choisit « Analyse de plaque ».
23. On met la croix du curseur au début de notre ligne rouge de 5 mm et on glisse jusqu'à la fin de la ligne et puis on relâche la souris. On a alors la volumétrie calculée dans la fenêtre de gauche.
24. Pour être certain que la lumière a bien été dessinée, on regarde notre segment analysé dans les fenêtres de bas (en transversale) en tournant la roulette.
25. Si on veut changer la ligne médiane dans la fenêtre de haut-gauche, on clique sur « Shift » et on le tient tout en changeant la ligne verte en cliquant sur les points verts et en les tirant. Ou sinon, on peut aussi changer la lumière en transversale en cliquant aussi sur « Shift » et en le maintenant on change le contour de la lumière dans la fenêtre de bas-gauche.
26. Et une fois que toutes les modifications sont faites, on peut cliquer « Cliquer ici pour recalculer » dans la première fenêtre de gauche et on obtient une nouvelle boîte avec les strates.
27. Pour choisir les paramètres dans la boîte de strates, on clique-droit sur la boîte et on peut changer les couleurs en choisissant « Modifier la carte de couleur » et on peut aussi monter un histogramme.
28. Maintenant, pour choisir un autre segment de 5 mm :

- On clique-droit sur les calculs de volumétrie et on choisit « Supprimer la mesure » (et pas « Supprimer toutes les mesures »)
- On met le curseur sur le bout proximal du segment de 5 mm qu'on a dessiné et une double-flèche oblique apparaît . Alors, on drag la flèche par le bout proximal vers le bas pour avoir une autre 5 mm. Et on recommence à faire les mesures à partir du step 22.
- Ainsi, on mesure la volumétrie de tous les blocs de 5mm dans l'intrastent. Si l'intrastent ne mesure pas le nombre entier (n) de multiplications de 5 mm (i.e. n x 5 mm), alors on élimine les millimètres distaux une fois que notre nombre maximal de n de 5 mm est atteint.
- Par exemple, pour l'intrastent de 16 mm de longueur axiale, on garde les 3 blocs de 5 mm (n max=3, 3x5=15 mm) et on élimine le dernier 1 mm distalement.

29. Prendre photos

- Avant de prendre la photo, on clique sur la double-flèche  pour n'avoir à l'écran que 4 fenêtres (cela va donner une meilleure résolution de l'image).
- On peut aussi effacer l'affichage des calculs dans la fenêtre de CPR/MPR de haut-gauche.
- Capturer tout en un (ctrl+alt+c)
- Capturer fenêtre principale, MPR et CPR (touche « c »)
- On prend la photo de (À revoir):
 - i. Endroit où il y a une plus grande sténose avec le curseur bleu sur un endroit de référence (segment sain) et le curseur rouge sur la coupe transversale de la sténose et les deux fenêtres longitudinales.
 - ii. Endroit où il y a un plus grand remodelage à l'œil sur la coupe transversale et longitudinale. Donc, on prend la photo de la coupe transversale de la lumière à l'endroit du plus grand remodelage (curseur rouge) avec la coupe transversale de l'endroit de référence (curseur bleu) et les deux fenêtres longitudinales.

Plus, on prend en photo les mêmes 4 fenêtres, mais cette fois on prend en photo le diamètre et aire **externes** dans la coupe longitudinales (curseur rouge).

30. (Facultatif) Dans l'onglet Album, transférer images dans PACS clinique

- Onglet Album > Envoyer > PACS
- Description de la série : inscrire initiale de l'observateur et date
- Si patient anonymisé, inscrire une note au responsable du PACS pour envoyer les images au PACS.
 - i. Lui informer de la date, patient et numéro de dossier

31. Sauvegarder les images aussi dans le commun ou sur la clé USB/ mémoire externe :

- Onglet Album > Sauvegarder
- Sélectionner dans Mes documents le dossier: Evguenia Zdanovich > patient # X
- Sauvegarder images dans ce dossier

32. (Facultatif) Aussi, on peut créer un lot d'images consécutives perpendiculaire à l'axe médiane :

- Cliquez droit sur la fenêtre de droite-haut et on va dans « Assistant Reconstruction » (Batch Wizard) et ensuite dans la fenêtre nouvellement apparue on clique sur « Perpendiculaire ». Ensuite, on garde la clique gauche enfoncé le long de la ligne verte.
- Cela permet de sauvegarder les couleurs en lien avec chacune unité de HU (chaque strate).

33. Dans la nouvelle fenêtre qui apparaîtra, on peut choisir la destination, si on veut sauvegarder en « AVI » ou dans « La Liste des patients ». On peut même y donner une description. Et à la fin on clique sur sortie.

34. Ce lot d'images consécutives se trouve dans « la Liste Patient ». Et on peut le visualiser si on clique sur le symbole Mise à jour. ()

35. On peut cliquer sur « Séries » et ensuite, « Envoyer Pacs ».

NOTA BENE :

- 1) Quand dans un des blocs l'artéfact crée une grande distorsion dans l'image axiale, j'exclue ce bloc de mes analyses et je ne l'inscris pas dans mes données.
- 2) La plupart des plaques est observée en proximal de stent. Donc, quand on exclut les millimètres distaux qui ne font pas partie d'un bloc, en majeure partie on n'affecte pas nos données de la plaque sous-stent.